TECHNICAL REPORT STANDARD TITLE PAGE

1. Report No.	2. Government Accession No.	3. Recipient's Catalog No.

4. Title and Subtitle	5. Report Date
Alternate Methods of Avalanche Control - Interim Report	July 1975
	6. Performing Organization Code

7. Author(s)	8. Performing Organization Report No.
C.B. Brown, R.J. Evans, J.B. Johnson, E.R. LaChapelle, J.A. Langdon, M.B. Moore, and P.L. Taylor	

9. Performing Organization Name and Address	10. Work Unit No.
Geophysics Program and Department of Civil Engineering University of Washington Seattle, Washington 98195	
	11. Contract or Grant No. Y-1637
	13. Type of Report and Period Covered INTERIM August 1974 - July 1975

12. Sponsoring Agency Name and Address	14. Sponsoring Agency Code
Washington State Highway Commission Department of Highways, Highway Administration Bldg. Olympia, Washington 98504	

15. Supplementary Notes

Cooperation with US Department of Transportation, Federal Highway Administration

16. Abstract

A collection of reports resulting from the first year's study Alternate Methods of Avalanche Control. The reports are entitled:

1. Air Bag System by E. R. LaChapelle and P.L. Taylor.
2. Gas Exploder System by E.R. LaChapelle and P.L. Taylor.
3. Snow Behavior Behind a Continuous Avalanche Defense Structure by J.A. Langdon.
4. Interface Modification Field Tests by E.R. LaChapelle.
5. Mechanical Resonance of Snow by J.B. Johnson and R.J. Evans.
6. The 1974-75 Winter by M.B. Moore.

17. Key Words	18. Distribution Statement
Avalanche, Snow, Weather, Creep, Glide, Avalanche Forecasting	

19. Security Classif. (of this report)	20. Security Classif. (of this page)	21. No. of Pages	22. Price
Unclassified	Unclassified	158	

Form DOT F 1700.7 (8-69)
UMV FORM 341-004

ALTERNATE METHODS OF AVALANCHE CONTROL

Co-principal Investigators
E. R. LaChapelle
C. B. Brown
R. J. Evans

Geophysics Program and
Department of Civil Engineering
University of Washington

INTERIM REPORT

Research Project Y-1637
Phase I

Prepared for
Washington State Highway Commission
Department of Highways
In cooperation with
US Department of Transportation
Federal Highway Administration

July 1975

The contents of this report reflect the views of the authors who are responsible for the facts and the accuracy of the data presented herein. The contents do not necessarily reflect the official views or policies of the Washington State Department of Highways or the Federal Highway Administration. This report does not constitute a standard, specification, or regulation.

TABLE OF CONTENTS

INTRODUCTION

This Interim Report summarizes results from the first year of investigation into alternate methods of avalanche control. This research project is designed to seek methods of either preventing or artificially releasing snow avalanches which do not depend on the conventional application of high explosives or use of artillery.

Four different methods of controlling snow avalanches are presently being investigated. These are:

(1) Artificial release by inflation of air bags under the snow.

(2) Artificial release by exploding a gas-oxygen mixture in special containers placed under the snow (gas exploders).

(3) Artificial release by initiating fracturing in snow through vibration.

(4) Modification of the snow-earth interface, either to inhibit avalanche formation (in the conventional sense of avalanche defense structures) or to enhance avalanching and prevent build-up of dangerous amounts of snow.

This research project has been organized to run for three years. During the first winter, strong emphasis has been placed on design and field-testing of the air bag and gas exploder systems. Fundamental studies are being carried out on sound transmission and mechanical resonance in snow as a background for the vibration method. Interface modification has been treated during the first year at the theoretical level except for some very minor field tests. It is anticipated that the second year of the project will continue field testing of air bags and gas exploders, with emphasis on technical

improvements. Vibration release of avalanches will be field-tested concurrently with further basic studies. Interface modification to enhance avalanching will be tested in the field while further theoretical studies continue.

Two locations were chosen for the field tests during the first winter. These are at Stevens Pass, Washington, and Red Mountain Pass, Colorado. The Washington and Colorado Highway Departments have contributed personnel and facilities support to the field tests at the respective passes. The Stevens Pass tests were installed and supervised by the Geophysics and Civil Engineering Departments at the University of Washington. Those at Red Mountain Pass have been managed by personnel of the Institute of Arctic and Alpine Research, University of Colorado (San Juan Avalanche Project). The two sites were chosen to assure a broad range of snow conditions for the tests and to offer better assurance that an adequate number of avalanche days would be encountered during the winter at least at one site even if an avalanche-poor winter was experienced at the other. In the case of winter 1974/75, substantial avalanche activity was experienced at both sites.

In the present Interim Report, the Chapters I and II on the air bag and gas exploder systems are narrative summaries of tests conducted the past winter and the current conclusions from these tests. Relevant technical details of the systems are summarized in appendices to Chapters I and II. Because the final forms of these systems for operational use have not yet been determined, the present conclusions and technical details are necessarily tentative. More complete and detailed systems descriptions and specifications will be presented in later reports as the designs become more clearly established.

Chapters III and IV on interface modification present the results of an on-going study on effects of barriers on snow creep. This stands as a detailed report on this particular aspect of the theoretical studies, with practical guidelines for engineering applications given in the appendix of Chapter III.

Chapter V summarizes the current background investigations into sound propagation in snow which have been conducted the past year as a prelude to designing a test of avalanche release through mechanical vibrations.

Chapter VI presents in some details the results from a concurrent study of conditions governing avalanche formation in the Cascades. This study began under previous Department of Highways contracts and has been carried forward under the present one in order to furnish an adequate background about avalanche release characteristics as a guideline for developing alternate methods of control. This chapter has also been presented as a key section of the Master of Science thesis submitted by Mark B. Moore to the University of Washington Department of Atmospheric Sciences in June of 1975.

Chapter I

AIR BAG SYSTEM

by

Edward R. LaChapelle and Philip L. Taylor

Background

The inflation of air bags underneath the snow cover is a simple means of disrupting the snow and inducing fracturing at the surface. The assumption of this method of avalanche control is that such fracturing induced at the right time and place will result in slab avalanche release. The basic idea was originally proposed by Don Anderson of the Washington Highway Department. It applies the same principle formerly used for aircraft de-icing which depended on inflation of a rubber boot along the leading edge of a wing. The only similar application to snow that has been discovered so far is a scheme used by the railways in Japan to empty snow out of gondola cars. (In certain areas of the Japanese Alps, snow accumulation removed from city streets is carried away by rail.) Rail cars loaded with snow on top of air bags are positioned over a bridge and the bags inflated, dumping snow into the river (D. Kuroiwa, personal communication).

The method is attractive in principle. Only very modest air pressure, in the order of 5 psi, is required to lift the weight of any reasonable winter snow cover of average density. Calculations show that, if the snow cover is very hard with a high tensile strength, pressures up to 20 psi may be needed to fracture the snow beam resting upon the air bag. Air at these pressures can readily be provided by small compressors or from high-pressure cylinders through reduction valves. Large compressors are required only if a fast inflation is desired.

Air bags are readily available commercially in the form of dunnage bags used to pack cargo securely in ships and rail cars. They are available in several sizes or can be fabricated to any size on custom order. The size adopted for these tests was 4 x 9 feet (1.3 x 3.2 meters). These bags are fabricated from nylon-reinforced neoprene with a separate neoprene air bladder inside (inner tube). They are rated at 10 psi maximum working pressure when restrained and have a nominal 30 psi bursting strength. Since completion of the first winter's test, plastic-coated paper dunnage bags have become available. These are now being evaluated for possible use in avalanche release at a much lower cost than the nylon-neoprene bags.

Once calculations had shown that the air bag system appeared highly feasible and availability of suitable bags had been established, an operational test was undertaken to see if the bags would in fact fracture snow in the manner anticipated. At this time (August 1974) little accessible snow was available in the normal Cascade avalanche paths, so the test was carried out at the University of Washington's field facility on the Blue Glacier, Mt. Olympus. At this site a deep layer of summer firn was available with a density of 600 kg/m^3 and a Kinosita hardness of 7-8 kg/cm^2, higher than that normally to be expected in a winter snow cover. A deep pit was dug in this firn with the aid of a chain saw (the snow was too hard to dig with a shovel) and an air bag inserted laterally from the bottom of the pit under an unbroken layer of snow 7 feet (2.2 meters) thick. The pit was refilled with packed firn and pressure applied from a small, portable compressor. The firn failed in tensile fracture with cracks appearing at the surface when pressure reached 28 psi. There was

no damage to the bag. This was considered to be an extreme test of combined snow weight and strength which was not likely to be matched in an ordinary winter snow cover. Air bag inflation did appear to be an effective means of fracturing snow.

Sites were then selected for winter field tests. At Stevens Pass, two sites were chosen for avalanche release tests in the fracture zones of known avalanche paths. One of these was a narrow chute adjacent to the Stevens Pass Ski Area, where a single bag was installed. The other site was near the crest of Skyline Ridge, at the head of a gully facing to the SSW. Neither of these sites involved avalanches which fell to the highway, a choice dictated by the need to experiment free from constraints of highway traffic control and maintenance. At Red Mountain Pass, a site was chosen where a series of cornices often formed and fell to trigger an avalanche which fell on a short slope directly to the highway (U.S. 550). In this case a test of the air bags was sought which would demonstrate their ability to remove cornices. This site was also a high-priority one for an alternate method of avalanche control. In past years the Colorado Highway Department had used artillery fire frequently on this path, but experienced serious difficulties due to shrapnel damage to adjacent power lines.

Details and specifications for the air bags and accessories used in the 1974/75 tests are listed in Appendix I.

Winter Field Tests--Red Mountain Pass

The Blue Point avalanche just north of Red Mountain Pass is a steep chute which plunges directly to the highway between rocky ridges. The

south ridge is crowned by an area of cliffs along which west and southwest winter storm winds build large cornices. These cornices reform with every storm and often provide a trigger for the avalanche path below when they fall. The path is very active, generating one or more avalanches with every significant snowfall. There is no run-out zone and all the sliding snow accumulates in the highway. Artificial release of the cornices to prevent their buildup is an excellent protective measure at this site. The fall of cornices so released often triggers avalanche snow on the slope below, providing a further stabilizing action. This site was selected for the cornice-release air bag test during a survey of the local terrain by project and Colorado Highway Department personnel in September 1974.

An air hose 600 feet long was installed running from the cornice site to the highway. This hose was buried in a trench and covered with flexible conduit where it was exposed above ground in order to prevent damage from pressures and to assure security from rodents (marmots are an especially troublesome problem in this area). The bags themselves were unprotected, but were installed after the marmot population had hibernated for the winter. Four air bags were deployed at the head of four small chutes among the rock cliffs where cornices were expected to form. Short lengths of air hose connected these bags to a manifold through separate valves, one for each bag. The manifold was located at the end of the air line running to the highway and mounted high enough on a tree stump to assure easy access during the winter.

The Colorado Highway Department furnished a trailer-mounted compressor supplying 90 psi air for use in the winter tests. This

compressor was stored in the equipment shop of Idarado Mining Company a couple of miles down the highway, from where it was towed to the test site to inflate the air bags. Connection to the air line running up to the bags was made with a quick-disconnect fitting. A valve and pressure gauge were installed at the lower end of this line to permit control of air flow and check of system pressure. The use of relatively high pressure was needed at this site in order to assure a reasonable rate of inflation through such a long line. But care has to be taken to monitor bag inflation and system pressure in order to avoid inflating the bags beyond their rated pressure.

The compressor, air hoses, and manifold system functioned without difficulty throughout the winter. Concern about icing of the lines from condensation did not appear to be justified, for no difficulties of this kind were encountered. Inflation rate was highly satisfactory, with full inflation of the four bags being achieved in 1½ to 2 minutes. In some cases evidence of snow displacement could be seen as little as 15 seconds after inflation began.

The air bags proved to be effective for removing cornices. A summary of tests and the results is listed in Table I, with a photographic sequence of an actual cornice release shown in Figure 1. Figures 2 and 3 show details of the installed air bags at the cornice site. Tests were conducted throughout the winter whenever snow conditions and cornice development permitted and were extended well into the spring owing to an unusually late winter and a prolonged series of March and April snowstorms.

Positioning of the bags is definitely critical. At the start of the season, the bags were placed on the near-vertical lee slopes just off the ridge crest. This proved satisfactory for early-season cornices, but

as the snow cover behind the ridge crest built up, the cornices tended to form far enough above the bags that these became less effective. Three of the bags were relocated on 10 March to positions on the ridge crest where they would be more effective in breaking the deep snow at the root of the cornices. A compromise bag position between these two may be more effective throughout the winter. One of the bags (No. 2, counting from the east) turned out to be in a site where little or no cornice formed. It was moved to a position west of No. 4 on 12 February where a substantial cornice was forming.

A persistent problem with the 1974/75 test installation was the tendency of the bags to inflate unevenly. The bags carrying the lightest snow load inflated first, with those more deeply buried following only after the first ones had accumulated considerable pressure. This same problem was encountered at Stevens Pass, where the dense, heavy snow cover of the Cascade Mountains led to more serious difficulties discussed below. At Red Mountain Pass, the principal consequence of this uneven inflation was reduced efficiency of release from that which might be gained by simultaneous bag inflation and snow rupture.

It is necessary to anchor the air bags securely so that they will resist the sometimes large snow pressures. For their designed use as dunnage bags, no firm points of attachment are required and none are furnished. It is necessary to provide a secure means of attaching anchors or tie ropes to the bags, which was done at the cornice site in two different ways. One was to punch a series of holes along one edge of the bag (through the outer bag but not the inner one) and lace a

stout line through these holes and around a pipe. The pipe in turn could then serve as a tie point for anchoring cables. The other method was to attach heavy loops of rubber belting to the outside of the bag by cold vulcanization. Both methods appeared to stand up well to the stresses of the winter tests. Both are time-consuming to prepare and the belting is relatively expensive. Other methods of bag anchoring are being explored.

The same test site will be used again in the winter of 1975/76, with some modifications to bag location, anchors and manifold connections.

Winter Field Tests--Stevens Pass

Two sites were chosen at Stevens Pass for the air bag tests under Cascade snow conditions. Both sites were in avalanche release zones and did not involve cornices. Neither site was an especially active avalanche path, but in this case they were chosen for the tests for reasons of accessibility and freedom from influence on the highway. A distinctly different situation prevails at Stevens Pass than at Red Mountain Pass, for a much heavier volume of traffic is found at Stevens Pass and any interruptions of traffic to insure safety during avalanche release tests would involve considerable inconvenience to the public and to the highway maintenance crew. A corollary to this consideration in selecting non-operational (in respect to highway problems) sites was the character of avalanching common to the Cascades. In this climate, avalanche hazard builds rapidly during storms, rain or thaw periods, but lasts for relatively short times, often diminishing again to zero in a few hours. Timing of the artificial release measures is thus much more critical than it is in

the cold, high-altitude snow found in Colorado, where unstable snow slabs may persist for many days or even weeks after formation. It was necessary to select sites which could be tested at times of choice independent of highway traffic considerations. In any case, it was recognized that the initial winter of testing in the deep, heavy snow-cover of the Cascades would be related more to evaluation of the air bag performance than to operational avalanche control.

One site was on Skyline Ridge immediately to the northwest of Stevens Pass. A series of gullies fall from this ridge to the south and southwest from which avalanches regularly fall each winter. One of these gullies, heading at about 4500 feet elevation, was chosen as the test site. It is accessible by a rough road in summer and can be reached by skis or oversnow vehicle in the winter. Four air bags were deployed across a shallow basin at the head of the gully in the expected area of the avalanche release zone. These bags were placed flat on the ground (heather surface) and anchored to stakes to limit downhill displacement by snow glide. An air hose was coupled to them as a single distribution line with a T-connection and stub line at each bag. Source of compressed air was cylinders of compressed dry nitrogen connected through a reducing valve to the air hose. As in the Red Mountain Pass installation, the hose was buried to protect it from snow pressures and rodents.

The other site was at the head of a narrow gully above the top of the No. 1 chairlift at the Stevens Pass Ski area. This location is easily accessible by a few minutes walk on skis from the top of the chairlift, but far enough removed from the ski area to avoid skier disturbance

of the snow. This gully faces to the northwest and is bordered by a moderately heavy stand of timber. A single bag was installed in the release zone of this small avalanche path, with an air hose brought out to an accessible point on a nearby tree where it could be connected to a reducing valve and dry nitrogen cylinder for inflation. This bag was also placed flat on the ground and anchored to stakes.

Although portable compressors could be used at both of these sites, inflation from compressed gas cylinders was chosen in order to test this mode of operation and to determine just how much gas would be required for effective inflation. No technical difficulties were experienced with this method of supplying compressed air to the bags. It is reasonably useful operationally for single bags, but requires a large number of gas cylinders for frequent inflation of a multi-bag system.

The air bag array on Skyline Ridge was tested by inflation on 16 and 24 February. These bags are number 1 through 4 from west to east. During the first test on the 16th, air from the cylinders was delivered to the air hose with the regulator valve set at a delivery pressure of 20 psi. The first cylinder was emptied in approximately 8 minutes of inflation, giving an initial bag system pressure of 11 psi which dropped to an equilibrated value of 6 psi after 3 to 4 minutes. Surface fractures in the snow were observed after 2 minutes at 4 to 7 psi system pressure. Two additional cylinders were then emptied into the hose with only a short period of rising pressure followed by a steady decline in system pressure. Investigation of the bags showed that No. 1 bag had ruptured along the upper seam during or after reaching full inflation. The snow

cover at this time was 6 feet (1.9 m) deep, hard, and contained many ice layers. Only bag No. 1 achieved full inflation; the others did not inflate under the deep snow cover and the excess pressure leading to rupture of No. 1 was applied while trying to inflate these other bags.

With No. 1 bag disconnected and its stub hose plugged, another inflation test was run on 24 February. At this time there had been an appreciable fall of new snow, but winds had scoured much of it away from the test area. The snow cover remained hard and ice, some 6 feet (1.6 m) deep. Again inflation proceeded at 20 psi delivery pressure. A system pressure of 10 psi was reached by the time the first cylinder was emptied. After 7 minutes of inflation and a system pressure of around 8 psi, the snow fractured over the No. 4 bag and was displaced some 2.5-3 feet above the surrounding snow surface. Air delivery continued with a second cylinder in order to inflate bags No. 2 and 3. After another 12 minutes the delivery pressure was raised to 30 psi and a final system pressure of 21 psi was achieved without any evidence of inflation of No. 2 and 3. After some 5 minutes of static conditions at this pressure, bag No. 4 ruptured along the upper seam. Inspection of No. 4 showed that the bag had levered up a slab of the very hard snow cover, forming a crack between snow and ground into which the rupture occurred. This bag failure at twice the design pressure also coincided with the points of attachment of belting loops for anchoring.

No further tests were conducted at Skyline Ridge, in view of the damaging consequences of multiple-bag inflation under the very hard snow cover. Both tests here demonstrated that inflation proceeds in those

bags which most easily break the snow cover, while failing to inflate at all those bags which apparently bear a heavier overburden. Multiple-bag systems in such circumstances need some refinement of air delivery controls to be effective.

Tests at the ski area site, where a single air bag was used, escaped the uneven inflation problem and offered convincing evidence that an air bag can fracture a deep and heavy snow cover. The first test was on 5 February, following a period of little snowfall and avalanche activity. No avalanche release was expected for this test. Inflation began from a compressed air cylinder with the regulator set for a delivery pressure of 20 psi. Within one half minute there was an audible thump from the snow, followed by more noises as bag pressure reached 2 to 4 psi and then by fracturing of the snow cover at the surface. Inflation continued until bag pressure reached 12 psi, by which time extensive cracking had appeared over an area of 15 x 21 feet (4.8 x 6 m), with the snow surface above the bag lifted about 20 inches. The snow on this 36^{o} slope was 10.5 feet (3.3 m) thick at this time, with a high density and numerous ice layers.

A second test at this ski area chute on 13 February produced similar results. Again the bag was filled with a delivery pressure of 20 psi. Fracturing of the snow surface occurred after 1½ minutes as the bag pressure progressed from 4 to 7 psi. Additional fracturing occurred when pressure reached 11.5 psi. Inflation was terminated at 15 psi bag pressure, with no further fracturing observed. The extensive cracking and lifting at the snow surface, pictured in Figure 4, extended farther

than in the previous experiment to cover an area of 20 x 25 feet (6.4 x 8 m). The snow cover was approximately 12 feet (3.8 m) thick at this time. Although a shallow layer of new snow was present at this time, it proved to be stable and no avalanche was released. The impressive extent of the fracturing, though, left no doubt that an unstable slab would easily be dislodged by such disruption of the snow cover.

Interim Evaluation

(1) The air bags are simple to install and have little that can go wrong. They appear to be unaffected by normal winter environment and use, except for failure due to overinflation.

(2) The bags are very effective in removing snow cornices. Positioning for this purpose is critical and may take one or more seasons of adjustment to reach an optimum at a given site.

(3) Full bag inflation produces extensive surface fracturing even in a deep and very hard snow cover. This takes place at pressures well within the rated operating characteristics of the dunnage bags used in this test. Although no slope avalanche releases have yet been achieved with this system, the extent of fracturing is deemed adequate to initiate the fall of unstable snow slabs.

(4) When several bags are connected to a common manifold or distribution air line, uneven inflation is the rule. In deep, heavy snow, some of the bags cannot be inflated even at pressures which rupture those which have already inflated. A more sophisticated system of metering air flow to each bag is required for multiple-bag installations.

(5) On the basis of the tests so far, installation of single bags appears feasible for operational use in cornice release or avalanche control on small paths.

Table I

Chronological record of 1974/75 air bag tests at Blue Point cornice site, Red Mountain Pass, Colorado

11/9/74	Four air bags installed at test site. The bags are numbered from east to west.
11/18/74	Inflation test of air bag system. Initial inflation was slow.
1/14/75	Inflation released a small cornice which fell to the highway.
2/1/75	No. 2 bag disconnected at manifold (no cornice forming at its location). Inflation of No. 1, 3, and 4 released cornices plus avalanching snow onto highway 10 m wide and 1 m deep.
2/5/75	No release with inflation of No. 1, 3, and 4. Bags too far downslope; 5 foot cornice remained in place.
2/11/75	Cornice built out over bags.
2/12/75	Old cornices at bag site removed with explosives and small avalanche ran to highway. No. 2 bag relocated to a cornice area just west of No. 4.
2/21/75	Small cornice from No. 1 and very small from 3 and 4 fell to road. Much displacement of snow cover with accompanying noise.
3/6/75	No. 1, 3, and 4 released very small pieces of cornice. Bag positions appear to need adjusting.
3/10/75	Cleared cornices with explosives and bag positions readjusted.
3/19/75	Bags No. 1, 3, and 4 released cornices.
3/24/75	Released cornices fell to highway.
3/28/75	Released cornices fell to highway and filled it.
4/23/75	Released cornices fell to highway and filled it.
Summary:	10 inflation tests with cornices
	9 instances of cornice release
	7 instances of falling cornices and avalanche snow reaching highway

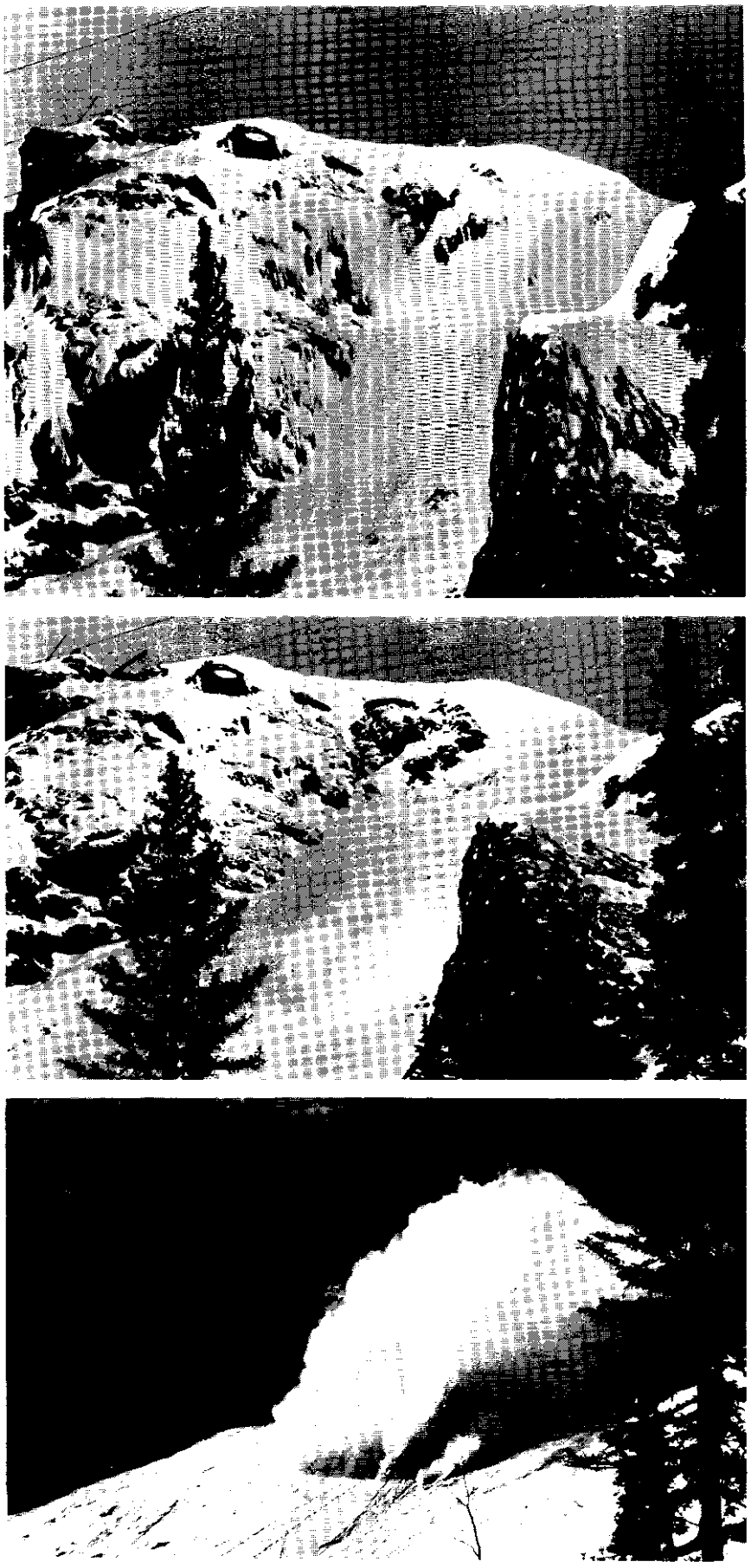

Figure 1 Blue Point cornice site at Red Mountain Pass, Colorado, 1 February 1975. Telephoto sequence showing falling cornices at instant of release by air bags, an avalanche triggered by the cornice fall, and the avalanche running toward the highway.

Figure 2 Blue Point cornice site, 1 February 1975. Exposed and partially deflated air bags following cornice release (see Figure 1).

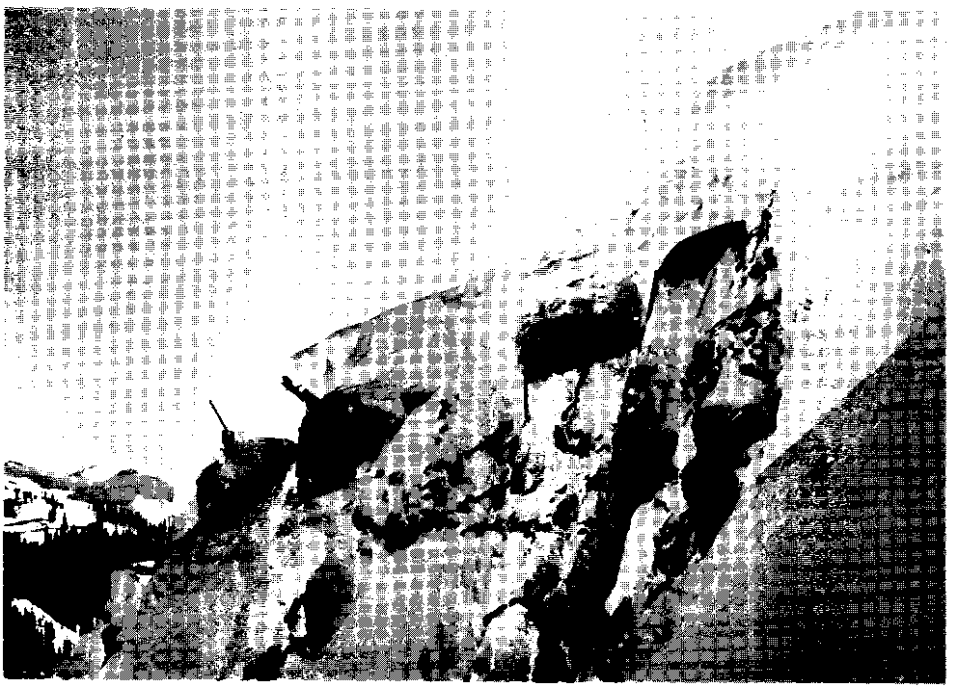

Figure 3 Blue Point cornice site, 12 February 1975. Air bags partially covered by newly-formed cornices.

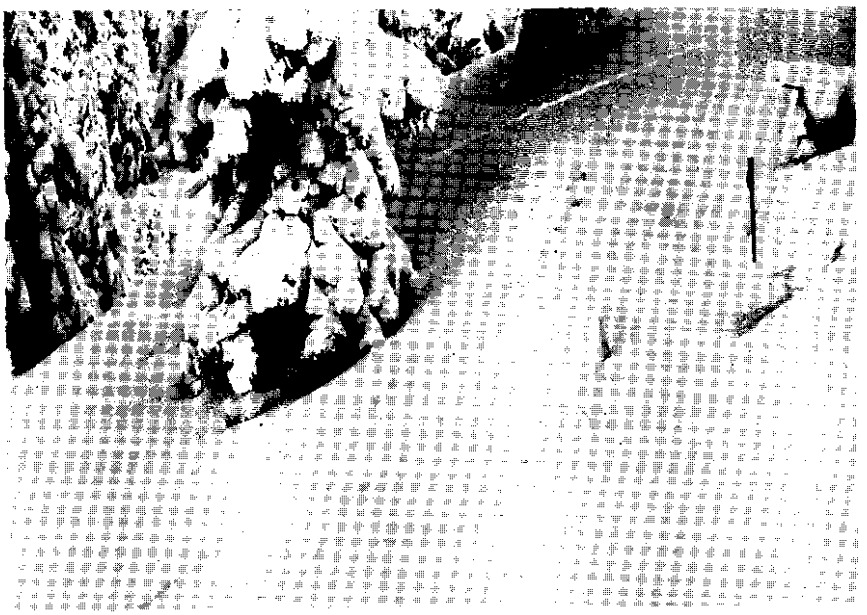

a

b

Figure 4 Stevens Pass ski area site, 13 February 1975. Fracturing of deep snow cover as a result of inflating a single air bag.

APPENDIX I

AIR BAG SYSTEM

Technical Description of Components

Air Bags

Uniroyal Dunnage Bag, 4' x 9' standard single strength, weight about 50 lbs, $200 ea. Inlet connection is Swagelok B1210-2-8 Male Elbow, brass, modified, @ $5 ea.

Bags are suspended utilizing 3/8" polyethylene line, 3/16" galvanized aircraft cable, and angle iron posts as required.

Hose

Hose is Uniroyal P-290, 1/2" I.D., 2 braid, 300 psi working pressure, $.70/ft, weight 20 lbs per 100 ft. Size is adequate for filling four bags through 600-900 ft in a few minutes.

Wedgon Couplings and Wire Clamps are used, installed in the field as required. Valves are standard 1/2 NPT Gate type, brass.

Air Supply

Any standard compressor rated 100 psi and at least 20 cfm, with shut-off valve and pressure gauge.

Alternate air supply used was size M bottle dry nitrogen, @ $1.25 ea, 112 ft^3, 7" x 46", weight 75 lbs. Regulator used on these bottles was Victor VTS-200C-580, rated 1500 scfm, @ $41 ea. Pressure gauge on regulator and bottle valve used for control.

CHAPTER II

GAS EXPLODER SYSTEM

by

Edward R. LaChapelle and Philip L. Taylor

Background

The basic idea of the gas exploder system is to deliver a repeatable explosive impulse to the snow cover without the use of conventional explosives. The application of this idea developed here is based on a proposal by Philip L. Taylor, Senior Engineer, University of Washington Geophysics Program, to adapt for avalanche release the principle of the seismic "thumper." This device is a large, truck-mounted cylinder which is charged with a mixture of propane and oxygen. When the mixture is detonated, a piston is driven violently against the ground, generating a seismic signal. Adaptation of this principle to avalanche control consists of inverting the "thumper," burying it in the ground, and driving a piston upward against the snow cover. In this case an arrangement is used which also permits the explosive discharge of vented gases to provide further disruption of the snow cover. The aim of such disruption is the same as that for conventional explosives: to fracture the snow cover and initiate slab avalanche release. It was expected that the efficiency of such disruption could be improved by installation of several gas exploders in a single release zone where they could be fired simultaneously. The big improvement over conventional explosives would stem from the fact that the exploders could be recharged with a gas mixture and fired as often as need, requiring only an initial installation at the beginning of a winter. The safety and convenience of handling separate gases in conventional pressure cylinders was also

expected to be a big improvement over the problems associated with conventional explosives. The system would be inherently safe to install and operate, for the explosive mixture would be formed and introduced into the cylinders only seconds before it was detonated.

Design and Development

Initial calculation showed that a useful amount of explosive energy could be obtained in a convenient volume, and that the most effective mixture would be oxygen and acetylene rather than propane and oxygen. Although acetylene has a lower heat value than propane, it has a much wider range of flammability, is less expensive, and permits the straight-forward adoption of standard oxy-acetylene welding components. A volume of 3 cubic feet of an optimum mixture of these contains the same chemical energy as 1 pound of TNT. While this amount of explosive is sub-marginal as a single charge for avalanche release, it was deemed to be useful when detonated in multiple charges in a single release zone.

Improvised gas metering equipment and a temporary cylinder cut from a water tank were assembled to test the principle. Ignition of the gas mixture was provided by a spark plug installed in the cylinder wall. Preliminary experiments at the Seattle Police Department Firing Range provided guidelines for regulating the gas mixture and charging the cylinder. The energetic detonations obtained in the experiments showed that a convincing amount of energy could be released in a cylinder of reasonable size.

The next step was to test the system in snow. A first model of a working

gas exploder cylinder was assembled from 16-inch steel pipe with 3/16 inch wall thickness. A steel plate was welded on the bottom. Instead of an internal piston, an external lid which could rise vertically on guide rods was installed. Heavy springs provided cushion at the end of the lid travel and returned the lid to the closed position following detonation. This design was adopted to provide both an impulse upward against the snow and to allow effective venting of the gases against the surrounding snow. The ultimate form of this basic design adopted for winter field tests is shown in Figure 1. At this time (August 1974), there was no readily accessible snow in the Cascade Mountains, so the initial field tests were conducted at the University of Washington field station on the Blue Glacier in the Olympic Mountains, along with simultaneous tests of the air bag system described in Chapter I. Here, the gas exploder was buried to various depths in hard summer firn, covered with packed firn, and detonated. Satisfactory disruption of this high-density form of snow was found at depths up to about 1 meter (3.1 ft.). Further experience was developed in regulating the gas mixture and charging the cylinder. A very useful discovery was the fact that the spark plug mounted in the wall of the cylinder was not necessary, for the gases could be ignited at the point of mixture and a flame would propagate down the hose used to charge the cylinder, igniting the mixture in the cylinder. This greatly simplified the operation of a system using multiple cylinders, for a single hose could be used both to charge and ignite the gas mixture and a single spark plug for ignition could be located at the gas metering controls.

Time was now growing short to fabricate and install working systems at both Stevens and Red Mountain Passes before the arrival of autumn snow storms.

Although it was recognized that alternate and perhaps preferred designs for the gas exploder might eventually be developed, a decision was made at this point to freeze the present design of the cylinder for the 1974/75 winter field tests. The first model of the cylinder had been shown to work in principle, but was found to possess inadequate strength for the stresses generated by the exploding gas mixture. Calculations based on deformation of the steel from these tests indicated that pressures in the order of 200 psi (14 kg/cm^2) were being generated inside the cylinder, resulting in a total initial upward thrust on the lid of around 40,000 lbs. (18,000 kg). A redesigned cylinder of the same size--16 inches (40 cm) diameter and 16 inches high, volume 1.8 cubit feet (.05 cubic meter)--was adopted which was fabricated from 1/4-inch (6.3 mm) steel. The guide rods for the lid were increased in size and in number from four to six and additional steel reinforcements were welded on the lid. The resulting design, which was installed for the winter field tests, is seen in Figure 1. A field installation is shown in Figure 2, where the gas exploder has been excavated immediately after an avalanche release.

A large amount of design and testing time was spent in perfecting a control unit for the gas exploder system. Although various configurations of the exploder itself might be used, the heart of the system is the method of metering gases into the exploder and firing it by remote control. The control unit has to be weatherproof and unaffected by very low temperatures, provide accurate control and mixing of the gases without leaks, provide reliable ignition for firing, and preferably function without service attention for several months at a time. The basic gas supply is provided by standard gas cylinders of the

type used in welding, equipped with high-quality gauges and reduction valves. From these reduction valves, standard welding hoses lead the gases to the control unit. Solenoid valves provide electrical control of the gas flow and the valves are protected by check valves. Mixing takes place in a standard oxyacetylene welding torch handle, where manual valve adjustment is made to regulate the mixture and flashback protection for the gas supply is obtained. The mixed gas flows through an ignition chamber and then through a distribution line to the gas exploders. Ignition is provided by a spark plug and automotive-type ignition coil. A sealed storage battery (Gel-Cel) provides power to operate the solenoid valves and ignition circuit. Control of the unit is exercised either by local switches or remotely through either wire or radio links. The 1974/75 field tests used wire links and detachable remote control switch boxes to control the charging and firing. The physical details of the control unit construction, mounted in a weatherproof fiberglass box, are shown in Figures 3 and 4, while further technical details are discussed in the Appendix to this chapter.

A key feature of the control unit design is the prevention of flashback from the ignition of the combustible mixture into the solenoid and reduction valves. Numerous experiments showed that it was not possible to improve on the use of a welding torch handle for this purpose, where flashback suppression is already a carefully-designed feature. The torch handle is also convenient because it permits quick disconnection of the mixed gas line and substitution of a torch tip so that the optimum gas mixture can be achieved by visual inspection of the flame. Experience showed that a slightly lean mixture

(leaner than would be optimum for welding) provided the most energetic detonation in the gas exploders.

Experience with the gas exploder system to date points to the crucial importance of using a correct gas mixture and to its efficient introduction into the exploder cylinder. For optimum explosive energy, the gas mixture ideally should displace the air in the exploder cylinder. In practice, partial displacement and partial mixture with the air appears to take place, thus reducing the efficiency from maximum. Experiments with the cylinders and with other exploder devices (discussed below) suggest that a manifold system of introducing the gas mixture at several points in the exploder will improve efficiency. The exploder cylinders used in the 1974/75 field tests had only a single point of gas entry and in many cases apparently did not produce their full designed energy impulse. Since the only place any displaced air can go is through the snow when the exploder is buried under the snow cover, the efficiency of the system will depend in part on snow porosity. Comparison of tests at Stevens and Red Mountain Passes seem to confirm this. Further development work will be aimed at more efficient charging of the exploders and better displacement of the air, possibly through a separate venting system. A basic obstacle to solution of the displacement problem is the fact that the optimum oxygen-acetylene mixture has a density very close to that of air.

Winter Field Tests--Red Mountain Pass

In cooperation with Colorado Highway Department personnel, a test site near Red Mountain Pass was selected for the gas exploder experiments. This

was an avalanche path called the Willow Swamp just north of the Pass where avalanches commonly fell to U.S. 550 each winter and which was a target for regular artillery control by the Department. There are three release zones in this path. The one selected for the test was the northern and largest, an open, shallow basin with a few scattered conifers and a ground cover of heather and grasses. This slide path lies immediately to the north of, but is higher than, the Blue Point site where the air bag system was tested (see Chapter I).

When the trench was dug to install the air hose to the Blue Point air bag site, a signal cable was also incorporated in the trench and this cable was extended on up the mountain side to the release zone of the Willow Swamp avalanche path. Total length of the cable was 2,000 feet (610 m). This was a four-conductor cable with a 10-mil copper shield. The main purpose of the shield was to prevent damage from gnawing rodents, although some extra electrical protection was also afforded from ground currents. Only two conductors were used for control of gas exploder system, the other two being reserved for other experiments. The control unit and gas cylinders were installed on a level bench above the ridge crest at the head of the avalanche path where they were safe from avalanche and snow creep damage. The control unit was placed inside a plywood box which rested in a shallow pit with the top exposed. The gas cylinders were placed upright at the foot of a nearby alpine fir.

Four gas exploder units were installed in the release zone late in the autumn. They were distributed across the shallow basin over a distance of about 250 feet (76 m). A single gas line (3/8-inch rubber hose) buried in a shallow trench provided gas feed and ignition, with distribution stubs from

tees to each exploder cylinder. The cylinders were buried in the ground with only the lid and 2-3 inches (5-7.5 cm) of the cylinder exposed above ground. Each cylinder was securely anchored to a large timber buried in the ground beneath it, for tests had shown that even the heavy steel cylinders tended to jump upward with considerable force when the lid reached the end of its travel on detonation. Hose length from the control unit to the nearest exploder was 200 feet (61 m). An initial test firing prior to snowfall showed the system to work as designed, with the simultaneous firing of four exploders providing an impressively loud concussion. Test firings were conducted during appropriate snow conditions throughout the winter from mid-December until late April. The dates of these tests and the results are summarized in Table I. The inoperative condition which developed in late January turned out on inspection to be due to loss of all the gas from the oxygen cylinder. This occurred when a snowshoe rabbit discovered a short section of the oxygen hose between reduction valve and control unit to be exposed and chewed a hole in it. The depleted bottle was replaced with a reserve one and the tests continued. Minor mechanical difficulties occurred on one occasion with the control unit, but these did not seriously impede the tests.

The Red Mountain Pass tests showed that the multiple-exploder array was capable of triggering avalanche during unstable snow conditions. The avalanche released on 10 February 1975 is illustrated in Figure 5. This avalanche released above exploders No. 3 and 4 (numbered south to north), with a jet of snow visible at the surface when the exploders were fired. On 12 February, No. 4 exploder was excavated for examination and photographed (Figure 2). The

winter experience at this site showed that the snow consistently fractured higher up the slope than the location of the exploder array. The array will be shifted farther uphill and closer to the fracture line position for the planned 1975/76 tests.

Winter Field Tests--Stevens Pass

In cooperation with Washington State Highway Department personnel, a test site was selected on the west side of Stevens Pass on the lower part of Old Faithful No. 7 slide path (see Cascade Passes Avalanche Atlas, Part 2). This site is an open boulder field adjacent to a timbered area from which avalanches often fall directly to U.S. 2, dropping over a steep, high cutbank without any outrun zone. Most avalanches originate in narrow chutes among the trees higher up on the ridge, but some occasionally release lower down on the open slope. This lower release zone was chosen for the test by reason of its accessibility in an area where rough ground and dense underbrush make equipment transport and travel difficult in the absence of snow.

Three exploder cylinders were deployed across the lower release zone of Old Faithful No. 7, with the gas line running horizontally to the west side of the path where the gas bottles and control unit were installed. The control unit was suspended from the trunk of a large conifer at a height which would permit access even with a deep snow cover (Figure 6). The rough, rocky ground did not permit direct burial of the hose, so it was laid among the rocks in such a fashion that it would be protected from snow pressures. A four-conductor control cable (approximately 2,200 feet in length) with 10-mil copper sheath was laid in similar fashion down the avalanche path to the

highway, through a culvert under the highway, and on down the slope below to a safe access point on the old Tye road. This access point was located on the snowcat route normally taken by the Department avalanche crew on their way to the gun tower used to control the Old Faithful slide paths. Thus, the exploder system could be fired as a convenient part of the regular avalanche control routine during hazardous conditions.

The exploder cylinders and gas cylinders were delivered to the site and installed prior to the first snow. The control unit was installed on 14 January 1975, when about 4 feet (1.3 m) of snow had accumulated on the lower release zone of Old Faithful No. 7. The bottom layer of this snow was old, wet and well-consolidated. The middle layers were poorly consolidated newer snow, topped by 10 inches (25 cm) of new snow. The system was fired at this time and the detonation of the gas mixture in the canisters could be heard, no effects were visible at the snow surface. The remote control box, used to trigger the system firing from the end of the control cable, was then turned over to the Department avalanche crew for operational use at their discretion. This control box contains a meter to indicate where the normal current flow to the control unit relays is flowing during the firing sequence.

Steve Reister, Avalanche Control Chief for the Department at Stevens Pass, reported that the system was fired on three subsequent occasions with the results noted below:

1/22 -- 1430 hours -- no release observed

2/21 -- 1135 hours -- no release observed

around 3/15 -- ---------- -- no release observed

When the system was dismantled on 11 June 1975, the gas flow and control unit were still normal and the system was fired for a final test, although the last snow had by this time melted from the slide path. The only difficulty with function of the system came from low voltage on one of the control unit batteries after five months in the field.

From these limited tests at Stevens Pass the first winter, it has not been possible to demonstrate the effectiveness of the gas exploder principle for use in Cascade snow conditions. Three factors, working either independently or collectively, appear to account for the failure to obtain successful avalanche releases:

(1) Inappropriate choice of test site. Slope angle and snow conditions here turned out to be marginal for frequent avalanche release. A higher site on the Old Faithful ridge would have been better, even at the cost of more difficult logistics for the test.

(2) Inadequate size of gas exploder for the deep and heavy Cascade snowpack. No effects were visible at the surface from any of the tests, unlike the situation in Colorado. It is probable that the equivalent energy in conventional explosives (1/2 lb. TNT) would also fail to produce any surface effects when detonated at the bottom of this snowpack.

(3) Inefficient charging of the exploder cylinders due to poor air displacement through the low-porosity snow and impervious ice layers found at the bottom of the Stevens Pass snowpack.

Extension of these tests to the 1975/76 winter will undertake to modify all three of these factors by selecting a different test site, enlarging the exploder size, and improving the gas charging methods.

Alternate Exploder Configurations

The exploder cylinder shown in Figure 1 was adopted for the first winter's tests in order to get a working model into the field in time. Alternate configurations have also been explored, with the aim both to extend the range of usefulness of the gas exploder principle and to seek simpler and more economical mechanisms.

One variation on the exploder was constructed and tested in two versions during the 1974/75 winter. This was a design intended to provide an explosive impulse extended along a line instead of concentrated at a single point. The first version was constructed from a 10-foot (3.2 meter) length of 6-inch (15 cm) aluminum electrical conduit. A threaded cap was screwed on each end and a row of 2-inch (5 cm) diameter holes drilled in a line along the full length of this pipe. Heavy rubber belting was then bolted over the holes to form a double movable flap. The flap would close the holes and allow a gas charge to be introduced in the pipe, but would separate on detonation of the gas mixture and allow the explosion to escape outward through the row of holes. In this case the piston impact of the exploder cylinder has been eliminated except for the limited motion of the flap, with disruption of the snow mainly being achieved by the explosive discharge of gases. The original intent of this design was to provide a means of breaking off a cornice. Overall appearance of the tubular cornice-breaker and its operation during a test in snow are shown in Figures 7 and 8.

The cornice breaker was tested in Utah in December for a demonstration for the U.S. Forest Service and on several occasions in Colorado, using a portable

control unit and gas cylinders. The principle of this design appeared to be effective, but two difficulties were discovered. First, the aluminum conduit pipe was too soft to sustain in the explosive forces and rapidly became deformed during the tests. Second, introduction of the gas charge through a single, central port resulted in poor distribution of the explosive gas mixture in the cylinder. Late in the winter, a second model was constructed using steel pipe and providing a gas distribution manifold for charging. Tests in Colorado with this improved version of the cornice breaker have been very promising. Operational tests in an avalanche path near Red Mountain Pass are planned for next winter.

Another pattern of gas exploder has been constructed on the basis of the first winter's experience with these systems and was tested late in the spring of 1975. In this case the exploder chamber consists of a 9.00-22 truck tire bolted along one rim to a 22-inch (56 cm) truck wheel minus the split ring. The other rim of the tire is left free to move. The gas mixture is introduced into the tire through four equally spaced inlet connections. On detonation, the exploding gases discharge through the free rim. Tests both in the free air and buried in snow indicate that this style of exploder may be able to deliver considerably more explosive energy than the other configurations used so far. It will be tested as part of the Willow Swamp gas exploder array next winter, as well as at a possible site in the Cascades.

Interim Evaluation

(1) The gas exploder system is effective for releasing avalanches in the snow conditions found at Red Mountain Pass.

(2) The gas exploder system in its present configuration does not appear to be effective for releasing avalanches in the snow conditions found at Stevens Pass. Further tests with a modified system are required.

(3) On the whole, the control unit design has been technically successful. Some minor modifications, especially in power supply batteries, are required to increase reliability.

(4) The initial design of steel cylinder adopted for the first winter's tests appears to be functional and durable. More effective and possibly more economical designs may be developed through further tests.

(5) A 100% shielding of the system from hungry rodents is essential for any sound field installation.

TABLE I

GAS EXPLODER TESTS

Chronological list of tests at Willow Swamp avalanche path, Red Mountain Pass, Colorado.

12/16/74 -- System fired. Slab fracturing, large cracks visible, snow stabilized in place.

1/14/75 -- System fired. Avalanche release, type HS-AT-2-G.

1/21/75 -- System fired in poor weather, no visible results.

1/29/75 -- Exploder system inoperative, Willow Swamp avalanche release by artillery fire.

2/2/75 -- System fired with low gas volume as test after repair of oxygen hose.

2/10/75 -- System fired. Avalanche release, type SS-AT-3-O (see Figure 5).

2/21/75 -- System fired in poor weather, no results visible.

2/26/75 -- Demonstration firing for Colorado Highway Department in stable snow conditions, no avalanche release.

3/6/75 -- System fired, a good detonation heard, no avalanche released.

3/9/75 -- System fired during natural avalanche cycle, bad weather with poor visibility, results could not be seen.

3/11/75 -- System fired with good detonation. Snow stable, no avalanche release.

4/23/75 -- System fired in very deep snow, no results visible, no avalanche.

Summary: 11 test firings

2 confirmed avalanche releases

3 firings in poor visibility, results could not be seen

5 firings with stable snow--no avalanches

1 low-energy test firing

APPENDIX I

GAS EXPLODER SYSTEM

Refer to Figure 9, the functional block diagram.

1. Gas Supply

   Oxygen bottle is size G, 220 ft^3, weight about 150 lbs, @ $2.70 ea.

   Acetylene bottle is size 5, 250 ft^3, weight about 180 lbs, @ $3.50 ea.

   Gives 20-30 cycles of a four canister array.

   Regulators are Victor, 2 stage, VTS-200C-540 (oxygen) @ $46 ea., and VTS-210A-510 (acetylene) @ $38 ea. Equipped with Harris 88-3CV Check Valves.

   Bottles and Regulators have a weatherproof cover (truck innertubes and heavy plastic was used).

   Supply Hose to the control box is 25 ft length standard twin 1/4" welding hose, $15, with flexible metal conduit cover where exposed (about $1/ft).

2. Control Box

   Stahlin J-1614H, 16" x 14" x 6", fiberglass, with Link-Lok Latch @ $34 ea. Weatherproof, mounted above snow line in protected, accessible spot near (typically 200 ft) canister array. Houses following components 3 through 7, equipped with hose and electrical disconnects.

3. Gas Valves

   Solenoid valves are Alco 204 CD-1/4 S-1/4 P, 24 VDC, 15 watts, degreased, $21 ea., equipped with Nupro B-4C4-1/3 outlet check valves, degreased, @ $7 ea. Dual 1/4" welding hose to Mixer.

4. Mixer

A Victor 315 Welding Torch with standard inlet adjustment valves is used. Allows gas ratio adjustments, mixes gasses, stops back-travelling flame upon ignition. Torch outlet is Victor 1T4 Tip modified to fit 3/8" I.D. hose given below. Tip may be temporarily replaced with standard Victor 3T4 Tip for visual adjustment of gas mixture.

5. Igniter

AC Spark Plug C47W with mating waterproof cap @ $8 ea. mounted in brass block connected with 3/8" I.D. hose given below. Ignition coil is Delco Remy 1115485, 12V @ 1.2 amps, with self-contained points @ $38 ea.

6. Outlet Hose

Hose is Uniroyal P-290, 3/8" I.D., 2 braid, 300 psi working pressure, $.45/ft, weight 18 lbs per 100 ft. Carries gas mixture to exploders (typical distance 200 ft), cover with flexible metal conduit where exposed. Hose disconnect at Control Box is standard 3/8 NPT Pipe Union. Wedgon couplings and wire clamps installed as required in the field.

7. Control Relays

Relays are Potter and Brumfield KRP11DG, 24 VDC, 472 ohms, DPDT, $8 ea. Activates gas solenoids and ignition coil in response to signals from either local control switches (located inside the control box) or from the remote control cable.

8. Battery

Batteries are Globe Gel-Cell, GC1245-1A, 12 V, 4.5 A-HR, rechargeable lead acid with gelled electrolyte, $23 ea. Two are connected in series. Power source for gas solenoids and ignition coil. Capacity for about 40 each 5 minute fill/fire cycles.

9. Cable

Electrical cable for remote control is either 2 or 4 conductor Anixter 19 AWG, Copper Armored, PVC Jacket, Direct Burial, .27" diameter, $174/1000 ft (2 cond); .325" diameter, $245/1000 ft (4 cond). Two conductors are required for each Control Box, typical length of cable is 1000-2000 ft.

10. Remote Control Trigger Box

Stahlin J-6044H, 6" x 4" x 4", fiberglass with Link-Lok Latch @ $15 ea. Contains batteries (3 ea. Eveready No. 266, 9 V, in series, @ 2.50 ea), and GE Panel Meter 250-101-JRJR @ $22 ea to operate main control box relays and to monitor cable current. Light-weight, portable, plugs into control cable. Batteries are rated for 40-50 each 5 minute fill/fire cycles.

11. Exploder Connections

Each gas exploder is connected in parallel to the 3/8" I.D. outlet hose utilizing a 3/8 NPT Pipe Tee, Whitey 1RF4 Brass Regulating Valve @ $9 ea., and 5/16" I.D. Armored Hydraulic Hose about 10 ft long @ $20. The regulating valve adjusts all canisters for the same flow rate by temporarily connecting a Dwyer RMB-55 Flowmeter @ $20 ea. The armored hose is used above ground for protection from rodents.

The gas exploding canisters are bolted to 2 ea., 8 ft long 4 by 4's, which are buried to the desired depth.

Figure 1. Gas exploder canister fabricated of one-quarter inch steel. The lid is shown in the fully extended position with the guide rods exposed. Heavy steel springs at the bottom of each guide rod return the lid to the closed position following gas mixture detonation.

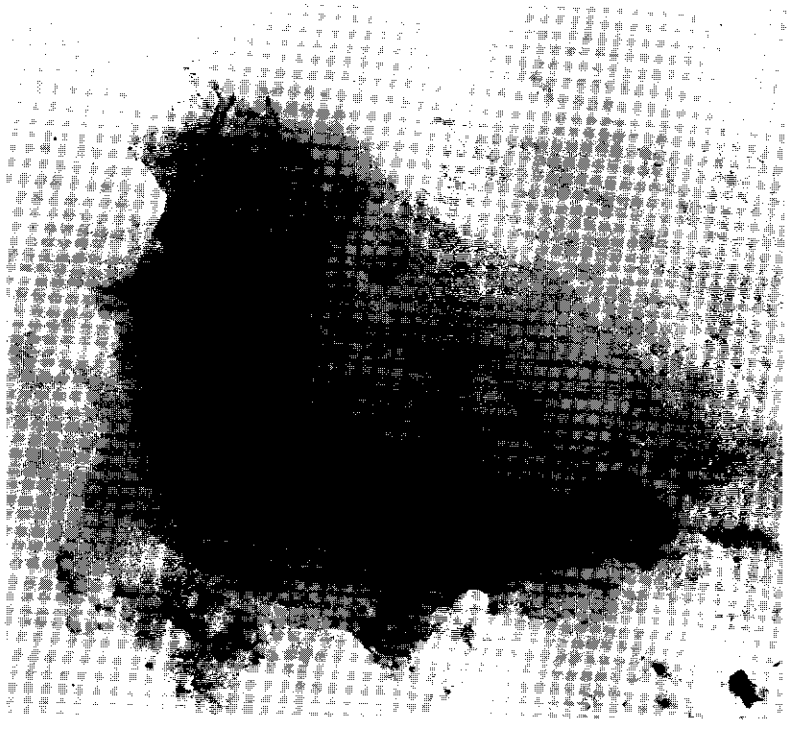

Figure 2. Gas exploder canister installed at Red Mountain Pass. It is buried in the ground with only the lid exposed. This canister was uncovered immediately following an avalanche release which slid on the surface visible immediately above the canister.

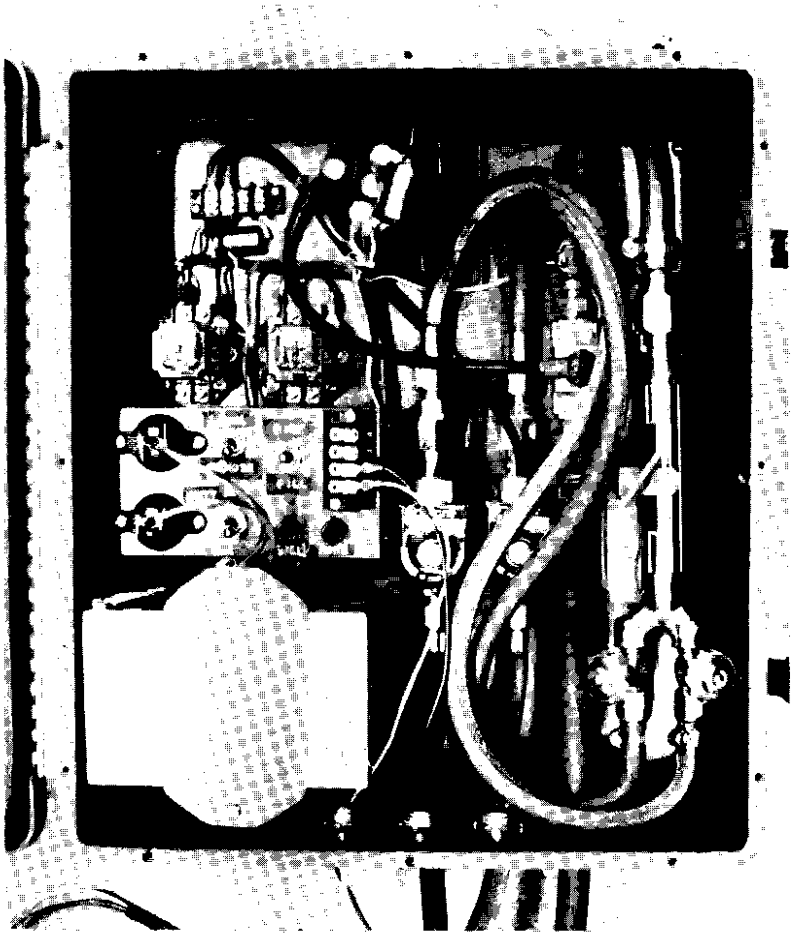

Figure 3. Gas exploder control box, showing arrangement of valves, mixing chamber, battery and electrical controls.

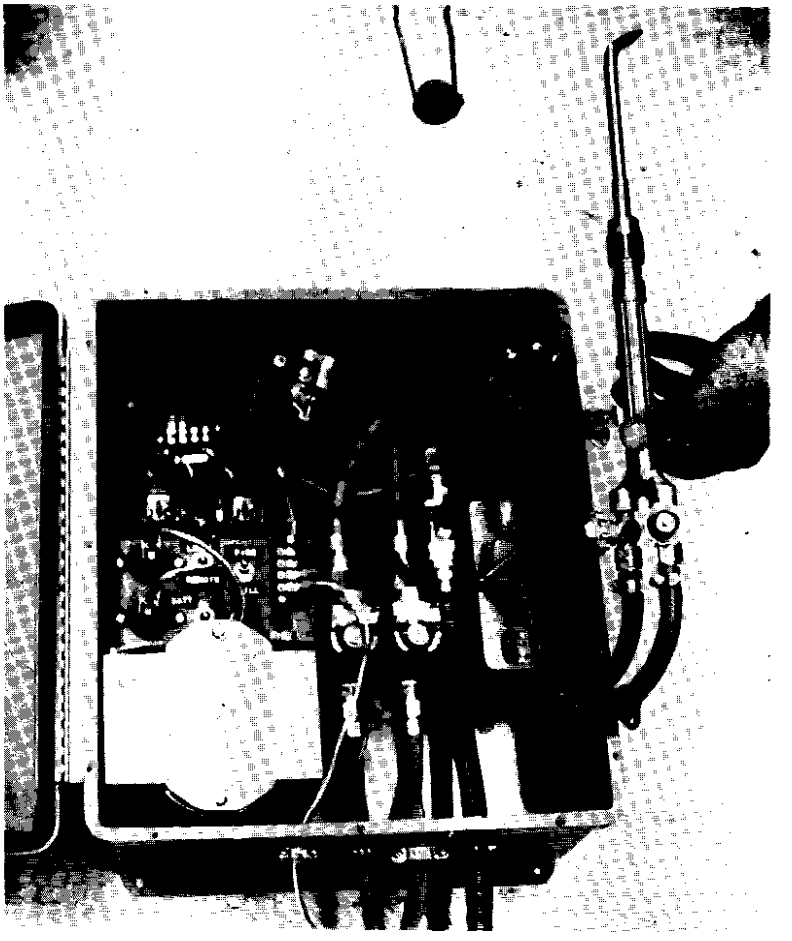

Figure 4. Gas exploder control box, illustrating method of adjusting gas mixture by attaching a torch tip to the mixing chamber (torch handle) so that a flame can be balanced for correct combustion.

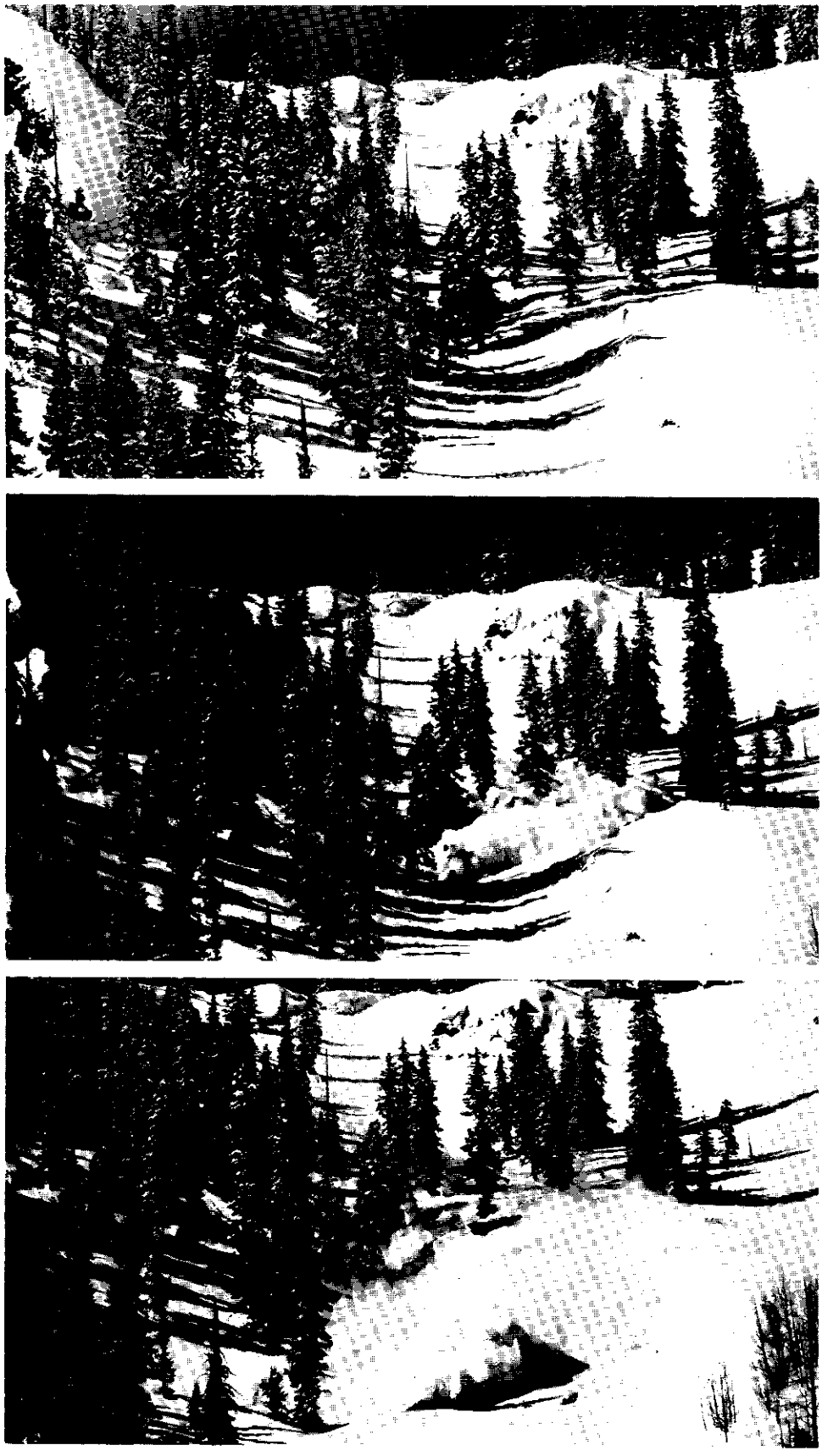

Figure 5. A telephoto sequence of a gas-exploder-triggered avalanche at the Willow Swamp test site, Red Mountain Pass, Colorado. Four gas exploder canisters are installed in the small basin above the trees in the middle distance.

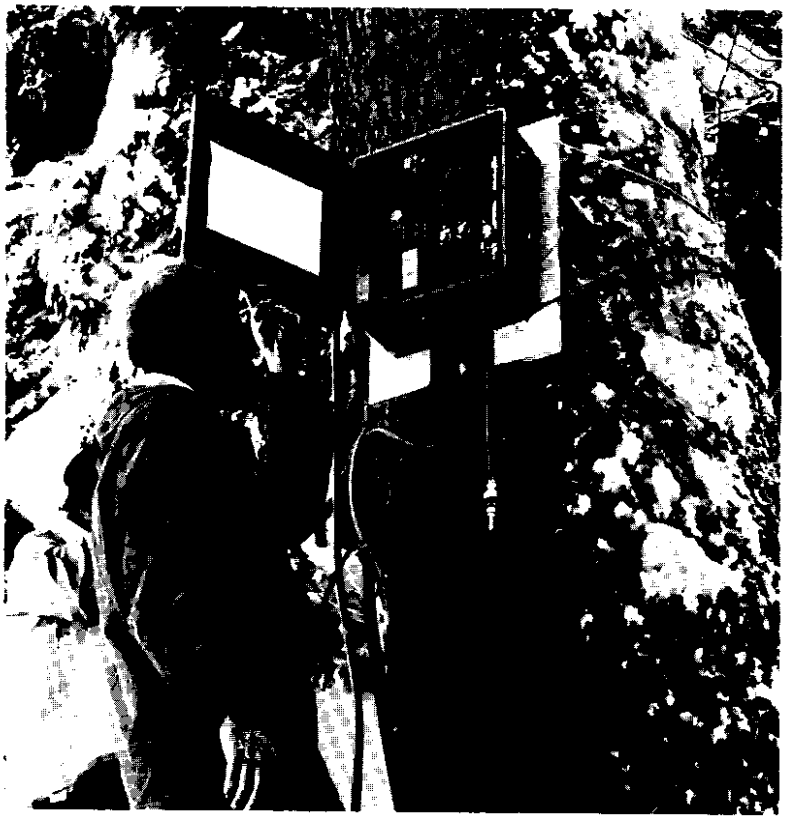

Figure 6. Gas exploder control unit installed at Old Faithful No. 7 slide path, Stevens Pass, Washington.

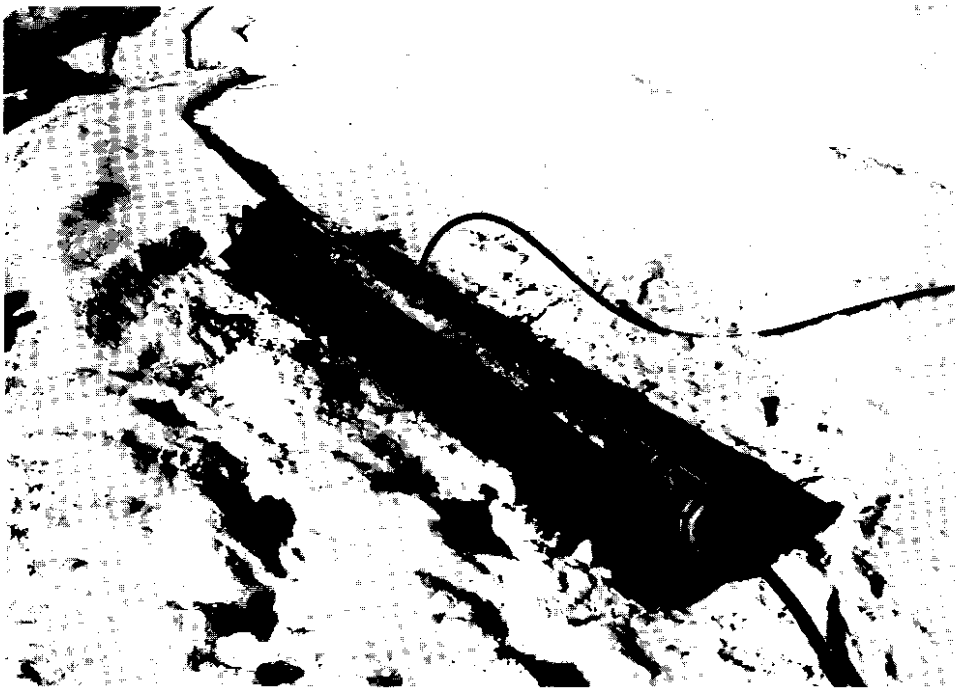

Figure 7. Experimental gas exploder device intended to break cornices. Flaps of heavy belting rubber cover a series of holes along the pipe from which the exploding gas mixture is discharged.

Figure 8. Field test of cornice-breaking exploder illustrated in Figure 7. The exploder has been fired while buried under 50 cm of packed new snow.

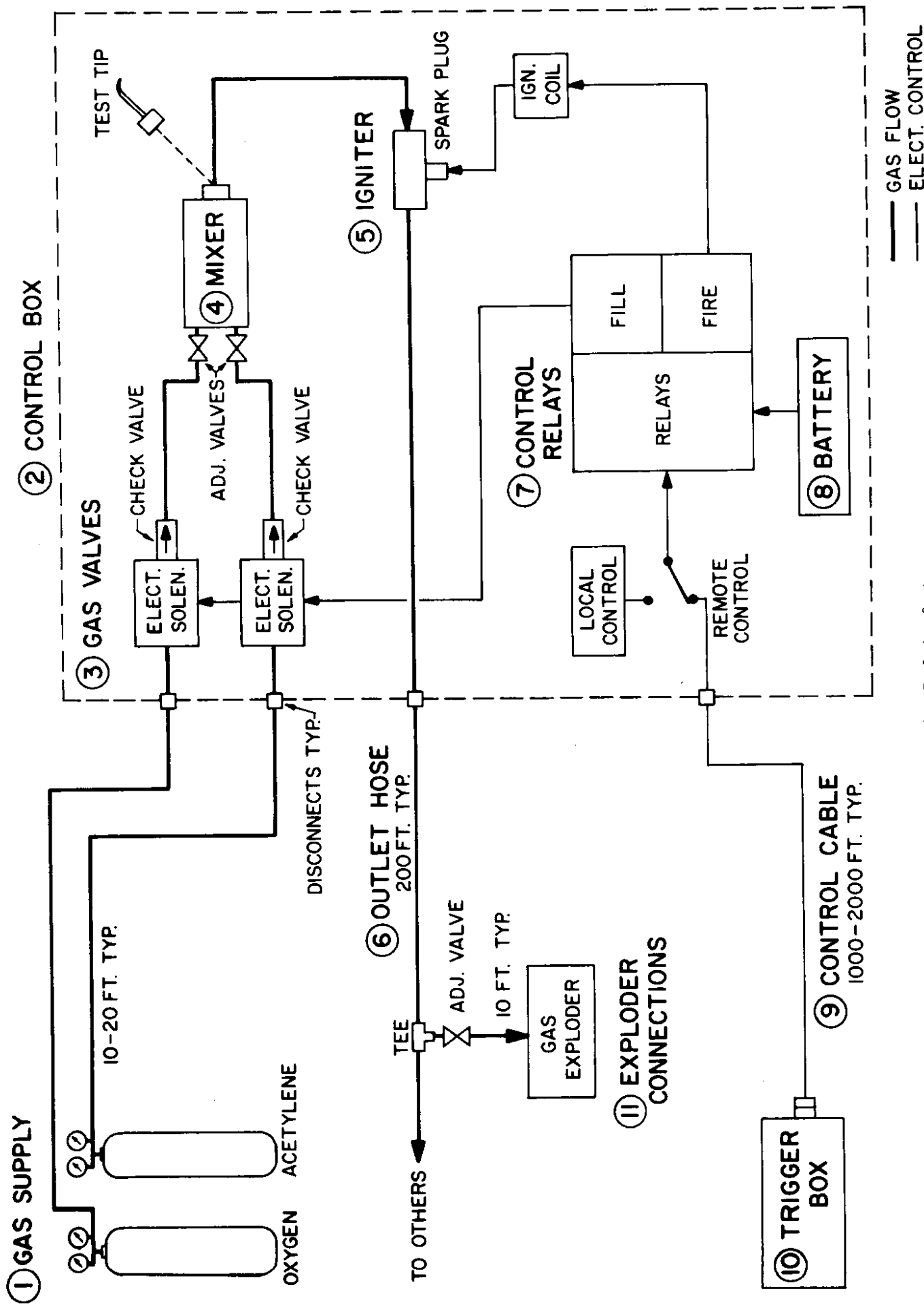

Figure 3. Gas Exploder System.

Chapter III

SNOW BEHAVIOR BEHIND A CONTINUOUS AVALANCHE DEFENSE STRUCTURE

by

James A. Langdon

ABSTRACT

A parameter study using a finite element numerical method leads to empirical expressions for forces acting on barriers, snow stresses, and glide behavior behind a continuous avalanche defense structure on a uniform slope for various snow properties and site conditions. Two constitutive laws are considered and compared using a linear glide law for basal slip. A slip boundary condition at the barrier face gives greater barrier forces than other boundary conditions and the empirical equations are developed for this case. The equations are functions of parameters which can be obtained through field measurements. An appendix contains tabulated values.

NOTATION

A	$1/G = S/h$
B	boundary condition type
C	non-dimensional empirical force coefficient
D	non-dimensional empirical stress coefficient
E	viscous modulus of snow at snow ground interface in neutral zone (effective for plane strain)
F	barrier force
G	non-dimensional number equal to $h/S = 2h\ (1+\nu)\ K/E = 1/A$
J	total glide force on the snow
K	glide stiffness
L	constitutive law type
S	stagnation depth of snow in neutral zone
T	slope angle in degrees
U	velocity in x direction
U_0	neutral zone glide velocity at snow ground interface
U_1	U at $x = h$
V_0	velocity in y direction at $x = 0$
V_1	velocity in y direction at $x = h$
b	exponential decay rate for U
g	gravitational acceleration
h	snow thickness measured in y direction
ρ	snow density
ν	Poisson effect (effective for plane strain)
ν'	Poisson effect = $\nu/(1+\nu)$
x	up slope direction

y direction normal to slope

z non-dimensional coordinate $1 - y/h$

σ_x stress in x direction

σ_y stress in y direction

σ_{xy} xy shear stress

The term force is synonymous with force per unit width.

The neutral zone is defined as the zone in which the rate of change of glide velocity is less than one tenth of one per cent of its initial value.

The feasibility of using continuous barriers as avalanche defense structures has been proven by European engineers. However, the theoretical basis for their design has not yet been perfected. In order to numerically evaluate previously developed concepts and reduce the complex concepts to a simplified yet accurate design procedure, a parameter study was pursued. Since design of an avalanche defense system depends upon the forces acting on the barriers and the influence the barriers have upslope, it is desirable to determine how snow properties and site conditions affect these factors.

McClung (1974) used a finite element procedure to calculate snow stresses, barrier forces, and basal glide. The present study extends the work of McClung to establish empirical relations between snow stresses, barrier forces, glide velocity, and snow viscosity, Poisson effects, slope angles, and glide stiffness. A linear glide law and two constitutive laws were considered. Approximate solutions were obtained from the finite element computer program, PLANE 2. Assumptions on geometry were that all barriers were continuous and facing perpendicular to the fall line, and that the slope was constant. The snow density was considered to be uniform. Possible creep constitutive laws that explain observed behavior have been suggested by Brown, Evans, and McClung (1972). The laws they considered that were used in the present study are:

(1) A viscous modulus that varies linearly with depth.

(2) A viscous modulus that is proportional to the bulk stress.

These laws were compared numerically.

Constitutive law (1) can easily be incorporated on PLANE 2. Figure 1 shows a typical element arrangement similar to that used by McClung. The viscous modulus in all elements in the bottom layer was set equal to 0.9E, that of the elements in the second layer was set equal to 0.7E, and that of the third to 0.5E, etc., and that of the top to 0.1E. A study using this law is simpler than that using law (2) where an iterative procedure is required.

When using law (2), the first run was made using the same procedure as for law (1); the viscous modulus in each succeeding iteration being calculated from the bulk stress of the previous run. The following approximate procedure was used:

(1) Selection of the viscous modulus E at the snow-ground interface in the neutral zone.

(2) Definition of an adequate number of materials having moduli in increments of E/20.

(3) Data recording of the bulk stresses for the center of each element from the previous iteration.

(4) Selection of the material with its modulus closest to being proportional to the bulk stress for each element for the successive iteration.

(5) Stress evaluation by the finite element program.

When using the above procedure, the average deviation of the viscous modulus in an element from the correct value is less than two per cent. A converged system was defined when the total barrier force changed less than one-half of one per cent in an iteration. Three to five iterations are required for convergence.

PLANE 2 provides the total glide force from all nodes as output. The barrier force was computed as the total body force less the glide force. The barrier force obtained in this way was in accord with that calculated by integrating σ_x through the elements adjacent to the barrier face and adding one-half the body force of these elements.

Barrier Force Equations

Consider the barrier force normal to the barrier as a function of 9 parameters:

$$F = f(T,\rho,g,K,E,\nu,h,L,B)$$

The boundary condition, B, at the barrier face has two extremes, slip or fixed. A few cases were studied treating B as a variable. Forces for the slip condition were found to be 10 to 13 per cent higher than the fixed condition.

We can consider ρg as one parameter. Known neutral zone behavior leads to the relation:

$$S = E/[2K(1+\nu)]$$

By defining a non-dimensional number:

$$G = 2h(1+\nu)K/E$$

Then:

$$F = f(T,\rho g,G,\nu,h,L)$$

And F varies as h^2 and as ρg, by similitude considerations.

This now reduces the study to four parameters. Defining the non-dimensional force coefficient C, then

$$F = h^2 \rho g \, C(T,G,\nu,L) \qquad (1)$$

Use of PLANE 2 has demonstrated the validity of this relation.

Now consider C as having two components.

(1) A static pressure due to Poisson effects exists in the intermediate zone as well as the neutral zone. For the elastic case, this force was deduced by Brown, Evans, and LaChapelle (1972) as

$$\tfrac{1}{2} h^2 \rho g \nu' \cos T/(1+\nu') \qquad (2)$$

In the present case it becomes $C_1 = \tfrac{1}{2}\nu \cos T$

(2) The remaining component is proportional to sin T. Hence

$$C = C_1 + \sin T \, C_2(G,\nu,L) \qquad (3)$$

Use of PLANE 2 has demonstrated the accuracy of the above considerations.

Consider law (1) and the effect of varying G. This relation is shown in Figure 2, with $\nu = 0$ and $T = 45$. Similar relations are found for other ν and T. Values of T studied were 0, 30, 45, and 90.

C_2 asymptotically approaches the value 0.592. In Figure 3 $\log (C_2 - .592)$ is plotted against log G. The relation approaches a straight line with a slope of -1. For G greater than one, the following relation approximates the curve.

$$C_2 = .592 + A - 0.4A^2 = .592 + 1/G - 0.4/G^2$$

Figure 4 shows how C_2 changes as ν increases for both constitutive laws. G equals 16.7 in this case. Similar relations for other values of G and T were studied. The slope of the lines are nearly constant and equal and only slightly depend upon G. The slope of the lines are approximately expressed as:

$$0.07\nu A + 0.4\nu$$

The change in C_2 from law (1) to law (2) is quite dependent upon G and T and has negligible dependence upon ν. It is approximately expressed as:

$$C_3 = (0.144 + 0.684A) \tan T \qquad (4)$$

The preceding considerations lead to the empirical expression for C:

$$C = 0.5\nu \cos T + \sin T(0.592 + A - 0.4A^2 + 0.4\nu + 0.07\nu A + C_3)$$

where C_3 is given by equation (4) for law (2) and is zero for law (1).

The barrier force is now given as:

$$F = h^2 \rho g C \qquad (5)$$

Values for C are tabulated in the Appendix for various conditions. Table 1 compares some results of C with the finite element results.

Glide Velocity Equations

The glide velocity, U, at the snow-ground interface is found to asymptotically approach that in the neutral zone. U is zero at the barrier and increases throughout the intermediate zone and exponentially

approaches U_0 in the neutral zone. Figure 5 shows this relationship for typical data.

Equilibrium considerations lead to the relation:

$$C_2 \sin T + J = \ell \sin T$$

If U changes exponentially,

$$J = \int_0^{\ell} KU_0(1 - e^{-\frac{x}{b}})dx \qquad (6)$$

where b is a constant to be determined. If $e^{-\frac{\ell}{b}}$ is taken as zero, then

$$J = KU_0(1 - b) \qquad (7)$$

Neutral zone equilibrium yields

$$\sin T = KU_0 \qquad (8)$$

Manipulation of (6), (7), and (8) yields $b = C_2$ and

$$U = U_0(1 - e^{-\frac{x}{C_2}})$$

Distribution of Stresses on Barrier

Using considerations similar to those for equation (1) an expression for σ_x can be obtained as:

$$\sigma_x = \rho g \, h \, D \, (T,G,\nu,L,z)$$

where $z = 1 - y/h$.

Since the force given by equation (2) is distributed linearly with depth, then

$$D = D_1 + \sin T \, D_2(G,\nu,L,z)$$

and

$$D_1 = \nu z \cos T$$

The remaining considerations for D are restricted to G greater than one. Also some accuracy is lost in order to simplify the expressions. However, the expressions give values of σ_x within ten per cent of the maximum value of σ_x.

For the case of $\nu = 0$ and $G = \infty$ and law (1), the stress distribution is approximated by the parabola:

$$D_3 = 0.175 + 2.5z - 2.5z^2$$

In a manner similar to that used for C:

$$D_4 = 2z(0.333 + z)\,(A - 0.4A^2)$$

The Poisson contribution is given by:

$$D_5 = 0.6z\nu(2-z) + 0.15z\nu A$$

And changing to constitutive law (2) contributes:

$$D_6 = z \tan T\,(1.37A + 1.52z^2 - 3.15z + 1.64)$$

Now

$$D = D_1 + \sin T\,(D_3 + D_4 + D_5 + D_6)$$

Figures 6 and 7 compare the empirical expression for σ_x from this study to the two cases which McClung (1974) studied.

Intermediate Zone Stresses

Neutral zone stresses are given by:

$$\sigma_x = \rho g h D_1 \qquad \sigma_y = \rho g h z \cos T$$

$$\sigma_{xy} = \rho g h z \sin T$$

An empirical approximation of stresses throughout the intermediate zone is to assume that they decay exponentially from values at the barrier to neutral zone values, the exponent being the same as for glide velocity. This gives:

$$\sigma_x (x,y) = \rho g h \left[D_1 + (D-D_1)\, e^{-\frac{x}{C_2}} \right] \pm 4\%$$

At the barrier $\sigma_y = 1.6\, \rho g h z \cos T \pm 10\%$. Assuming exponential decay,

$$\sigma_y (x,y) = \rho g h z \cos T \,(1 + 0.6 e^{-\frac{x}{C_2}})$$

σ_{xy} is zero at the barrier and:

$$\sigma_{xy} (x,y) = \rho g h z \sin T \,(1 - e^{-\frac{x}{C_2}}) \pm (15/z)\%$$

Discussion

The empirical equations are functions of parameters which can be obtained through field measurements. T, ρ, and h are easily measured. A relation for ν' found from neutral zone behavior is:

$$\nu' = (\tfrac{1}{2} - Q \tan T)/(1 - Q \tan T)$$

where

$$Q = (V_1 - V_0)/(U_1 - U_0)$$

A value for A is given by:

$$A = 1/G = S/h = U_0/(U_1 - U_0)$$

At present there is little experimental evidence that either of the constitutive laws will give accurate results. Nor has the linear glide law been satisfactorily justified. A case was studied where glide stiffness was a linear function of the bulk stress in the lower elements. This glide law gave about ten per cent less barrier force.

REFERENCES

Brown, C. B., Evans, R. J., LaChapelle, E. R., "Slab Avalanching and the State of Stress in Fallen Snow," Journal of Geophysical Research 77(24); 4570-4580, 1972.

Brown, C. B., Evans, R. J., McClung, D., "Incorporation of Glide and Creep Measurements in Snow Slab Mechanics," Advances in North American Avalanche Technology; 1972 Symposium, 7-13.

McClung, D., "Avalanche Defense Mechanics," Ph.D. Dissertation, University of Washington, 1974.

TABLE 1

Comparison of C with Finite Element Values

v	G	L	C	finite element
0	2.43	1	.6617	.6283
0	3.18	1	.6127	.5879
0	3.18	2	.8666	.8594
0	12.8	1	.4721	.4681
0	16.8	1	.4597	.4571
0	16.8	2	.5906	.5966
0	874	1	.4194	.4192
0	874	2	.5221	.5238
.3	1.14	1	1.026	1.027
.3	3.18	1	.8083	.7918
.3	3.18	2	1.062	1.065
.3	11.4	1	.6709	.6664
.3	16.8	1	.6515	.6479
.3	114	1	.6159	.6121
.3	1140	1	.6102	.6061

T=45 for above cases.

APPENDIX

Use of Appendix

To find the force, F, per unit width and its point of action on a continuous barrier:

(1) Obtain the following (see Figure 8):

- h snow thickness measured perpendicular to the slope
- ρ snow density
- g gravitational acceleration
- T slope angle in degrees
- U_0 glide velocity or snow velocity parallel to the slope at the snow-ground interface
- U_1 snow velocity component parallel to the slope at the surface
- V_0 snow velocity component perpendicular to the slope at the snow-ground interface
- V_1 snow velocity component perpendicular to the slope at the surface

(2) Calculate the following:

$$A = U_0/(U_1 - U_0)$$

$$Q = (V_1 - V_0)/(U_1 - U_0)$$

$$\nu' = (\tfrac{1}{2} - Q \tan T)/(1 - Q \tan T)$$

$$\nu = \nu'/(1-\nu')$$

(3) Find a value for C for known T, A, and ν from the tabulated values. Two values of C are given for the two constitutive laws suggested.

(4) Calculate F as:

$$F = h^2 \rho g C$$

As a hypothetical example typical of measurements made by McClung (1974) on Mt. Baker, use:

$T = 25$

$h = 400$ cm (157.5 in.)

$U_0 = 0.020$ cm per day (.00787 in. per day)

$U_1 = 0.220$ cm per day (.08661 in. per day)

$V_0 = 0.005$ cm per day (.00197 in. per day)

$V_1 = 0.134$ cm per day (.05275 in. per day)

$\rho g = 0.005$ Nt per cm^3 (.0184 lbs per $in.^3$)

Thus $A = 0.10$

$Q = 0.645$

$\nu' = 0.285$

$\nu = 0.40$

and from the tables for law (1)

$C(1) = 0.541$ $R(1) = 0.412$

and for law (2)

$C(2) = 0.583$ $R(2) = 0.417$

giving $F_1 = 433$ Nt per cm (247 lbs per in.)

acting 165 cm (64.9 in.) above the ground

$F_2 = 466$ Nt per cm (266 lbs per in.)

acting 167 cm (65.7 in.) above the ground

Note that the greatest value of ν' measured by McClung (1974) was 0.32.

T	A	V	C(1)	C(2)	R(1)	R(2)
15.0	.000	.200	.271	.281	.431	.436
15.0	.000	.300	.329	.339	.415	.419
15.0	.000	.400	.388	.398	.404	.408
15.0	.000	.500	.446	.456	.395	.399
15.0	.100	.200	.296	.310	.418	.421
15.0	.100	.300	.355	.369	.405	.409
15.0	.100	.400	.413	.428	.396	.399
15.0	.100	.500	.472	.487	.389	.392
15.0	.200	.200	.319	.338	.408	.410
15.0	.200	.300	.378	.397	.397	.400
15.0	.200	.400	.437	.456	.390	.392
15.0	.200	.500	.496	.515	.384	.386
15.0	.300	.200	.340	.364	.400	.402
15.0	.300	.300	.399	.423	.391	.393
15.0	.300	.400	.458	.483	.384	.387
15.0	.300	.500	.518	.542	.379	.382
15.0	.400	.200	.359	.388	.393	.395
15.0	.400	.300	.418	.447	.386	.387
15.0	.400	.400	.478	.507	.380	.382
15.0	.400	.500	.537	.566	.376	.378
15.0	.500	.200	.376	.410	.388	.389
15.0	.500	.300	.435	.469	.382	.383
15.0	.500	.400	.495	.529	.377	.378
15.0	.500	.500	.555	.588	.373	.374
15.0	.600	.200	.391	.429	.384	.385
15.0	.600	.300	.450	.489	.378	.379
15.0	.600	.400	.510	.549	.374	.375
15.0	.600	.500	.570	.608	.370	.371
15.0	.700	.200	.404	.447	.381	.381
15.0	.700	.300	.463	.507	.375	.376
15.0	.700	.400	.523	.567	.371	.372
15.0	.700	.500	.583	.626	.368	.369
15.0	.800	.200	.414	.462	.378	.378
15.0	.800	.300	.474	.522	.373	.374
15.0	.800	.400	.534	.582	.369	.370
15.0	.800	.500	.595	.642	.366	.367
15.0	.900	.200	.423	.476	.376	.376
15.0	.900	.300	.483	.536	.371	.372
15.0	.900	.400	.543	.596	.368	.369
15.0	.900	.500	.604	.656	.365	.366
15.0	1.000	.200	.429	.487	.374	.374
15.0	1.000	.300	.490	.547	.370	.370
15.0	1.000	.400	.550	.608	.367	.367
15.0	1.000	.500	.611	.668	.364	.365

T	A	V	C(1)	C(2)	R(1)	R(2)
20.0	.000	.200	.324	.342	.441	.448
20.0	.000	.300	.384	.402	.426	.432
20.0	.000	.400	.445	.463	.414	.420
20.0	.000	.500	.506	.524	.406	.411
20.0	.100	.200	.357	.384	.426	.430
20.0	.100	.300	.418	.445	.414	.418
20.0	.100	.400	.479	.505	.405	.409
20.0	.100	.500	.540	.566	.398	.402
20.0	.200	.200	.388	.423	.414	.417
20.0	.200	.300	.449	.484	.405	.408
20.0	.200	.400	.510	.545	.397	.400
20.0	.200	.500	.571	.606	.391	.395
20.0	.300	.200	.416	.459	.405	.407
20.0	.300	.300	.477	.520	.397	.400
20.0	.300	.400	.538	.582	.391	.394
20.0	.300	.500	.600	.643	.386	.389
20.0	.400	.200	.441	.493	.398	.399
20.0	.400	.300	.502	.554	.391	.393
20.0	.400	.400	.564	.616	.386	.388
20.0	.400	.500	.626	.678	.381	.384
20.0	.500	.200	.463	.524	.392	.393
20.0	.500	.300	.525	.585	.386	.388
20.0	.500	.400	.587	.647	.381	.383
20.0	.500	.500	.649	.709	.378	.380
20.0	.600	.200	.483	.552	.388	.388
20.0	.600	.300	.545	.614	.382	.383
20.0	.600	.400	.607	.676	.378	.380
20.0	.600	.500	.669	.738	.375	.376
20.0	.700	.200	.500	.577	.384	.384
20.0	.700	.300	.562	.639	.379	.380
20.0	.700	.400	.624	.702	.375	.376
20.0	.700	.500	.687	.764	.372	.374
20.0	.800	.200	.514	.600	.381	.381
20.0	.800	.300	.576	.662	.377	.377
20.0	.800	.400	.639	.725	.373	.374
20.0	.800	.500	.701	.788	.370	.371
20.0	.900	.200	.525	.620	.379	.378
20.0	.900	.300	.588	.683	.375	.375
20.0	.900	.400	.651	.745	.371	.372
20.0	.900	.500	.714	.808	.369	.370
20.0	1.000	.200	.534	.637	.377	.376
20.0	1.000	.300	.597	.700	.373	.373
20.0	1.000	.400	.660	.763	.370	.370
20.0	1.000	.500	.723	.826	.367	.368

T	A	V	C(1)	C(2)	R(1)	R(2)
25.0	.000	.200	.375	.403	.449	.457
25.0	.000	.300	.437	.465	.434	.442
25.0	.000	.400	.499	.528	.423	.430
25.0	.000	.500	.561	.590	.414	.421
25.0	.100	.200	.416	.458	.432	.437
25.0	.100	.300	.478	.520	.420	.426
25.0	.100	.400	.541	.583	.412	.417
25.0	.100	.500	.603	.645	.405	.410
25.0	.200	.200	.454	.509	.419	.422
25.0	.200	.300	.516	.572	.410	.414
25.0	.200	.400	.579	.635	.403	.407
25.0	.200	.500	.642	.697	.397	.401
25.0	.300	.200	.488	.557	.409	.411
25.0	.300	.300	.551	.620	.401	.404
25.0	.300	.400	.614	.683	.396	.399
25.0	.300	.500	.677	.746	.391	.394
25.0	.400	.200	.519	.601	.401	.403
25.0	.400	.300	.582	.665	.395	.397
25.0	.400	.400	.646	.728	.390	.392
25.0	.400	.500	.709	.792	.386	.388
25.0	.500	.200	.547	.642	.395	.396
25.0	.500	.300	.610	.706	.390	.391
25.0	.500	.400	.674	.770	.385	.387
25.0	.500	.500	.738	.834	.382	.384
25.0	.600	.200	.571	.680	.390	.390
25.0	.600	.300	.635	.744	.385	.386
25.0	.600	.400	.699	.808	.381	.383
25.0	.600	.500	.763	.872	.378	.380
25.0	.700	.200	.592	.715	.386	.386
25.0	.700	.300	.656	.779	.382	.382
25.0	.700	.400	.720	.843	.378	.379
25.0	.700	.500	.785	.907	.375	.377
25.0	.800	.200	.609	.746	.383	.382
25.0	.800	.300	.674	.810	.379	.379
25.0	.800	.400	.738	.875	.376	.377
25.0	.800	.500	.803	.939	.373	.374
25.0	.900	.200	.623	.773	.381	.380
25.0	.900	.300	.688	.838	.377	.377
25.0	.900	.400	.753	.903	.374	.374
25.0	.900	.500	.818	.968	.371	.372
25.0	1.000	.200	.634	.797	.379	.377
25.0	1.000	.300	.699	.863	.375	.375
25.0	1.000	.400	.764	.928	.373	.372
25.0	1.000	.500	.830	.993	.370	.370

T	A	V	C(1)	C(2)	R(1)	R(2)
30.0	.000	.200	.423	.464	.454	.464
30.0	.000	.300	.486	.528	.440	.450
30.0	.000	.400	.549	.591	.429	.439
30.0	.000	.500	.613	.654	.421	.430
30.0	.100	.200	.471	.533	.436	.442
30.0	.100	.300	.535	.596	.425	.432
30.0	.100	.400	.599	.660	.417	.424
30.0	.100	.500	.662	.724	.410	.417
30.0	.200	.200	.516	.597	.422	.426
30.0	.200	.300	.580	.661	.414	.418
30.0	.200	.400	.644	.725	.407	.412
30.0	.200	.500	.708	.789	.402	.407
30.0	.300	.200	.557	.658	.412	.414
30.0	.300	.300	.621	.722	.405	.408
30.0	.300	.400	.685	.786	.399	.403
30.0	.300	.500	.750	.851	.395	.399
30.0	.400	.200	.593	.714	.403	.405
30.0	.400	.300	.658	.779	.398	.400
30.0	.400	.400	.723	.843	.393	.396
30.0	.400	.500	.788	.908	.389	.392
30.0	.500	.200	.626	.767	.397	.398
30.0	.500	.300	.691	.832	.392	.393
30.0	.500	.400	.756	.897	.388	.390
30.0	.500	.500	.821	.962	.385	.387
30.0	.600	.200	.655	.815	.392	.392
30.0	.600	.300	.720	.880	.387	.388
30.0	.600	.400	.786	.946	.384	.385
30.0	.600	.500	.851	1.011	.381	.383
30.0	.700	.200	.680	.859	.388	.387
30.0	.700	.300	.745	.925	.384	.384
30.0	.700	.400	.811	.991	.381	.381
30.0	.700	.500	.877	1.057	.378	.379
30.0	.800	.200	.700	.900	.384	.383
30.0	.800	.300	.766	.966	.381	.381
30.0	.800	.400	.832	1.032	.378	.378
30.0	.800	.500	.899	1.098	.375	.376
30.0	.900	.200	.717	.936	.382	.381
30.0	.900	.300	.783	1.003	.379	.378
30.0	.900	.400	.850	1.069	.376	.376
30.0	.900	.500	.916	1.136	.374	.374
30.0	1.000	.200	.730	.969	.380	.378
30.0	1.000	.300	.796	1.036	.377	.376
30.0	1.000	.400	.863	1.102	.374	.374
30.0	1.000	.500	.930	1.169	.372	.372

T	A	V	C(1)	C(2)	R(1)	R(2)
35.0	.000	.200	.467	.525	.459	.470
35.0	.000	.300	.531	.589	.445	.457
35.0	.000	.400	.595	.653	.435	.446
35.0	.000	.500	.659	.717	.427	.438
35.0	.100	.200	.523	.609	.439	.446
35.0	.100	.300	.588	.673	.429	.437
35.0	.100	.400	.652	.737	.421	.429
35.0	.100	.500	.716	.802	.415	.423
35.0	.200	.200	.575	.687	.425	.429
35.0	.200	.300	.639	.752	.417	.422
35.0	.200	.400	.704	.817	.411	.416
35.0	.200	.500	.769	.882	.405	.411
35.0	.300	.200	.621	.762	.414	.416
35.0	.300	.300	.686	.827	.408	.411
35.0	.300	.400	.751	.892	.402	.406
35.0	.300	.500	.817	.957	.398	.402
35.0	.400	.200	.663	.831	.405	.407
35.0	.400	.300	.729	.897	.400	.402
35.0	.400	.400	.794	.962	.396	.398
35.0	.400	.500	.860	1.028	.392	.395
35.0	.500	.200	.701	.896	.398	.399
35.0	.500	.300	.767	.962	.394	.395
35.0	.500	.400	.833	1.028	.390	.392
35.0	.500	.500	.899	1.094	.387	.389
35.0	.600	.200	.734	.957	.393	.393
35.0	.600	.300	.800	1.023	.389	.390
35.0	.600	.400	.866	1.089	.386	.387
35.0	.600	.500	.933	1.155	.383	.385
35.0	.700	.200	.762	1.012	.389	.388
35.0	.700	.300	.829	1.079	.385	.385
35.0	.700	.400	.895	1.146	.382	.383
35.0	.700	.500	.962	1.212	.380	.381
35.0	.800	.200	.786	1.064	.385	.384
35.0	.800	.300	.853	1.131	.382	.382
35.0	.800	.400	.920	1.198	.380	.380
35.0	.800	.500	.987	1.265	.377	.378
35.0	.900	.200	.805	1.110	.383	.381
35.0	.900	.300	.872	1.178	.380	.379
35.0	.900	.400	.940	1.245	.377	.377
35.0	.900	.500	1.008	1.313	.375	.375
35.0	1.000	.200	.820	1.152	.381	.379
35.0	1.000	.300	.887	1.220	.378	.377
35.0	1.000	.400	.955	1.288	.376	.375
35.0	1.000	.500	1.023	1.356	.374	.373

T	A	V	C(1)	C(2)	R(1)	R(2)
40.0	.000	.200	.509	.586	.462	.476
40.0	.000	.300	.573	.650	.450	.463
40.0	.000	.400	.637	.714	.440	.453
40.0	.000	.500	.701	.778	.432	.445
40.0	.100	.200	.571	.686	.442	.450
40.0	.100	.300	.636	.750	.433	.441
40.0	.100	.400	.700	.815	.425	.434
40.0	.100	.500	.765	.879	.419	.428
40.0	.200	.200	.629	.780	.427	.432
40.0	.200	.300	.694	.845	.420	.425
40.0	.200	.400	.758	.910	.414	.420
40.0	.200	.500	.823	.975	.409	.415
40.0	.300	.200	.681	.870	.416	.418
40.0	.300	.300	.746	.935	.410	.413
40.0	.300	.400	.812	1.000	.405	.409
40.0	.300	.500	.877	1.066	.401	.405
40.0	.400	.200	.728	.954	.407	.408
40.0	.400	.300	.794	1.019	.402	.404
40.0	.400	.400	.860	1.085	.398	.401
40.0	.400	.500	.926	1.151	.394	.398
40.0	.500	.200	.770	1.033	.400	.400
40.0	.500	.300	.836	1.099	.396	.397
40.0	.500	.400	.903	1.165	.392	.394
40.0	.500	.500	.969	1.231	.389	.392
40.0	.600	.200	.807	1.106	.394	.394
40.0	.600	.300	.874	1.173	.391	.391
40.0	.600	.400	.940	1.240	.388	.389
40.0	.600	.500	1.007	1.306	.385	.387
40.0	.700	.200	.839	1.175	.390	.389
40.0	.700	.300	.906	1.242	.387	.386
40.0	.700	.400	.973	1.309	.384	.384
40.0	.700	.500	1.040	1.376	.382	.383
40.0	.800	.200	.865	1.238	.386	.385
40.0	.800	.300	.933	1.306	.384	.383
40.0	.800	.400	1.001	1.374	.381	.381
40.0	.800	.500	1.068	1.441	.379	.379
40.0	.900	.200	.887	1.297	.384	.381
40.0	.900	.300	.955	1.365	.381	.380
40.0	.900	.400	1.023	1.433	.379	.378
40.0	.900	.500	1.091	1.501	.377	.377
40.0	1.000	.200	.903	1.350	.382	.379
40.0	1.000	.300	.972	1.419	.379	.377
40.0	1.000	.400	1.040	1.487	.377	.376
40.0	1.000	.500	1.109	1.556	.375	.374

T	A	V	C(1)	C(2)	R(1)	R(2)
45.0	.000	.200	.546	.648	.466	.481
45.0	.000	.300	.610	.712	.454	.469
45.0	.000	.400	.673	.775	.444	.460
45.0	.000	.500	.737	.839	.436	.452
45.0	.100	.200	.615	.765	.445	.453
45.0	.100	.300	.679	.829	.436	.445
45.0	.100	.400	.743	.893	.429	.439
45.0	.100	.500	.807	.958	.422	.433
45.0	.200	.200	.678	.877	.429	.434
45.0	.200	.300	.743	.941	.422	.428
45.0	.200	.400	.807	1.006	.417	.423
45.0	.200	.500	.872	1.071	.412	.419
45.0	.300	.200	.736	.983	.417	.420
45.0	.300	.300	.801	1.048	.412	.416
45.0	.300	.400	.866	1.113	.407	.412
45.0	.300	.500	.931	1.178	.403	.408
45.0	.400	.200	.787	1.083	.408	.409
45.0	.400	.300	.853	1.149	.404	.406
45.0	.400	.400	.919	1.214	.400	.403
45.0	.400	.500	.984	1.280	.396	.400
45.0	.500	.200	.834	1.178	.401	.401
45.0	.500	.300	.900	1.244	.397	.398
45.0	.500	.400	.966	1.310	.394	.396
45.0	.500	.500	1.032	1.376	.391	.393
45.0	.600	.200	.874	1.267	.395	.394
45.0	.600	.300	.941	1.333	.392	.392
45.0	.600	.400	1.007	1.400	.389	.390
45.0	.600	.500	1.074	1.466	.387	.388
45.0	.700	.200	.909	1.350	.391	.389
45.0	.700	.300	.976	1.417	.388	.387
45.0	.700	.400	1.043	1.484	.385	.385
45.0	.700	.500	1.111	1.551	.383	.384
45.0	.800	.200	.938	1.428	.387	.385
45.0	.800	.300	1.006	1.495	.385	.383
45.0	.800	.400	1.074	1.563	.382	.382
45.0	.800	.500	1.141	1.630	.380	.380
45.0	.900	.200	.962	1.499	.384	.381
45.0	.900	.300	1.030	1.568	.382	.380
45.0	.900	.400	1.098	1.636	.380	.379
45.0	.900	.500	1.166	1.704	.378	.377
45.0	1.000	.200	.980	1.566	.383	.379
45.0	1.000	.300	1.049	1.634	.380	.377
45.0	1.000	.400	1.117	1.703	.378	.376
45.0	1.000	.500	1.186	1.772	.376	.375

T	A	V	C(1)	C(2)	R(1)	R(2)
50.0	.000	.200	.579	.711	.468	.486
50.0	.000	.300	.642	.774	.457	.475
50.0	.000	.400	.705	.836	.448	.466
50.0	.000	.500	.767	.899	.440	.458
50.0	.100	.200	.654	.848	.447	.456
50.0	.100	.300	.717	.911	.438	.449
50.0	.100	.400	.780	.975	.432	.443
50.0	.100	.500	.844	1.038	.426	.437
50.0	.200	.200	.722	.979	.431	.436
50.0	.200	.300	.786	1.043	.424	.431
50.0	.200	.400	.850	1.107	.419	.426
50.0	.200	.500	.914	1.170	.414	.422
50.0	.300	.200	.785	1.104	.419	.421
50.0	.300	.300	.849	1.168	.414	.417
50.0	.300	.400	.913	1.232	.409	.414
50.0	.300	.500	.978	1.297	.405	.411
50.0	.400	.200	.841	1.222	.409	.410
50.0	.400	.300	.906	1.287	.405	.407
50.0	.400	.400	.971	1.352	.401	.404
50.0	.400	.500	1.036	1.417	.398	.402
50.0	.500	.200	.891	1.335	.402	.401
50.0	.500	.300	.956	1.400	.398	.399
50.0	.500	.400	1.022	1.466	.395	.397
50.0	.500	.500	1.087	1.531	.393	.395
50.0	.600	.200	.935	1.441	.396	.395
50.0	.600	.300	1.001	1.507	.393	.393
50.0	.600	.400	1.067	1.573	.390	.391
50.0	.600	.500	1.133	1.639	.388	.389
50.0	.700	.200	.973	1.542	.391	.389
50.0	.700	.300	1.039	1.608	.389	.388
50.0	.700	.400	1.106	1.675	.386	.386
50.0	.700	.500	1.172	1.741	.384	.385
50.0	.800	.200	1.004	1.636	.388	.385
50.0	.800	.300	1.071	1.703	.385	.384
50.0	.800	.400	1.139	1.770	.383	.382
50.0	.800	.500	1.206	1.837	.381	.381
50.0	.900	.200	1.030	1.724	.385	.381
50.0	.900	.300	1.098	1.791	.383	.380
50.0	.900	.400	1.165	1.859	.381	.379
50.0	.900	.500	1.233	1.927	.379	.378
50.0	1.000	.200	1.049	1.806	.383	.379
50.0	1.000	.300	1.118	1.874	.381	.378
50.0	1.000	.400	1.186	1.942	.379	.377
50.0	1.000	.500	1.254	2.010	.377	.376

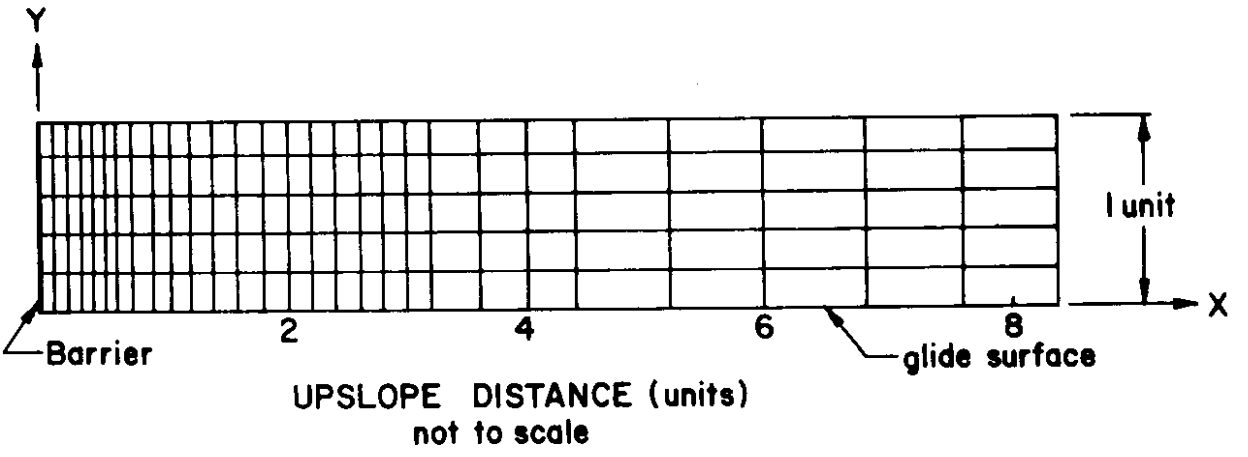

Figure 1. Finite element grid

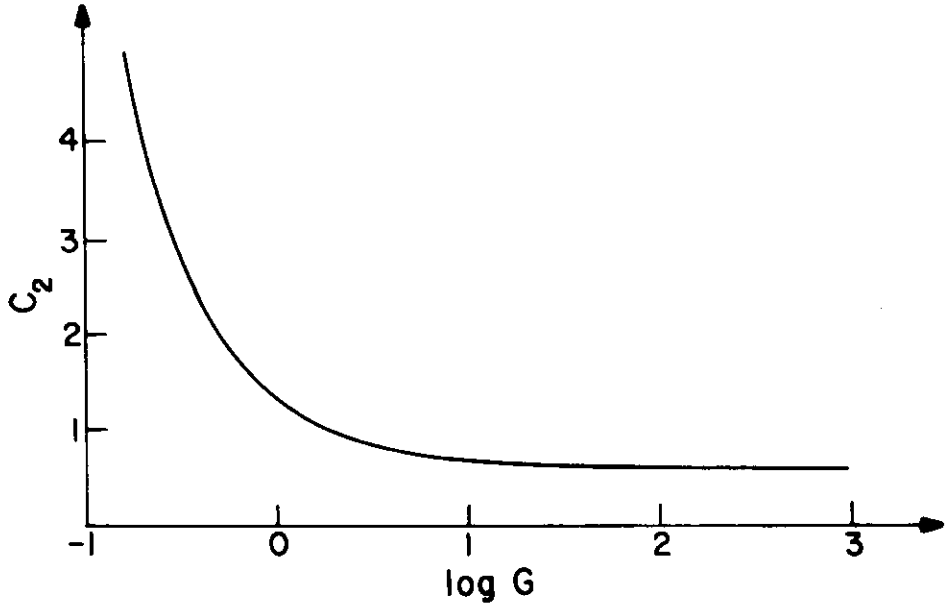

Figure 2. Finite element results for C_2; L = 1, T = 45, ν = 0

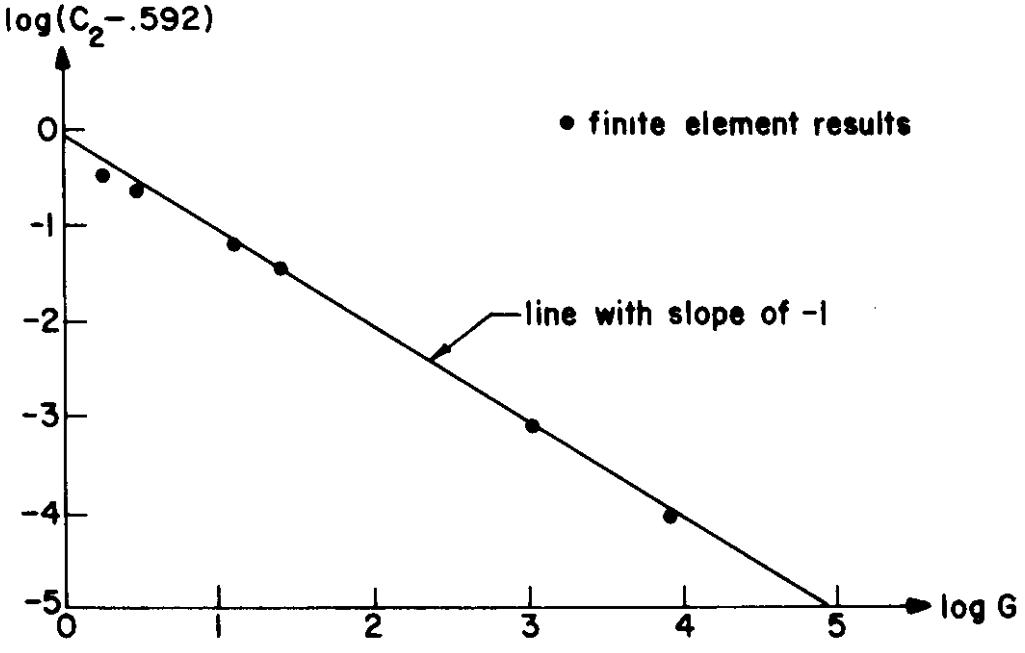

Figure 3. Typical log-log plot of C_2 - .592 and G

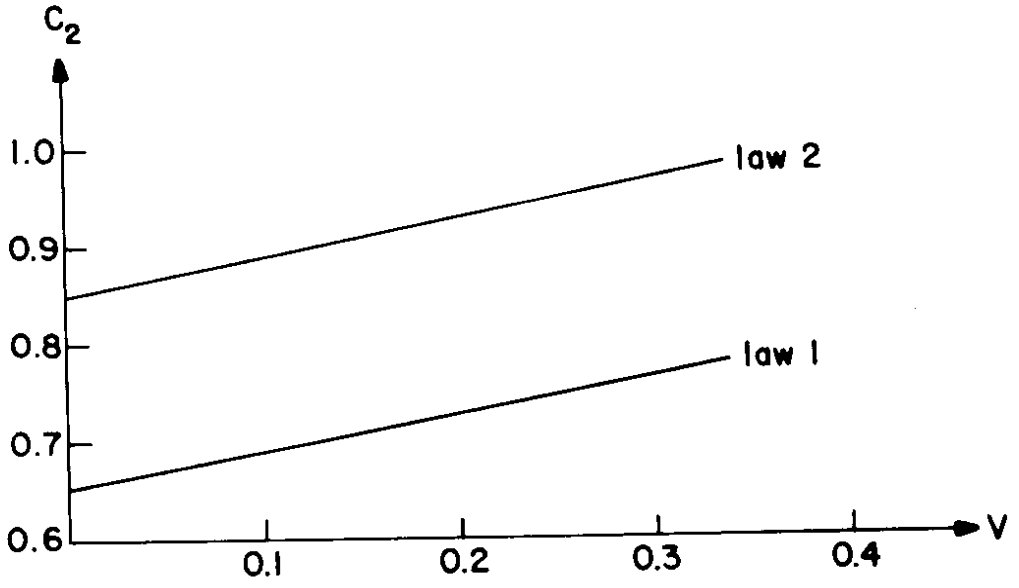

Figure 4. C_2 versus ν; G = 16.7, T = 45

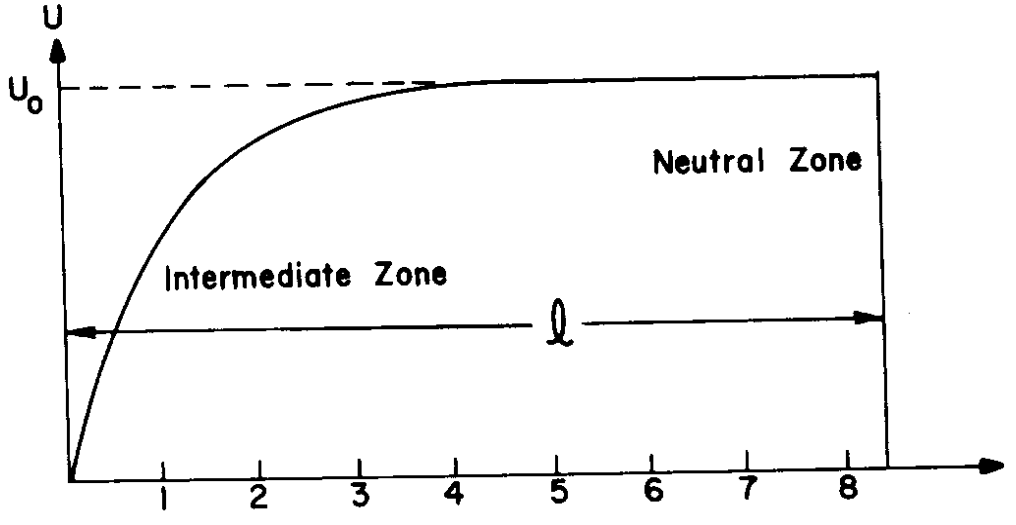

Figure 5. Typical glide velocity

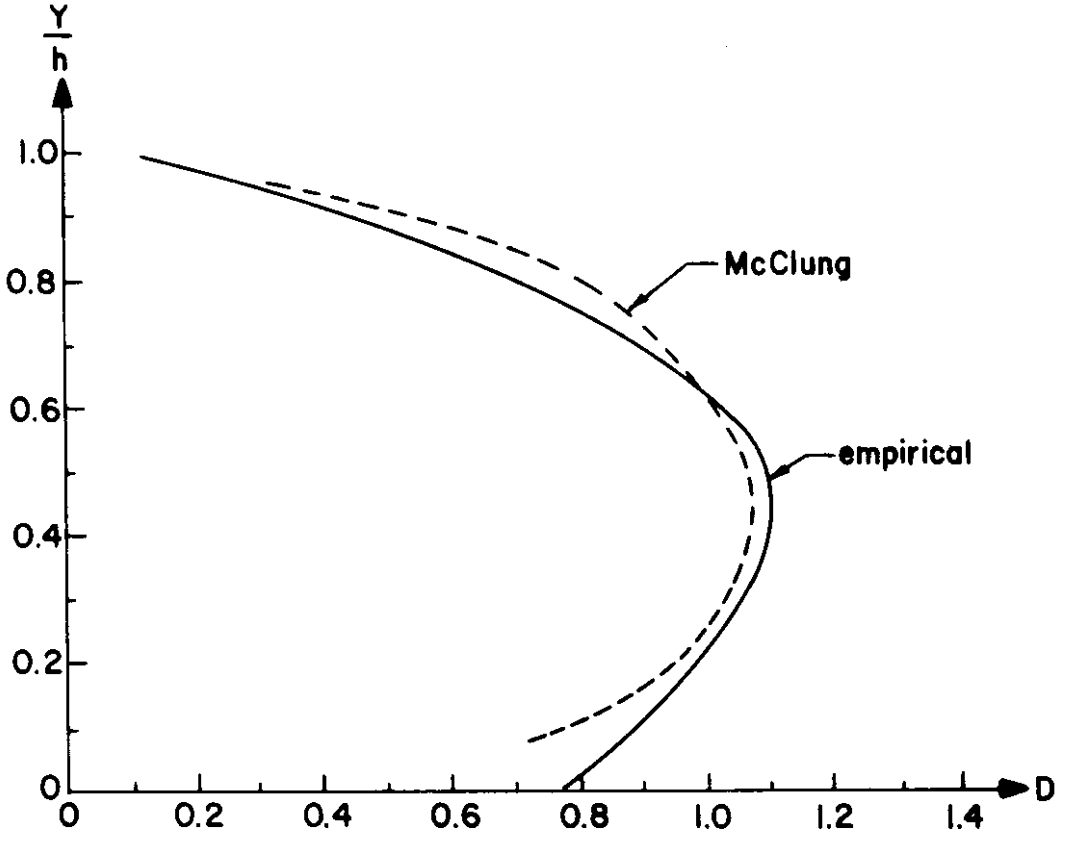

Figure 6. Comparison of results, T = 45, G = 16.7, $\nu' = .3$

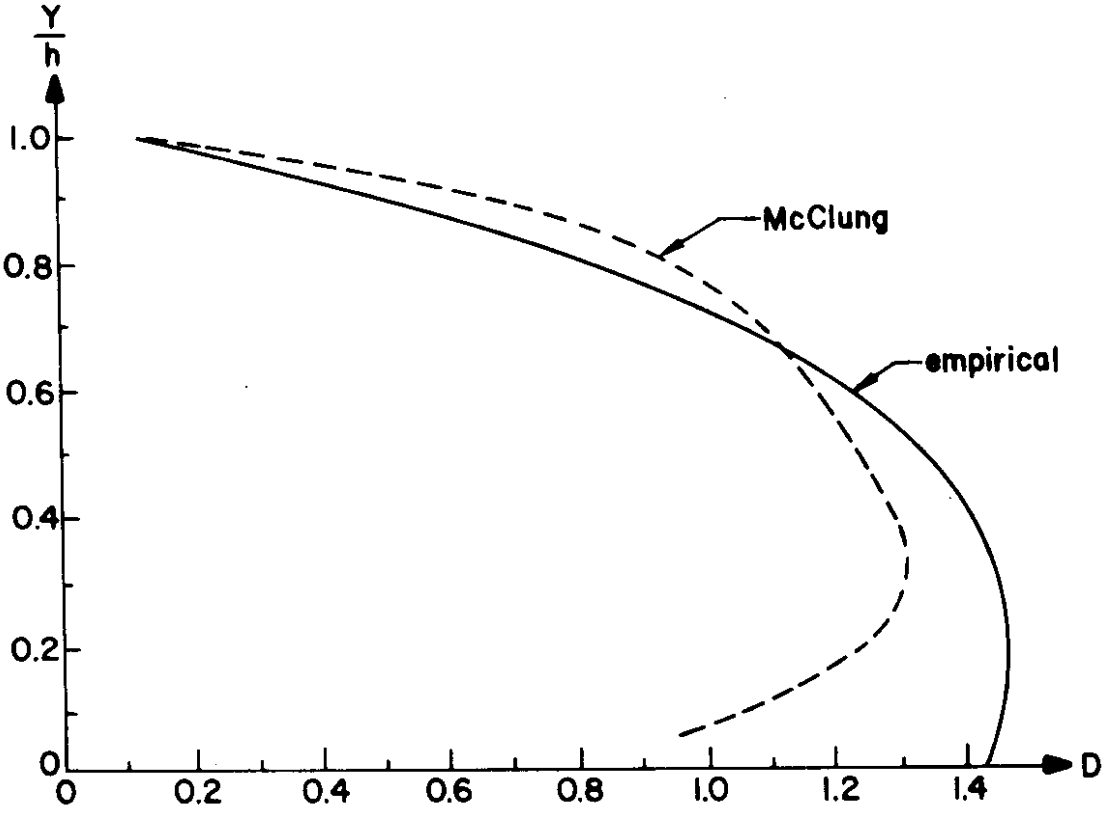

Figure 7. Comparison of results, T = 45, G = 3.18, $\nu' = .3$

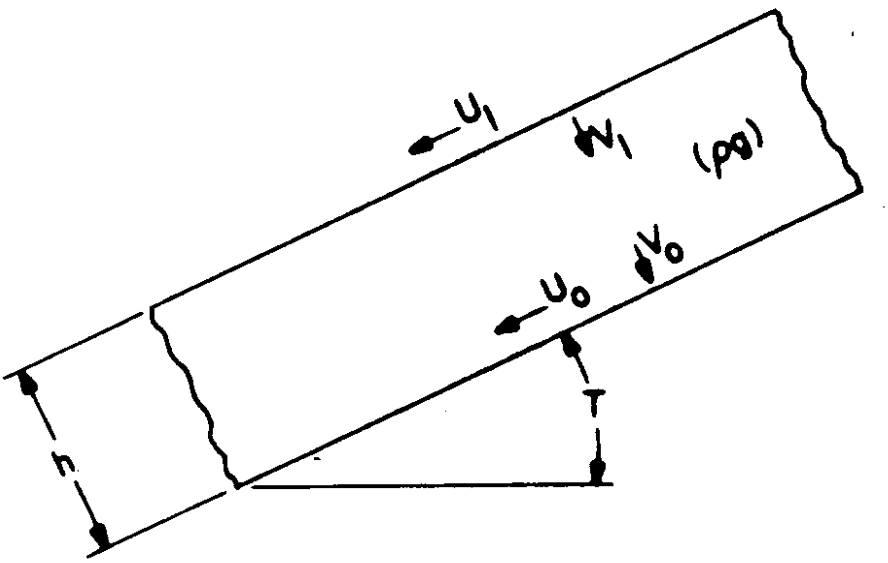

Figure 8. Parameters for calculation of barrier force

Chapter IV

INTERFACE MODIFICATION FIELD TESTS

by

Edward R. LaChapelle

Some informal field tests were conducted at Red Mountain Pass to examine the possibility of using plastic membranes to alter the bond between deposited snow and underlying old snow or earth.

(1) A sheet of black polyethylene, 2 x 3 meters, was installed in the release zone of a small avalanche path next to the Pass. One avalanche release was observed early in the winter on the plastic while the snow cover was still very shallow (10-30 cm).

(2) A sheet of texture-tempered polyethylene, 8 x 15 meters, was placed on a cornice-forming ridge adjacent to the Willow Swamp avalanche path just north of Red Mountain Pass. This was placed after snow was on the ground and difficulty was experienced in securing a proper anchor for the plastic sheet. High winds subsequently destroyed the inadequate anchors and damaged the plastic. The experiment was terminated before effects on cornice formation could be determined.

(3) Two sheets of texture-tempered polyethylene, each 8 x 8 meters, were placed in separate small avalanche paths. Snow continually slipped off these sheets during precipitation until the snow cover reached a depth of about 0.5 meter on the surrounding ground. Thereafter the snow started accumulating on the sheets as anchorage for the snow developed at the sides and bottom. After the plastic sheets became buried under snow, the glide rate of the snow over the sheets remained noticeably greater than for the surrounding snow which rested on the ground.

A large accumulation of snow accumulated by gliding at the foot of one of the sheets.

We deduce from these highly preliminary tests that cold snow adheres very poorly to polyethylene and that the use of this material to modify the snow-ground interface may be useful in inhibiting snow accumulation in avalanche release zones and especially on cornice sites. More thorough tests are planned to explore this possibility in the winter of 1975/76. It is obvious that proper and secure anchorage of the plastic to the ground is essential, especially at windy cornice sites.

Chapter V

MECHANICAL RESONANCE OF SNOW

by

J. B. Johnson and R. J. Evans

Introduction

The basic purpose of studying vibrations and wave propagation within the snow pack is to investigate the possibility of initiating avalanches by vibrations introduced either at the snow surface or at the snow-ground interface. From another point of view, however, useful information on the mechanical and crystallographic properties of snow can be obtained from acoustical measurements (1, 2*).

Standing waves, or vibrations, are the consequence of wave propagation in a bounded medium. For an isotropic elastic medium, the governing equation for the displacement vector, $\vec{u}$, is

$$(\lambda + \mu)\, \nabla^2\vec{u} + \mu\nabla\cdot\nabla\vec{u} = \rho\, \frac{\partial^2\vec{u}}{\partial T^2} \qquad (1)$$

where λ and μ are Lame's constants and ρ is the mass density. Thus for plane compressional waves the equation becomes

$$(\lambda + 2\mu)\, \frac{\partial^2 u}{\partial x^2} = \rho\, \frac{\partial^2 u}{\partial T^2} \qquad (2)$$

which, in a medium of depth L, leads to standing waves of frequency

$$\nu = \sqrt{\frac{(\lambda + 2\mu)\, n^2}{4\rho L^2}} \qquad (3)$$

where n = 1, 2, etc.

---

* Reference numbers

The fundamental frequency is given when n = 1 and it would, ideally, be this mode which would be excited in order to initiate avalanching.

The actual situation in the snow pack is, of course, far more complex than that described by equation (1). The snow is anisotropic and dissipative, the latter effect being particularly important in that damping, where large enough, can completely suppress standing waves. The fact that snow is porous means that the snow may exhibit behavior of a two-phase material and thus one may expect to see modes of vibration corresponding to vibration of entrapped air in addition to vibration of the snow. Also, the granular structure of the snow means that there will be high frequency standing waves associated with grain vibrations. The presence of ice layers will further complicate the situation because these layers will cause partial wave reflection and apparent depth effects.

Field Experiments

In the summer of 1974 preliminary tests were made at Mount Olympus, Washington with regard to acoustic energy losses; other experiments have been concerned with attempts to generate and measure standing waves.

Energy Loss Tests

A 1 m^3 hole was dug in a snow field on the Upper Blue Glacier of Mount Olympus. An electric jack hammer on an aluminum plate was used as a wave generator and the response was measured at distances of 8, 4, and 2 m and at angles of 0, 45^0, 90^0, 135^0, and 180^0 to the direction of the vibrator. The response was measured by an accelerometer (Kistler QA-116-16) connected to a portable oscilloscope. Results are shown in

Figure 1 and Table 1. From these F. Budding deduced a damping factor of approximately 0.1, rather high in comparison with results obtained from snow samples (3); present measurements are too tentative to allow definite conclusions to be drawn.

Experiments of this nature do require snow of considerable depth in order to calculate the loss factor; such depths are not generally available in areas of seasonal snow cover. On the other hand, variation of snow properties with depth was unknown at the particular location used, and increasing density with depth would mean that calculated loss factor was low (see Figure 1).

Resonance Experiments

These were made in the autumn at Mount Baker and in the winter at Stevens Pass and at Red Mountain Pass in southwestern Colorado. The Mount Baker snow consisted mostly of firn with ice layers throughout the snow pack. Snow in the Stevens Pass area is characterized by relatively small temperature gradients and equitemperature metamorphism; the San Juan Mountains snow is characterized by relatively large temperature gradients and temperature gradient metamorphism.

The study consisted of mechanically vibrating the snow using various audio-electrically driven transducers. The frequencies of the transducers and hence the frequency of snow vibrations were varied while keeping the input amplitude fixed. Kistler QA-116-16 accelerometers were used to record the amplitude of the resulting snow vibrations. These experiments were geared to locate possible resonance frequencies and to determine their changes with snow conditions, i.e., snow depth, crystal structure, water content, etc.

It was seen from the first experiments that relative amplitude enhancement did exist at specific frequencies in the snow. The frequencies at which this enhancement occurred were also seen to vary with general snow type and density, as was the amount of enhancement.

The type of transducers and their placement caused changes in the amount of enhancement. Thus four transducers in a rectangular pattern caused a larger enhancement of amplitude than a single transducer. Similarly, at Mount Baker, a sound generator mounted on a metal plate directly in contact with the snow surface produced different resonant frequencies at a given location than did a loudspeaker. The latter transducer presumably was acting on the air at the snow surface rather than on snow grains, producing different types of motion than did the former.

A series of experiments at Stevens Pass did not show any dependence of resonant frequency on snow depth (Figure 2). Instead, resonant peaks were observed which were independent of depth and appeared to be related to some internal feature of snow structure. This type of intercrystalline resonance was also observed by F. Budding in his experiments at Red Mountain Pass, Colorado.

Results so far would indicate a need for a more concerted effort to determine the type of resonance being observed. Thus we have not so far detected any vibrations which can clearly be associated with standing waves throughout the entire depth of the snow pack. It may be that the energy losses due to radical propagation from the surface source are large enough that, together with other dissipative losses inherent in the snow, all standing waves over depths so far encountered have been effectively damped out.

Accordingly, our next experiments will make use of snow columns of varying lengths with which longitudinal wave propagation and vibration will be investigated. This should enable types of vibration to be identified so that we can distinguish between boundary induced vibrations and intergranular vibrations.

Table 1. Response Amplitudes

Test Hole Number	Response	Test Hole Number	Response
1	60 mV	9	125 mV
2	20 mV	10	200 mV
3	10 mV	11	1 V
4	noise level	12	.4 V
5	noise level	13	.25 V
6	45 mV	14	.2 V
7	40 mV	15	.1 V
8	75 mV		

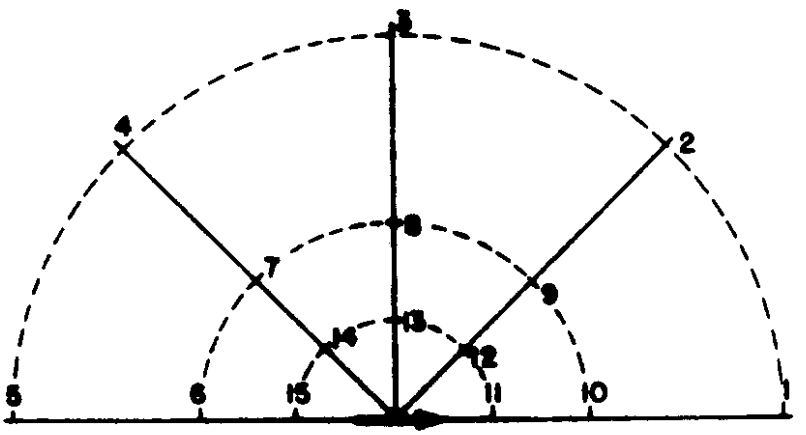

Figure 1. Response measurement location

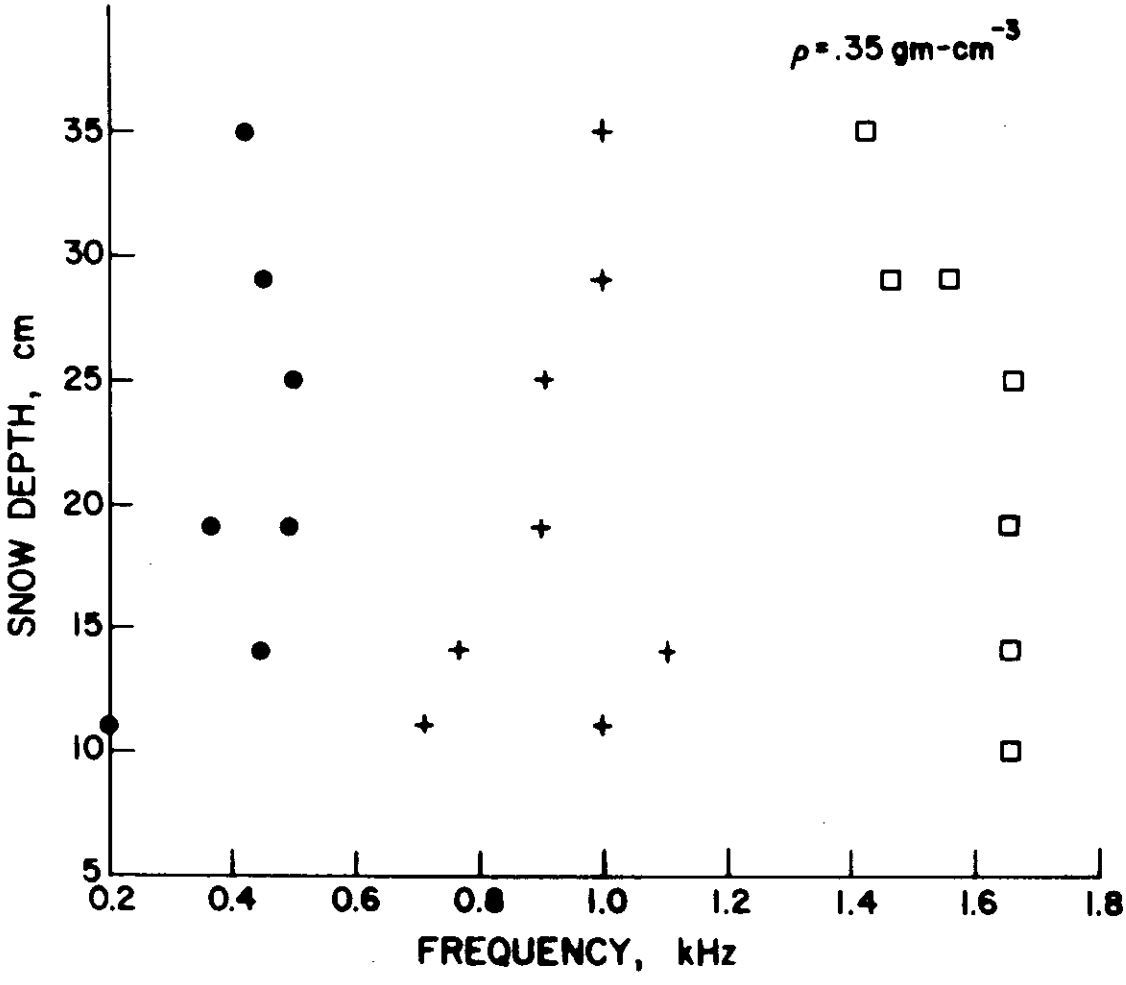

Figure 2. Resonance frequency versus snow depth

CHAPTER VI

THE 1974-75 WINTER

by

Mark B. Moore

VI.1 Introduction

For the 1974-75 winter, correlation of avalanche occurrences with local and synoptic weather conditions began in January, when extensive field data in the form of snowpits and fracture-line profiles became available. No field data were collected in November and December. Studies for the 1974-75 winter concentrated largely on the developing Stevens Pass snowpack and its cycles of instability characterized by both natural and artificial avalanching, although data from most reporting Cascade stations were ultimately incorporated into the analysis.

It should be emphasized that whenever personal field observations of the snowpack by this author were not possible, data from field work and observations by snow rangers, ski area personnel, and highway department avalanche crews were available and utilized in analysis of possible weather to avalanche correlations. Especially good cooperation of field personnel at Stevens Pass was an important determining factor in the choice of Stevens Pass as the primary snow study site.

The 1974-75 winter analysis below is divided into sections on the basis of the general surface weather conditions and their effect on the Cascade snowpack for that specific time period. At the start of each section, the principal weather conditions for that period are given, followed by a brief summary of the important variations

in weather or snowpack evolution which had an effect on Cascade avalanching. In the more detailed description following each section heading, probable causes for (in terms of synoptic weather conditions) and effects of local weather variables (e.g., temperature, wind, snowfall) on the snowpack and on Cascade avalanching are presented.

VI.2 Comparison of Local and Synoptic Weather Conditions with the Developing Snowpack and Observed Avalanche Occurrences

VI.2.1 January 1-11 (moist and cool, cold later in period); intermittent breaks in winds and snowfall, regional snowfall variations, wind slab deposition, cold easterly winds

From the 1st through the 4th of January, a large, developing upper level low in Alaska brought fairly consistent and cool temperatures into the Cascades along with a gradual southward shifting of the jetstream from British Columbia and consequently much stronger zonal flow into Washington by the 3rd. Weak surface fronts associated with the low, and resulting instability in the following flow, brought light to moderate orographic precipitation to the central and northern Cascades through the 3rd. As a result snowfall amounts in most Cascade areas were great enough during this period to yield sufficient snowpack instability for artificially induced avalanches. From analysis of snow, weather and avalanche observations by ski area personnel and USFS snow rangers, it is reasonable to infer that sliding surfaces or lubricating layers for any slides occurring during this period resulted from wind direction shifts and variations in wind speed associated with frontal passage, or variations in snowfall intensity between fronts.

A fairly intense surface cold front passed through Washington the night of the 3rd and early morning of the 4th. Here the center of surface low pressure moved directly onto the central Washington coast from the west late on the 3rd, with accompanying circulation producing a strong, moist, westerly flow into the southern Washington Cascades, but a much drier easterly flow over most of the central to northern Cascades (see Figure 1). Strong southwesterly winds were reported at Crystal Mountain and Paradise through the morning of the 4th, while Stevens Pass reported easterly winds during this time. As a result, Crystal Mountain and Paradise reported heavy precipitation--Crystal reported 17 in. (43 cm) of snowfall by 0800 on the 4th--while more northerly stations reported only light to moderate amounts of snowfall. With this regional variation in snowfall along the length of the Cascades, a similar pattern in avalanching also followed, with heavy avalanching reported at Crystal on the 4th and only light avalanching at Stevens Pass and more northerly areas.

With a strong westerly flow aloft over Washington through the 7th, surface cold fronts of the 5th and 7th affected the entire length of the state. Due to strong pressure gradients associated with each front, very strong winds were reported prior to and during both storms (Stevens Pass recorded wind gusts up to 26 and 28 m/sec (58 and 63 mph) for the 5th and 7th, respectively.) This wind combined with increased snowfall gave rise to moderate to severe snow slab avalanching in all reporting areas.

At Stevens Pass, Snoqualamie Pass and Crystal Mountain late night on the 4th end early morning of the 5th, instability in the surface

flow following frontal passage on the 4th resulted in the deposition of light orographic snow during low winds and low temperatures, resulting in a very cold low density layer. When this snowfall was followed by passage of a strong front later in the morning of the 5th (see Figure 2), which brought increased snowfall intensity and an east to west wind shift with accompanying stronger winds and initially higher temperatures (in the warm sector preceding the cold front), extreme instability in the snowpack resulted. From field records (snow and weather data, and observations of fracture-line depths) provided by snow rangers and highway department avalanche crews, it appears as if the very cohesive and high-density, wind-blown snow critically loaded the underlying layer of low-density snow, with the apparent result that the low density layer failed internally in shear. Severe avalanching at the ski areas and onto the major pass highways ensued on the morning of the 5th, and closure of I-90 and U.S. 2 at Snoqualamie and Stevens Passes, respectively, followed.

This avalanche situation emphasizes the importance of evaluating interrelationships among temperature, wind and snowfall in assessing avalanche hazard. A similar frontal passage on the 7th produced similar heavy avalanching at most reporting stations, and emphasized further the importance of such relationships. Again a cohesive wind-deposited slab, produced by the strong winds associated with the front, slid on a cold, low density snow layer deposited by moist, decreasing winds following the cold front of the 5th.

Another frontal system on the 9th and 10th affected the Cascades similarly to that storm described for the 3rd and 4th, where again only southernmost reporting stations were substantially affected by heavy

snowfalls. Despite this primary southerly affect of the front, though, some avalanching associated with this front and the following flow did occur at Stevens Pass on the 11th, and is characterized in Figure 3. Here a short decrease in wind and snowfall intensity is shown to be important in relating the observed avalanche to its associated sliding surface and hence is of value in predicting avalanche hazard for the Cascades. The avalanche exhibited in Figure 3 was observed as typical of those occurring throughout the area--a direct action avalanche triggered by explosives. The 20-25 cm of new snow at the surface in the starting zone corresponds well to that snowfall recorded at the pass level overnight (deposited in the instability of the following flow behind the front), given the existence of additional light wind loading in the upper area. This new layer slid out on the stronger more cohesive sliding surface (D = 23-35 cm in Figure 3) which had settled and hardened during the early morning of the 10th, when no snowfall and a sharp decline in wind--in response to decreasing post-frontal pressure gradients--was reported. The deeper layer below 35 cm in the figure is inferred to result from the 9 in. (23 cm) of snowfall reported on the morning of the 9th at the pass level, again given the additional wind loading in the starting zone which occurred overnight on the 8th.

The fact that most reporting station temperatures--especially those recorded on the passes--remained so low during this period (see Figures 4 and 5) was due to the influx of cold air from eastern Washington prior to the arrival of each front in response to the strong east to west pressure gradients ahead of fronts. These low temperatures at the passes were particularly evident in response to the very cold

east winds produced by extremely strong pressure gradients prior to frontal passage over the Cascades on the 12th. Such extremely cold air had been brought into eastern Washington by cold continental air advection at the surface and a strong, northwesterly upper level flow on the 11th (see Figure 6). As will be shown later, this cold air pattern plays an important role in Cascade avalanching.

VI.2.2 January 12-25 (very warm and moist); warming during snowfall, heavy rain lubrication, cooling during snowfall, rainshielding by melt-freeze crusts, warm air overriding at the passes

By early morning of the 12th, the offshore upper level high, which had brought such cold temperatures to eastern Washington and the passes, had moved rapidly onshore, and another well-developed upper level low moved southward from the Gulf of Alaska, bringing with it a new set of intense surface fronts. The first front, with a preceding intense east-west pressure gradient and corresponding warm sector, approached the Washington coast on the early morning of the 12th. Overrunning of the cold air at Stevens Pass (and in fact all the central and southern Cascades) by this warm moist air on the 12th, followed by heavy wet snowfall with some rain at all areas except Washington Pass, was apparently responsible for the heavy avalanche cycles reported the morning of the 13th. Characteristic of the Cascade warming on the 12th, temperatures at Stevens Pass rose from an early morning low of -17°C (2°F) to a high of 2°C (35°F) that afternoon. U.S. 2 at Stevens Pass was closed at 0915 on the 13th due to slides, and heavy wet loose avalanche activity was likewise reported at Crystal Mountain during morning control work by ski patrol. Here an excellent example of

often-recurring Cascade slide cycles is represented by the avalanching associated with the snowfall and temperature trends from the 9th to the 13th. A few days (the 9th-11th) of cold dry snow followed by abrupt warming and heavy snowfall deposition led to critical loading and subsequent snowpack failure, as bonding of the wet dense snow to the underlying cold and dry, low density snow was minimal. These avalanche-producing trends relate quite well to the observed northwesterly to southwesterly shift of the upper air flow during the same period.

Strong onshore flow in the upper levels brought heavy orographic precipitation on the 13th at all areas, and severe avalanching occurred again on the 14th. This time snow slid on the transitional melt-freeze crust of the 12th, which had formed in response to heat conduction from this warmer rain-soaked layer downward into the lower colder layers (evidenced by initial crust formation upward from the bottom of the rain-soaked layer). In his avalanche report on the 14th, the Stevens Pass snow ranger reported that all slide paths released naturally on the rain-produced melt-freeze crust, running full length of their slide paths with 61-66 cm slab depths. The fact that many of the slides that released were sympathetic (i.e., being triggered by neighboring paths) demonstrated the extreme instability of the snowpack at this point. Considerable densification and warming of the snowpack by the morning of the 15th is evident in the fracture profile of Figure 8, which is characteristic of many of the avalanches occurring at Stevens Pass both on the 14th and 15th. Following the light rain which occurred on the 12th, evidenced by the melt-freeze crust at D = 95 cm in Figure 7, relatively dense snow fell (D = 65-95 cm) prior to actual passage of the cold front

late on the 12th. Upon this denser, wetter layer increasingly colder and lighter snow was deposited early on the 13th following frontal passage (D = 30-65 cm), resulting in the icy crust (D = 65 cm) and the transitional layer (D = 58-65 cm) of denser to lighter snow which was probably formed when the lower part of the light snow layer hardened somewhat in response to initial warming from below followed by heat loss to the colder snow deposited above. As a result of such hardening, the transitional layer produced a poor bond with the upper, lighter layer. With increased loading by subsequent snowfall (D = 0-30 cm) through the 14th, and explosive control of this area on the 15th, this weakness in bonding resulted in snowpack failure and the slab release described by the accompanying figure.

On the 15th surface high pressure in eastern Washington brought cold continental air over the passes. However, in response to strong warming from the south by a stationary front, higher temperatures were recorded aloft than at pass level on the morning of the 15th, due to overriding by the warm air. At 0730 on the 15th, Stevens Pass reported -7°C (20°F) at the 4000 ft. (1220 m) level and -1°C (31°F) at the 5000 ft. (1520 m) level, with light snow at both levels. This situation brought only minor surface sluffing to the pass areas on the 16th as most areas had already experienced substantial sliding on the 13th-15th, but is worthy of note as it is potentially hazardous in certain instances (e.g., see VI.2.7, where significant warming aloft at Snoqualamie Pass prior to frontal passage resulted in substantial avalanching).

This hazard results from the fact that warming of starting zone snowpacks may not necessarily be noticed at the lower levels, and hence

may create avalanche hazard which remains unidentified without access to current weather data (via weather telemetry systems or synoptic weather maps).

Warming with increased orographic precipitation and heavy rain continued through the 18th in the Cascades, as an associated warm front lingered near Washington most of 16th, 17th and 18th, advecting considerable warm and moisture-laden air northward (see Figure 8). In general, such rain deposition onto an unconsolidated snowpack usually results in severe wet slab or wet loose avalanching. In this instance, however, considerable snowpack stabilization and settling of the more recently deposited snowpack had already occurred on the 14th and 15th, and only light to moderate avalanching ensued with the initial rainfall on the 16th. Under continued heavy rain, though, percolation and decreased cohesion penetrated deeper and deeper layers, and ultimately the more general rule prevailed as a major wet slab cycle affected much of the Cascades late on the 17th and 18th, closing the Stevens Pass highway in the early morning of the 18th. Most slides observed during this period, however, primarily involved snow deposited after the rain on the 12th. This absence of extensive climax and/or full-depth avalanches during this heavy rain period was due to the rain-shielding effect on underlying layers of the now strong melt-freeze crust formed from the rain on the 12th and particularly a thin ice layer associated with the crust. That is, the rainfall from the present storm period of the 16th-18th only percolated down to the fairly impervious rain crust of the 12th, whereupon it flowed out on this strong, icy layer rather than percolating further downward. In absence of such blocking layers, such heavy rainfall as

occurred could easily have percolated much deeper, causing even more serious avalanche problems. The increasingly wet state of the upper snowpack at this time is shown in Figure 9, where both the newly rain-soaked layer (D = 0-40 cm) and the rain crust and ice layer of the 12th (D = 40-42 cm) are clearly visible. Note that the snow has remained sub-freezing below the shielding ice layer at D = 40 cm.

After an extended period of limited precipitation, mild temperatures, and some clearing, a new surface front passed through the Cascades on the 22nd. Initially, temperatures continued high as most of the frontal push was westerly, and thus rain again occurred at all but the most northerly areas. Rain continued until a stronger frontal push and following colder flow dropped Cascade temperatures on the 23rd, whereupon light to moderate snowfall occurred through the 26th. The initial snow which fell at warm temperatures bonded well to the rain-soaked layer and therefore only wet loose surface slides occurred on the 24th. Falling temperatures, however, produced a fine sliding surface through rapid hardening and melt-freeze crust formation in the initially deposited snow layer. Hence small but highly unstable slides occurred on the 25th and 26th at all Cascade areas as a result of poor bonding at the developing melt-freeze crust interface.

In general, cooling during snowfall produces a much more stable and much less avalanche-prone layering than the opposite trend (warming during snowfall), since the underlying wet snow usually freezes and the upper, colder, looser snow stabilizes itself through surface sluffing. In the case above, though, rapid hardening of the very wet underlayer produced a sliding surface rather than a merely cohesive snow layer, and

in the absence of surface sluffing prior to artificial control, the observed avalanches ensued. At Stevens Pass on the 25th, each gully that slid had a double 10 cm fracture line, where in response to explosive control, the top 10-12 cm of new snow deposited overnight began to slide, dynamically loading the underlying layer of snow from the previous day which also slid. This is shown graphically in Figure 10, where the double fracture slab (D = 0-18 cm) slid on the partially crusted underlying surface described above. Note again the rain crusts of the 16th-18th; the crust of the 12th is no longer discernible as a separate layer and has become a part of the 16th-18th rain crust (D = 25-45 cm in Figure 10).

VI.2.3 January 26-February 8 (very cold and dry); rain crust decomposition--extended temperature gradient metamorphism in the Cascade snowpack, wind-slab deposition, regional variations in Cascade weather

An increasingly cold and relatively dry weather situation for the Cascades prevailed from the 26th-30th of January, as an upper level trough, directly to the west of or over Washington during this period, effectively brought cold dry air aloft from the Arctic into the northwest, with strongest onshore flow occurring well to the south (see Figure 11). Only slight modification of this cold and dry synoptic situation for the Cascades occurred through the 6th of February, as a second upper level low assumed a somewhat stationary position off the Washington coast from the 31st through the 6th of February. Only light amounts of precipitation occurred in the Cascades through the 6th, as the majority of the flow both at the surface and aloft continued to be brought onshore much farther south--in northern and central California

(see Figures 11 and 12). Temperatures in the Cascades, while moderating somewhat late in this period (the 1st-6th), remained for the most part well below freezing (especially in the passes and the northern Cascades--see Figures 4 and 5), since the primary surface flow over the Cascades at this time was very cold, dry and easterly as a result of the strong east-to-west pressure gradient, the low 500 mb heights, and substantial cold, continental air advection into eastern Washington at the surface (see Figure 13).

As a result of this cold and dry weather situation, very little slide action, but extensive internal snowpack modification occurred in the Cascades through the 6th of February. Response of the Stevens Pass snowpack to the synoptic situation through the 1st is shown in Figures 14 and 15, where the snowpack has set up considerably and strong ice lenses exist at both upper and lower elevations. The observed temperature gradient of close to 10°C/m in the upper layers of both figures is of extreme importance here, for it equals on the average the critical value necessary for substantial water vapor diffusion and recrystallization in the snowpack.[1] This mechanism seems likely responsible for the loss of grain bonds and the deterioration in mechanical strength of the refrozen rain-soaked layer of the 16th-18th noted in later snowpits and related to subsequent slide releases. The fracture-line profile observed in Figure 15 is of little value insofar as slide genesis is concerned, but

---

[1] It is clear from Yosida (1963) and Eugster (1952) that the critical value of 0.1°C/cm does not imply a strict division between different metamorphic processes, but rather indicates where a shift in trends from predominantly equitemperature to predominantly temperature-gradient metamorphism takes place.

is retained primarily for the stratigraphy, temperature and density study it contains. It represents a soft slab of low-density new snowfall (of the 31st and 1st) sliding on a partial wind and sun melted surface of the 29th-30th which had refrozen.

Avalanches which did occur from the 1st-6th of February resulted primarily from wind-slab deposition (in response to the continued strong east to west pressure gradients) on the increasingly unstable rain crust of the previous month, which continued to decompose in the strong surface snowpack temperature gradients. Such continued weakening of the upper section of the rain crust (of the 16th-18th of January) is evident by the low ram resistances (less than 2.0 kg) down to D = 50 cm in the Stevens Pass snowpit of the 5th (Figure 16), where effective temperature gradients on the order of 10°C/m continued to be observed in the upper layer (D = 0-60 cm) of the snowpack. Here the layer from D = 25-55 cm showed definite grain angularity which implies temperature gradient metamorphism in this case.

With a primarily cold northerly flow aloft into Washington on the 7th and 8th, large temperatures gradients in the snowpack continued through the 8th, being interrupted for only brief periods prior to weak frontal passage. One such weak front passed over Stevens Pass late on the 6th, where light snows and strong winds (still in response to the strong surface pressure gradient) produced slab conditions and ensuing avalanching with artificial control on the morning of the 7th. One of the slab avalanches generated on the morning of the 7th is shown in Figure 17, and is representative of most slides occurring in the area that day. The slab layer itself (D = 0-25 cm) was produced the night

before, corresponding well to the 6.5 in (16 cm) of snowfall recorded at the base of the ski area (pass level) if additional wind loading is considered. The light surface sun crust shown developed the morning of the 7th as the day dawned clear and cold, but rapidly warmed. The underlying layer (D = 25-48 cm) resulted from low intensity, wind-deposited snowfall at Stevens Pass from the 1st to the 5th, with the actual sliding surface generated on the 5th, a clear but very cold day. Again, the evolving weak structure of the coarse-grained layers within the previously rain-soaked portion of the snowpack (D = 48-102 cm) is evident through low ram resistances in Figure 17, and such weakening in the snowpack structure was also observed by the snow ranger at Crystal Mountain on the 7th.

The different response of Crystal Mountain in this storm situation insofar as observed local weather of reporting stations is concerned is notable. On the morning of the 7th, Crystal reported .36 in (9 mm) of rain, suggestive again of its geographical isolation from pass weather, and specifically from cold, easterly pass winds. That this response is probably true in any area situated on the western slope like Crystal is worthy of mention, for substantially different avalanche situations than occur in the passes should be expected in these more western areas.

VI.2.4 <u>February 9-15 (warming and very moist); rain-crust decomposition, rain on unconsolidated snow, wind scouring, warming with occlusions</u>

On the morning of the 9th, the period of extended cold temperatures in the Cascades ended, as both surface and upper level flows into Washington increased and shifted to substantially more southwesterly,

and the offshore upper level low pressure formed an intense center along the British Columbia coast (see Figure 18). The dominating cold east winds in the passes shifted to strong westerly with passage of a cold front that afternoon. Very heavy snowfall and slowly moderating temperatures followed throughout the Cascades through the 13th, as subsequent surface low pressure centers lingered and passed over the Washington-Canadian border, and a strengthening jetstream moved southward and established itself directly over the Cascades.

The impact of the temperature-gradient snow metamorphism associated with the preceding extremely cold, dry weather following heavy rain in the Cascades now became evident, as severe avalanching resulted at all areas the 10th through the 15th, with many climax snow slides releasing on the well-decomposed rain crust of January 16th-18th. In response to the very warm flow preceding and following an oncoming occluded front, slide action was particularly heavy on the 12th, as rain falling on large amounts of unconsolidated snow deposited the 10th and 11th precipitated large slab avalanche releases. Separate types of slide cycles resulting initially from heavy snowfall at lower temperatures and then from continued heavy snowfall followed by rain, were recorded at both Stevens and Snoqualamie Passes on the 11th and 12th. Here avalanching on the 11th through the early morning of the 12th consisted of direct action loose or soft slab as a result of the high intensity snowfall and therefore heavy snowpack loading. However, those avalanches occurring later in the morning and afternoon of the 12th involved soft or wet slabs primarily due to the lubricating effect of the rainwater and the gradually destabilizing conditions inherent in the rapidly rising

temperatures preceding the approaching occluded front on the 12th. Both Stevens and Snoqualamie Passes were closed off and on the 11th to the 13th by heavy natural and artificial avalanche activity, as 90-120 cm fractures released from many chutes, sliding on the weakened rain crust.

The scouring effect of strong winds on certain exposed areas is also essential in characterizing some of the natural slides which occurred on the 12th, and in this case, Skyline Ridge at Stevens Pass is a good example. Here strong west winds on the 10th following frontal passage were observed to remove most of the snow overlying the weakened rain crust found in all areas. Subsequent low density snow on the 11th bonded poorly to this exposed surface, and with the deposition of increasingly denser snows with rain and significant warming on the morning of the 12th, a large natural soft slab slide occurred on this low angle, otherwise relatively stable area.

The extreme instability in the snowpack during this entire time is shown graphically very well in both Figures 19 and 20, where sliding in both instances centered around the temperature-gradient weakened, coarse-grained layers developed throughout the initial part of the month. In Figure 19, critical loading by new snow followed by explosive control brought about general shear failure within the top portion of the weak temperature-gradient layer (D = 85-95 cm). The very weak state of this upper portion of the January rain crust is obvious in the ram profile of Figure 19, where ram resistances decreasing rapidly from above 10.0 kg (at D = 70-85 cm) to below 4.0 kg (at D = 85-90 cm) indicate substantial loss of mechanical strength in the weak crust. Note also the rapid increase in density in the uppermost portion of the

decomposed rain crust (D = 85-95 cm), where the effect of temperature-gradient weakening was most pronounced. The decrease in density found in the lower portion of the involved weak layer (D = 95-100 cm) is possibly due to earlier variable sub-layer retention of meltwater within the weak layer. The avalanche situation described in Figure 20 indicates that poor bonding between the temperature-gradient weakened layer (D = 120-172 cm) and the underlying hard ice layer (D = 172-179 cm) led to the observed large snow slab release.

From the standpoint of Cascade avalanche forecasting, it is also very instructive to note here the specifics of the generally northward-moving warming trend affecting the Cascades on the 12th. Such warming associated with the strong southerly flow prior to the arrival of the occluded front was reported at Crystal Mountain early on the 12th, as rain occurred from 0000 to 0600 while southwesterly wind gusts over 45 m/sec (100 mph) and lowering temperatures by noon showed arrival of the front later that morning. At the passes, however, warming at the surface and hence accompanying rain did not occur until well after the front had passed through the Cascades, due to the attending orientation of the isobars accompanying such an occlusion and the resulting continued easterly pass winds through late morning of the 12th. See Figure 21(a) and compare this surface flow on the 12th following frontal passage with that occurring after strong cold frontal passage on the 19th of February shown in Figure 21 (b).

It must be emphasized here that passage over the Cascades of either an occluded front or a cold front sometimes brings warming to the passes, due to the possible presence of extremely cold air masses in

eastern Washington and strong, easterly pass winds prior to frontal arrival. The occlusion discussed above was accompanied by slow but substantial warming which was associated with the observed avalalching. This occluded frontal passage is quite different from that of cold front passage where accompanying strong temperature gradients limit warming behind the front. Consequently the relative timing of any warming behind the two types of fronts can be substantially different, with warming in occluded front situations generally occurring later and more substantially than any warming associated with cold fronts.

VI.2.5 February 16-22 (cool and moist); pass versus non-pass weather, settlement of cold snowfall, wind-slab deposition, strengthening of earlier weak temperature-gradient layers

A strong offshore upper level ridge brought about drier and more stable air into the Cascades through the 18th, and relatively light snowfall and lower temperatures produced no avalanching (see Figures 4-5, 22-25) and considerable stabilization of the snowpack during this period. Overnight lows of -5°C to -13°C brought about substantial solidification of previously wet layers. However, as the high moved onshore and another strong low pressure established itself offshore by late on the 18th, heavy snowfall and generally increasing daytime temperatures on the western slope of the Cascades heralded strong frontal arrival late on the 19th. While warming occurred to the west, though, colder temperatures prevailed in the passes most of the 19th during the heavy snowfall, as first an east wind in response to the pre-frontal pressure gradient kept pass temperatures low, and then strong, cool west winds

at the surface following frontal passage brought continued cooling (see Figure 21(b)).

Again the singular response of Crystal Mountain and Paradise to frontal passage on the 19th are noted, as without the prevailing easterly pass winds prior to frontal passage, these southwesterly areas warmed considerably on the 19th. Crystal Mountain reported a high of 3°C (38°F) on the 19th with rain in the morning, while Paradise also reported above-freezing temperatures.

Especially heavy snowfall at Snoqualamie Pass during this storm on the 19th (79 cm in 24 hours) resulted as the center of surface convergence passed directly over this area of the central Cascades. Yet even with this large amount of snowfall, only light to moderate avalanching followed, as the very low density snowfall at low temperatures and low winds stabilized considerably throughout the storm period by surface sluffs, and net new snow settlement of over 50% in this area eliminated severe hazard. Stevens Pass also reported only light avalanching at this time, with characteristically occurring slides on the 20th represented in Figure 26. Here the lubricating weak layer (D = 33-40 cm) resulted from low-temperature snowfall deposited at low winds on the 19th prior to frontal passage, while subsequent more intense snowfall at higher west winds during and after frontal passage late on the 19th and early on the 20th produced the upper slab layer (D = 0-35 cm in Figure 26).

The fact that only light avalanching occurred at both Stevens and Snoqualamie Passes on the 20th given the heavy snowfall throughout the day on the 19th is worthy of further emphasis, for such snowfall deposition occurring with or followed by warming temperatures would have undoubtedly

led to heavier avalanching: compare this slide cycle with those of January 9-13 and February 12, both of which were characterized by strong warming with increased snowfall or rain, and severe avalanching. However in this case, with a strong cold post-frontal flow, initially cool with increasingly colder temperatures throughout the snowfall period (-2°C dropping to -7°C at Snoqualamie Pass) was accompanied by substantial snowpack settlement and stabilization through surface sluffing action, resulting in much less snowpack instability than might have otherwise been expected.

With colder but still moist northwesterly flow returning to the upper levels by the 21st, all reporting areas continued to record loose and slab avalanches through the 21st as continued very strong west winds following earlier frontal passage--and in response to offshore surface high pressure--deposited considerable wind-slab snow on lee slopes. Such wind-slab deposition was particularly evident at Stevens Pass on the 22nd, and is shown in Figure 27. Here the weakness of a cold snow lubricating layer is particularly apparent in the ram penetrometer data, where ram resistances of less than 2.0 kg are found in the low density layer at D = 73-85 cm, which was probably deposited during cold temperatures and low winds on the 16th. The upper 73 cm of the fracture line slab is inferred to be storm deposition recorded during high winds on the 19th and 20th. Note also the continued presence of the crust formed by rain in mid-January (D = 178-250 cm). This lower, previously mechanically weakened rain crust is shown here to have strengthened considerably with the stable addition of new overlying snow and accompanying settlement,

Cascade temperatures ranged from approximately 3 to 12°C--brought only small wet loose, surface slides to the Cascades, as most previous recent small snowfalls had stabilized by either earlier slides or by settlement and equitemperature metamorphism. Also, the rain-shielding effect of the earlier formed melt-freeze crust of the 22nd and 23rd on underlying snow layers was very much in evidence, as no observed slides involved layers beneath this crust, indicating only limited (if any) percolation of the new rain through this old crust layer.

A continued difluent and weak upper level flow in the northwest (see Figure 29), brought only very light precipitation and sporadic periods of clearing to the Cascades through the 11th of March. Response of the Cascade, and in particular Stevens Pass, snowpack to this continued period of mild daytime temperatures, cool nights and rain early in the month was basically one of further settlement and substantial densification, as found by field snowpack observation on the 10th. Comparison of snowpit studies taken at Stevens Pass on the 2nd and 10th of the month serve to emphasize this snowpack solidification. Densities in the upper 70 cm of the 0°C isothermal snowpack of the 2nd ranged from 0.25-0.30 gm/cm^3, with lower layer (D = 70-200 cm) densities from 0.40-0.45 gm/cm^3. On the 10th, densities in the upper 70 cm of a similarly isothermal snowpack situated at a slightly lower elevation (1310 versus 1520 m) had increased to 0.35-0.40 gm/cm^3, while lower layers (D = 70-200 cm) were found to have densities uniformly greater than 0.45 gm/cm^3. However, despite the general settlement and density stabilization of the snow during this period, both snowpits showed some weakening in mechanical strength of all layers due to the high snowpack

temperature. Free water was really not evident except in extreme upper layers, though, and hence wet loose avalanching except at the surface did not occur. Some partial decomposition of the well-densified, uppermost rain crust layers was also noticed in the snowpit of the 10th and at Crystal Mountain as a result of some clear, cold nights with strong radiational cooling and ensuing temperature gradient metamorphism in the surface snow layers. These evolving weaker layers played an important part in later avalanche release at both Crystal Mountain and Stevens Pass. This again stresses the importance of snowpack metamorphism and its relationship to surface and synoptic weather in prediction of possible avalanche hazard.

VI.2.7 March 12-21 (cool and very moist); temperature-gradient weakening of melt-freeze crusts, regional snowfall variations, timing of warming trends, breaks in the affecting weather

With a slow return to stronger zonal flow into Washington on the 11th and 12th, an accompanying surface cold front deposited moderate to heavy snowfall on the probable temperature-gradient weakened layer at Stevens Pass and Washington Pass on the 12th, leading to both natural and artificial avalanching on the 13th. In Figure 30 (at Stevens Pass), snowpack stratigraphy, low ram resistances and low densities observed from D = 40-55 cm all suggest a definite mechanical weakness in this relatively old snow layer.

Figure 30 also shows the sliding and lubricating layer at Stevens Pass on the 13th to correlate well with the previously observed decomposed rain crust layers of earlier March snowpits. In this avalanche analysis,

therefore, it appears as if the weak layer (D = 40-55 cm) failed internally in shear with the critical loading imposed by the new snow (D = 0-40 cm) and explosive control.

By late on the 14th, much more coherent definition returned to the upper level flow over the Cascades for the first time in over two weeks, as a series of very intense upper level lows moved consecutively southeastward out of the Gulf of Alaska, reuniting the different upper level flow and bringing with them an almost constant supply of moisture to the northwest through the 26th.

A series of associated strong frontal passages on the 16th and 17th deposited substantial snowfall at all areas and moderate to heavy avalanching in the Cascades ensued through the 18th. At Stevens Pass, most slides were observed as running only on the old snow surface of the 12th and 13th, while at Crystal Mountain many ran on the temperature-gradient affected melt-freeze (rain -crust of the 1st and 2nd of the month). Differences between sliding surfaces here probably resulted from the differences in previous snowfalls and subsequent stabilization of the weak layers. At Stevens Pass on the 16th, a snowpit dug in an upper elevation potential fracture area (see Figure 31) showed considerable snowfall (D = 0-35 cm) resting on top of the weakened underlayer (D = 35-58 cm), while Crystal Mountain on the same day showed very little new snow above the rain crust due to the substantial snowfall differences between the two areas in previous March storms (see Figures 22 and 24). Thus, the exposed weak rain crust at Crystal continued to degenerate during cold nights, while the added snow above the rain crust at Stevens Pass acted as an insulating layer which greatly inhibited

any further weakening effects of temperature-gradient metamorphism on this icy layer. However, the fact that some avalanches at Stevens Pass did run on the weakened crust indicated the continued marginal instability of that weak layer.

The meteorological timing of potential hazard and natural avalanche release accompanying strong frontal passage on the 17th is also very important in terms of avalanche forecasting in the Cascades. Comparison of snowfall, temperature and weather records available from Snoqualamie Pass indicates that snowfall early on the 17th occurred at cold temperatures brought about by accompanying east winds prior to an approaching frontal passage that afternoon. Rapid warming from -6°C to 0°C (22-32°F) at the 3800 ft (1150 m) level in the afternoon of the 17th immediately preceding this front precipitated substantial natural avalanching. Here the bonding of the new snow to the old snow surface or the rain crust of the 1st-3rd (depending on location) at the low temperatures of the initial snow deposition was weak at best, and this weakness combined with a decrease in tensile strength of the new snow during the rapid warming apparently resulted in the observed natural avalanches.

Comparison of the surface weather patterns accompanying this heavy avalanche-producing situation with that weather associated with the heavy avalanching of February 12th and the relatively light avalanching on February 19th is of further value in aiding prediction of avalanche hazard for the Cascades. In both heavy avalanching situations, where substantial warming occurred following passage of an occluded front, surface winds behind the front were zonal to southwesterly

and quite warm (see Figures 21(a) and 32). However, with the light avalanching situation of the 19th of February, low temperatures dominated throughout the snowfall period, due to strong temperature gradients behind this sharply defined front (see Figure 21(b)). As a result, warming associated with frontal passage never really occurred in the passes (a combination of cold east winds followed by cold westerly winds kept pass temperatures low throughout).

As more and more snowfall accumulated above the March 1st-3rd rain crust at all areas through the 20th, avalanches (especially those occurring naturally) increasingly involved just the newly deposited layers, where decreased precipitation and wind between fronts and even between meso-scale precipitation bands became more and more important in determining snowpack instability and just which layers would be involved in slide activity. Such breaks in weather may introduce poor surface bonding between older and newer snows through solidification and metamorphism of old snow before ensuing snowfall, or possibly through generation of sun crusts and hard wind-slab surfaces in the older snow prior to resumed snowfall.

VI.2.8 March 22-31 (warm and relatively dry); cooling during snowfall, regional variations in snowfall, breaks in weather, increasing radiation into the snowpack

Avalanching continued sporadically in all areas through the 26th, as light to moderate and occasionally heavy snowfall continued. During a frontal passage and accompanying snowfall period on the 22nd, where Snoqualamie Pass was the only reporting avalanche-prone area substantially affected, initial snowfall occurring at higher temperatures followed by

increasing snowfall at lower temperatures, assured good bonding of the new snowfall to the fairly stable underlying layers, and hence no natural avalanching in the pass area was reported. The surface flow here roughly paralleled that associated with snowfall on February 19th, where in both instances cooling was associated (at least in part) with the gradual shift of surface winds from southwesterly to northwesterly, as a surface high pushed northeastward behind the easterly-moving low pressure center.

The effect of topography and geographical location on Cascade weather was very essential in attempting to explain the substantial regional snowfall variations (and accompanying avalanche variations) for the post-frontal period on the 22nd. In this storm situation, Washington Pass, Stevens Pass and Crystal Mountain reported 15, 15 and 8 cm new snowfall respectively on the 22nd, while Snoqualamie Pass and Paradise reported 38 and 32 cm snowfall respectively. Here the dominant surface winds throughout the period in question were strongly out of the southwest in the southwestern Cascades and easterly in the northern Cascades, as surface low pressure centered immediately off the Washington coast (see Figure 33). Hence Paradise on the southwest slopes of Mt. Rainier received strong orographic precipitation with Crystal Mountain in the lee receiving relatively light amounts. Also Snoqualamie Pass, far enough south to still provide an orographic barrier to the strong southwesterly flow, received heavy precipitation, while Stevens Pass, farther north and east and hence more in the easterly flow, received accordingly lighter snowfall.

Such geographic and topographic effects are also suggested by the extreme local and regional variations in reported snowfall on the

morning of the 26th, where no reporting station except Crystal Mountain (which recorded 41 cm) received more than 8 cm of new snowfall. During this time predominantly easterly winds occurred in Washington as a surface low pressure center moved eastward over central Oregon on the 25th (see Figure 34), but this alone provides little clue to the observed discrepancies in snowfall amounts, unless Crystal's closer location to the low pressure center, and the lee side exposure of Paradise--the only other extreme southerly station--for this particular flow configuration are also considered.

These examples here and throughout this chapter of regional snowfall variation are presented since they are produced by the interaction of surface winds and topography, and they directly relate to associated avalanche variations and hence avalanche forecasting in the Cascades. While each surface flow situation in any given winter which produces such variations will naturally differ a great deal from another, these instances of substantial regional snowfall variations nevertheless serve to emphasize the importance of topography and geographical location within the Cascades on prediction of snowfall amounts and associated avalanche hazard from a given surface flow pattern. Such variability in regional weather observations points up an obvious need in the avalanche data collection network for more, reliable southerly Cascade reporting stations. In general, though, a definite need exists for both additional northerly and southerly reporting stations, for with this added input, coherent explanations for greatly varying regional meteorology would be greatly enhanced.

The final avalanche situation of the season was associated with the above-mentioned storm occurring only at Crystal Mountain on the

26th, and resulted from rapid accumulation of new snowfall at low temperatures during an extremely short period in the early morning of the 26th. The Crystal Mountain snow ranger reported snowfall beginning at 0015 and ending by 0800. Partial clearing and lowering temperatures the day before effected considerable hardening of the sliding layer to which the subsequent cold, low-density snow only weakly adhered. With these slide releases at Crystal Mountain, March avalanche activity in the Cascades decreased to near zero for the remainder of the month, as high pressure at the surface and aloft brought clearing and a stabilizing snow cover through the 31st. However, as a result of accompanying intense late season radiation into the snowpack, wet loose avalanching of still unconsolidated snow pockets did occur. Paradise and Washington Pass reported wet loose natural slides on the 29th and 30th, respectively.

SUMMARY AND CONCLUSIONS

In an overall fashion, the studies presented here support the findings of Fox (1973), especially in regard to the geographic progression of avalanching in the Cascades in response to similarly progressing frontal systems, and the generally destabilizing effect of warming with or without rain on the Cascade snowpack (see below).

More specifically, probable relationships were established between avalanche associated layers and the weather which produced them, and between regional meteorology variations and similar regional variations in reported avalanching. The general snowpack or meteorological phenomena indicated by this study to have an effect on Cascade avalanching are given below, along with a brief description of how these phenomena occurred and how they affected avalanching.

(a) Melt-freeze crusts--these crusts were produced by refreezing of snow following either radiation-induced surface melt or the introduction of rain into the snowpack (associated with a warm, moist southwesterly flow at the surface). They were observed as the sliding surface in numerous avalanche situations (VI.2.4) due to poor bonding with overlying snow layers. The presence of impervious ice layers within these melt-freeze crusts appeared to be quite important in limiting the depth (and therefore severity) of subsequent slide action by inhibiting downward rainwater percolation (VI.2.2, VI.2.6).

(b) Warming trends, timing of warming--warming during snowfall (VI.2.2, VI.2.7), alternating cooling and warming during snowfall (VI.2.8), heavy rain after significant snowfall (VI.2.2, VI.2.4) and warm air overriding at the passes (VI.2.2) all played significant roles in generation of Cascade avalanche activity through their basic destabilizing effect on bonding within the existing snowpack, and generally associated high rate of snowpack loading due to accompanying dense, wetter snowfall. The passage of one or more cold front systems or occlusions in a general southwesterly upper level flow was responsible for all of these avalanche-generating meteorological situations as cold air from east of the Cascades was dislodged from the passes, resulting in a warming trend. In heavy avalanching situations, substantial but sometimes slow warming accompanied the occlusions, while lighter avalanche occurrences and less warming tended to accompany the cold fronts (VI.2.7).

Given the destabilizing influence of these various phenomena on the Cascade snowpack, the timing of such warming trends in the various avalanche-prone areas is apparently very important. This timing was also examined in regard to various surface winds preceding and following cold fronts and occlusions in the Cascades, and rough guidelines for relative timing of warming on the western slope and the passes were established for the investigated instances. These rough guidelines indicate that in instances with warm west-southwesterly surface winds both preceding and following (occluded) frontal passage, warming at

the passes occurred much later than on the western slope, and substantially later than would have occurred in a warm front-cold front situation with following northwesterly winds (VI.2.4).

(c) Temperature-gradient weakening of rain crusts (refrozen rain-soaked layers)--warm and very moist southwesterly, upper-level flow followed by extended periods of strong and cold, northwesterly flow aloft and predominantly cold, easterly pass winds at the surface, resulted in substantial weakening of developed rain crusts through the effect of temperature-gradient metamorphism (VI.2.4). Strong radiational cooling at the surface associated with clear nights was shown to play a similar function in snowpack decomposition and later avalanche release (VI.2.6, VI.2.7). It is important to emphasize here that such temperature-gradient weakening of the snowpack has been previously considered to be a major problem only in more continental climates (e.g., the Rockies). However, given certain weather and snowpack conditions in the Washington Cascades, it is apparent that such temperature-gradient metamorphism can be a significant factor in Cascade avalanche release as well.

(d) Regional weather variations, pass versus non-pass weather--regional snowfall variations were observed to produce related regional variations in avalanche activity in the Cascades. Possible reasons for the various differences in snowfall between different areas are related to surface flow patterns (VI.2.1), geographical location (VI.2.2, VI.2.8), and topography (VI.2.8). An example was found where consistently different new snowfall amounts between two areas (Stevens Pass and Crystal Mountain) following generation of a weak temperature-

gradient layer within the snowpack led to substantial differences in the character of sliding surfaces (VI.2.7).

Substantial variations in local meteorological conditions (e.g., temperature and wind) between pass and non-pass areas were observed, and explained by the presence (or absence) of cold, easterly surface winds prior to frontal passage (VI.2.3, VI.2.5). The relationship of cold, easterly pass winds to avalanche-generating layers in the Cascade snowpack was also discussed (VI.2.1), and the adverse effect of extended periods of such cold easterly winds on the Cascade snowpack was demonstrated in the temperature gradient weakening of surface snow layers discussed in (c) above.

(e) Wind--wind-slab deposition (VI.2.1, VI.2.3, VI.2.5), and breaks in wind and snowfall (VI.2.1, VI.2.7) were found to be related to changing surface pressure gradients accompanying frontal passages and associated wind-slab avalanching. Temporal variation in wind speed was shown to be a significant factor in producing snowpack instability in both cases.

Wind removal (scouring) of surface snow down to a fairly hard but unstable underlayer (a weakened melt-freeze crust) followed by heavy snowfall was found to be related to subsequent avalanche release in exposed locations (VI.2.4). The strong winds evidenced by such scouring were associated with an intense west to east pressure gradient following strong cold-frontal passage, and the ensuing heavy snowfall resulted from strong, moist, onshore flow both at the surface and aloft.

(f) Cooling during snowfall--lowering temperatures during heavy snowfall, in response to cold post-frontal surface winds, generally

produced stabilization of the snowpack through hardening of the older, warmer snow, good bonding in transitional layers, and rapid settlement and sluffing of the newer, colder snow (VI.2.8). However, with heavy snowfall and very rapid drops in temperature immediately following rain and warm, wet snow deposition, some instability in the snowpack was observed resulting from crust formation in the warm, wet layer through conduction cooling (VI.2.2).

REFERENCES

Eugster, H. P., 1952: Beitrag su einer Gefüge Analyse des Schnees, Betr. z. Geologie der Schweiz. Geotech. Serie-Hydrologie, Lieferung 5.

Yosida, Z., 1963: "Physical Properties of Snow," Ice and Snow (Proc. of M.I.T. Conf., 1962), pp. 493-495.

Figure 1. Surface Weather Map for 2200 PST, 1/3/75. Isobars indicating surface pressure in mb are shown as continuous lines; plotted station weather data follow the international code form for surface weather reports.

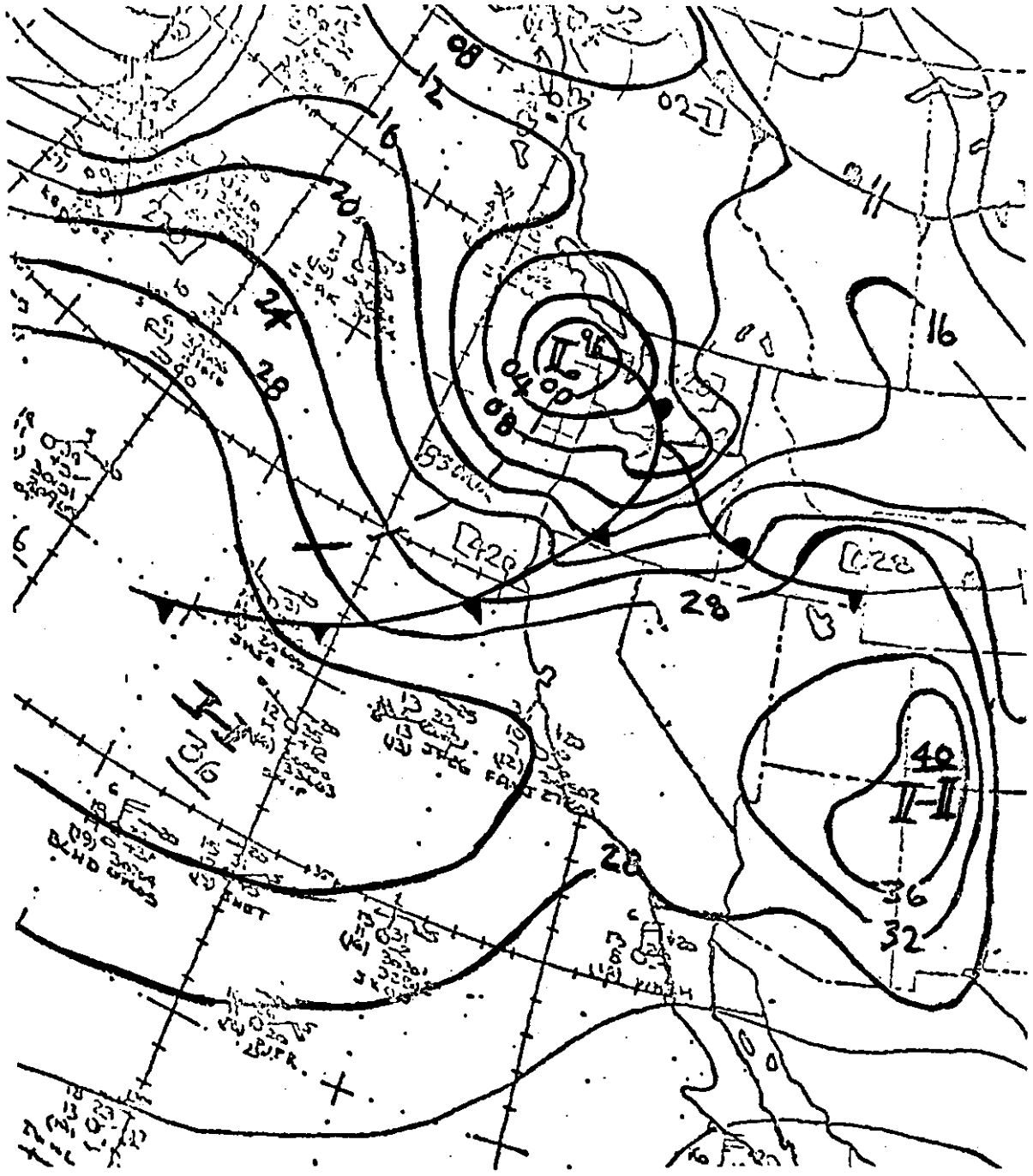

Figure 2. Surface weather map for 0400 PST, 1/5/75. Surface isobars and plotted station weather data are shown, and are described in Figure 1.

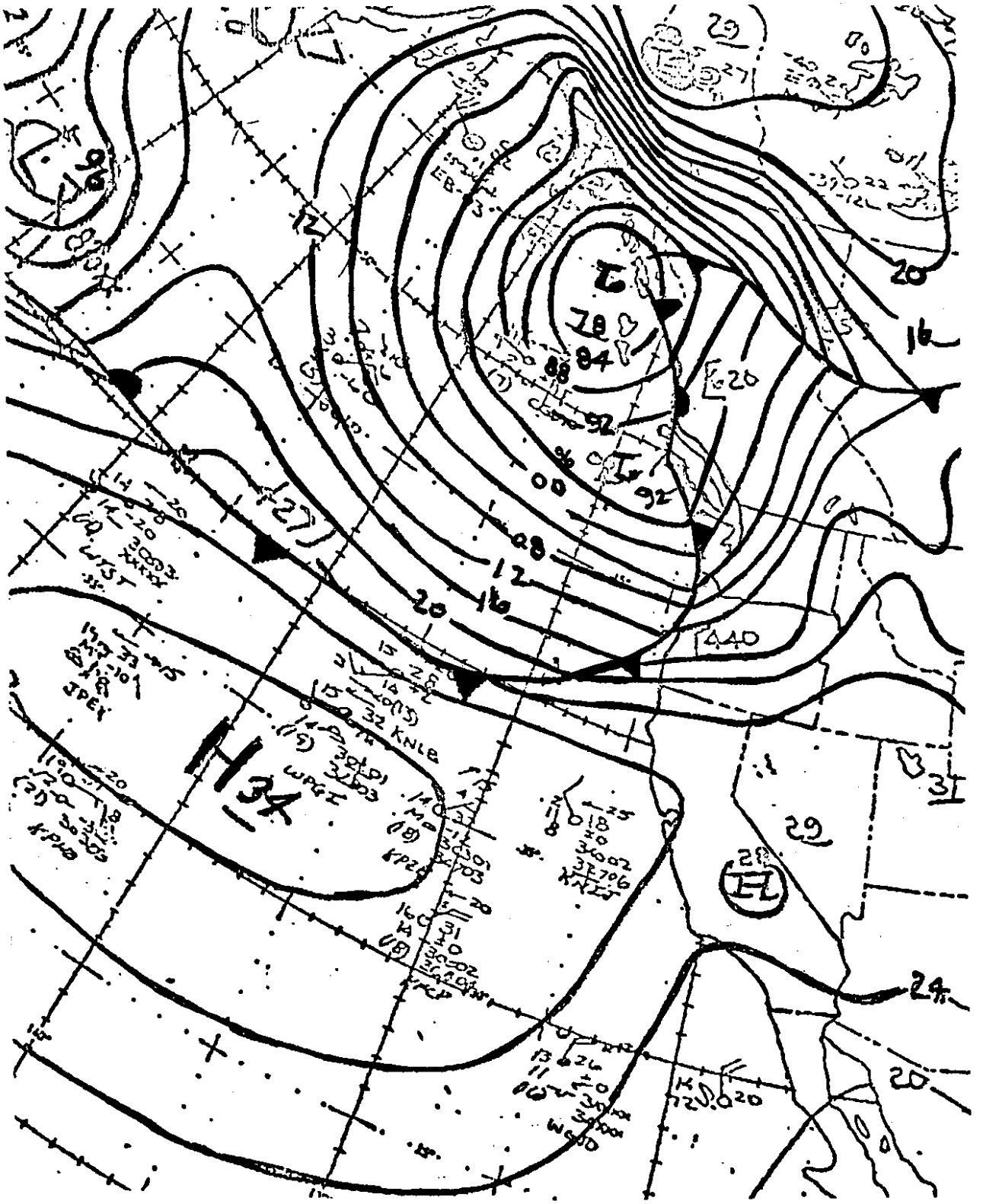

Figure 3. Fracture-line Profile of Slab Avalanche at Stevens Pass, 1/11/75. Variations with snow depth of density (▲), temperature (●), rain resistance (▨) and stratigraphy (shown on left of figure) for the particular time and area indicated are shown. Interpretation of abbreviations and symbols used in the stratigraphy is given in Figure 3(a).

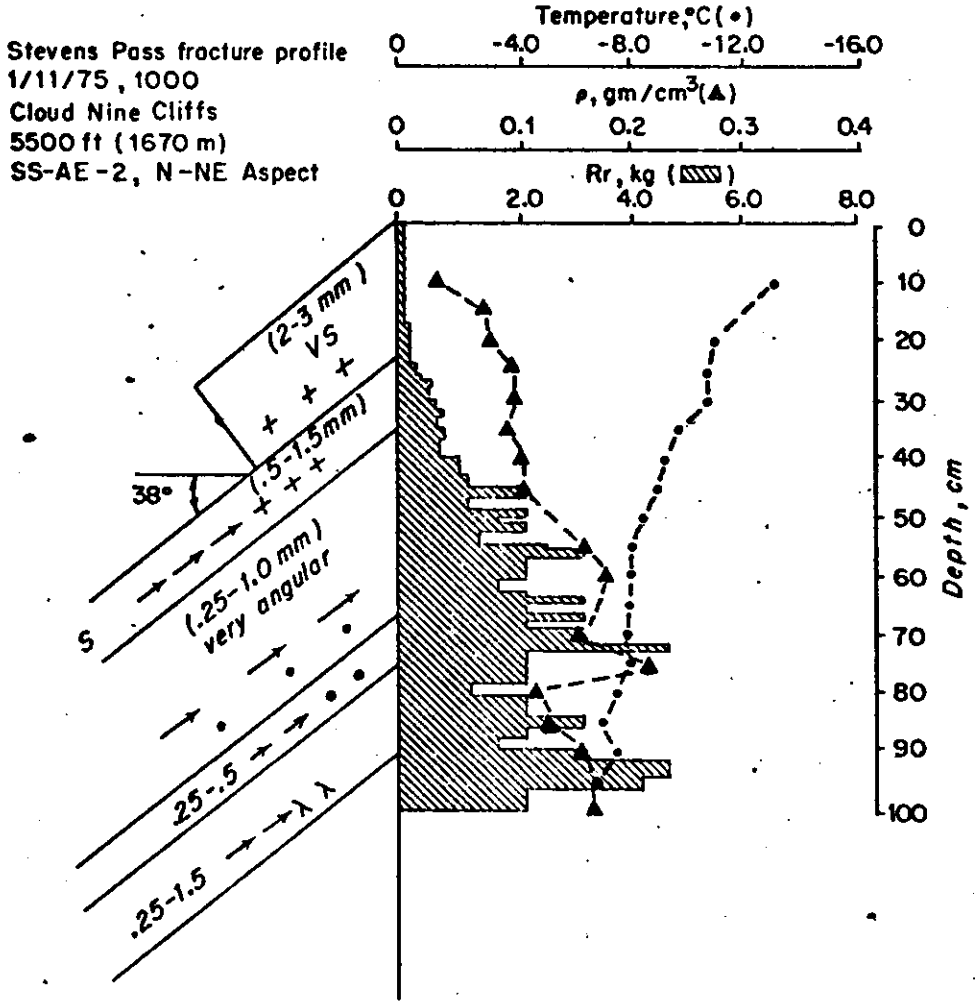

Figure 3(a). Interpretation of Snow Profile Symbols and Abbreviations.

Basic Crystal Classification (after personal communication with E. R. LaChapelle)

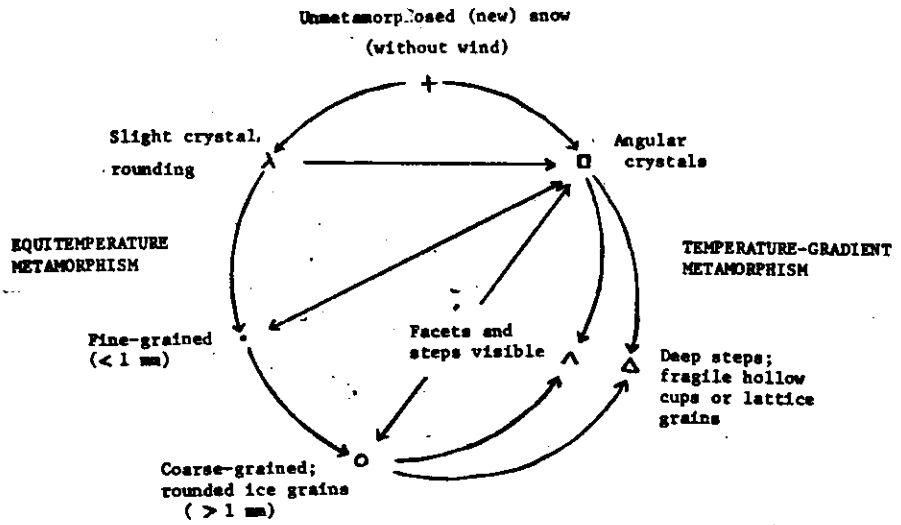

Transitions between stages are designated with an arrow (e.g., • ⟶ O).

Arrows alone or with one crystal type indicate wind action with various degrees of fragmented crystals (see below).

Additional layering symbols

Symbol	Meaning
→→ ++	Wind action shown by slightly fragmented new snow (no rounding)
→→ ʎʎ	Wind action shown by slightly fragmented new snow with some crystal rounding
→→ • •	Heavy wind action shown by newly-deposited, angular, fine-grained snow
	Rain crust (refrozen rain-soaked layer)
	Rain-soaked layer
	Sun crust
	Decomposed layer, probable temperature-gradient metamorphism acting
	Ice layer

Abbreviations Used

FG	--	fine-grained
CG	--	coarse-grained
MF	--	melt-freeze
SS	--	soft slab
HS	--	hard slab
AS, AE, AA	--	refer to mechanism of artificial avalanche release--by ski (AS), explosive (AE) or artillery (AA)

Rough Snow Strength Designations

VS	--	very soft
S	--	soft
M	--	medium
MH	--	medium hard
H	--	hard
VH	--	very hard

Avalanche Classifications

In each fracture-line profile the observed avalanche in classified as to type, method of release, and size. Abbreviations for type and method of release are given above. Size classification follows the scheme of the U. S. Forest Service using a scale from 1-5, where 1 denotes a sluff and 5 stands for the maximum possible size that a slide could attain in its particular chute. Hence, SS-AE-3 represents a medium-sized, soft-slab avalanche released artificially by explosives.

Figure 4. Twenty-four Hour Maximum and Minimum Temperatures for Snoqualamie Pass, Stevens Pass, and Paradise, January-March, 1975. The abbreviation NA has the same meaning as given in Figure 23.

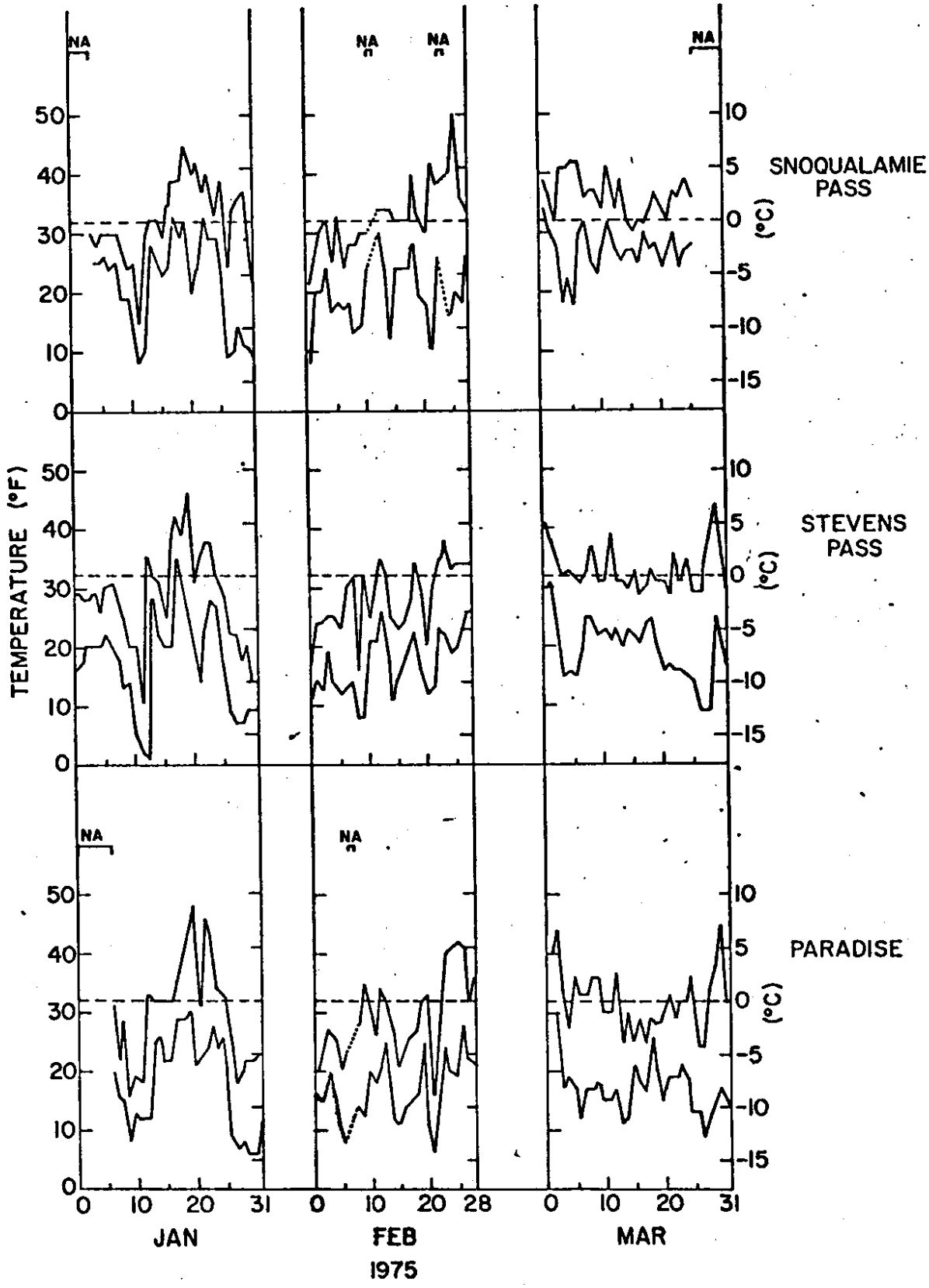

Figure 5. Twenty-four Hour Maximum and Minimum Temperatures for Washington Pass and Crystal Mountain, January-March, 1975. The abbreviation NA has the same meaning as given in Figure 23 .

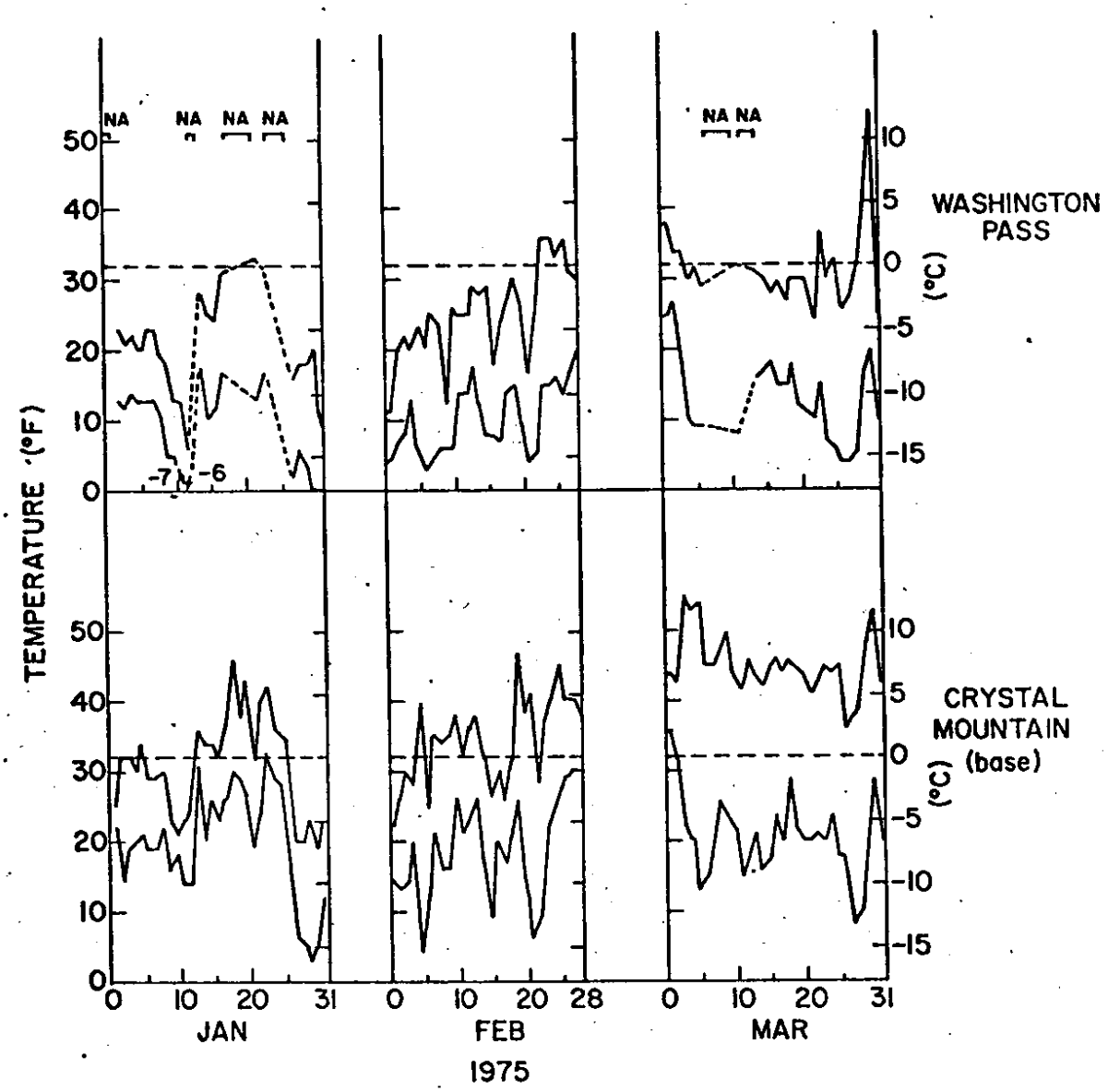

Figure 6. Surface and 500 mb Weather Maps for 0400 PST, 1/11/75.

(a) Surface Map, 0400 PST, 1/11/75. Surface isobars and plotted station weather data are shown, and are described in Figure 1.

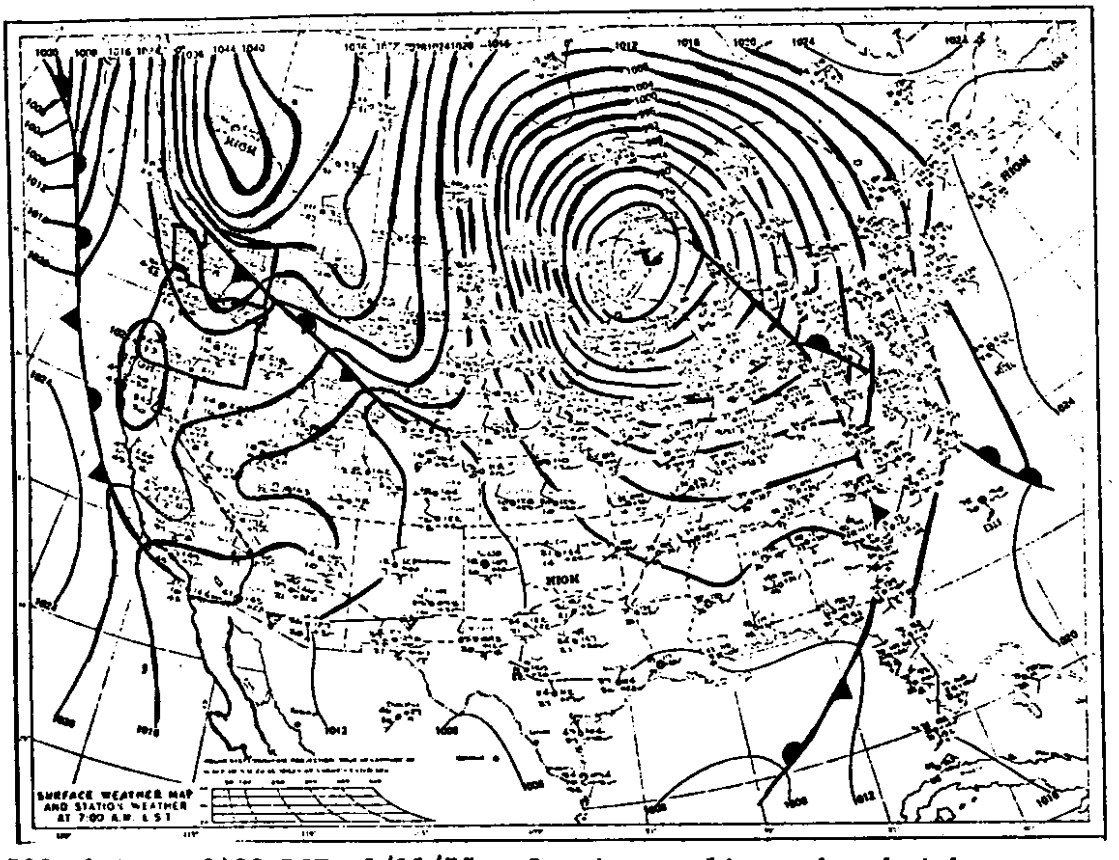

(b) 500 mb Map, 0400 PST, 1/11/75. Continuous lines show height contours of the 500 mb pressure surface labeled in feet above sea level. Dashed lines represent isotherms labeled in degrees Celsius. Arrows show the wind direction and speed at the 500 mb level.

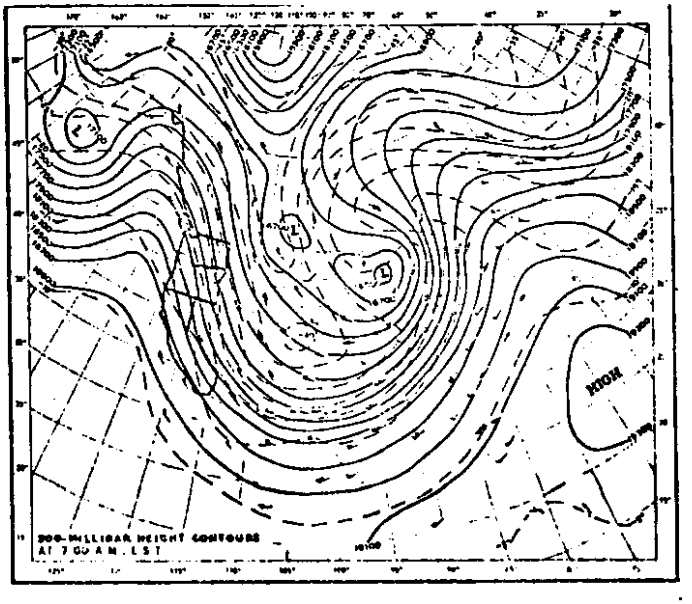

Figure 7. Fracture-line Profile of Slab Avalanche at Stevens Pass, 1/15/75. See Figure 3 for explanation of snow profile data.

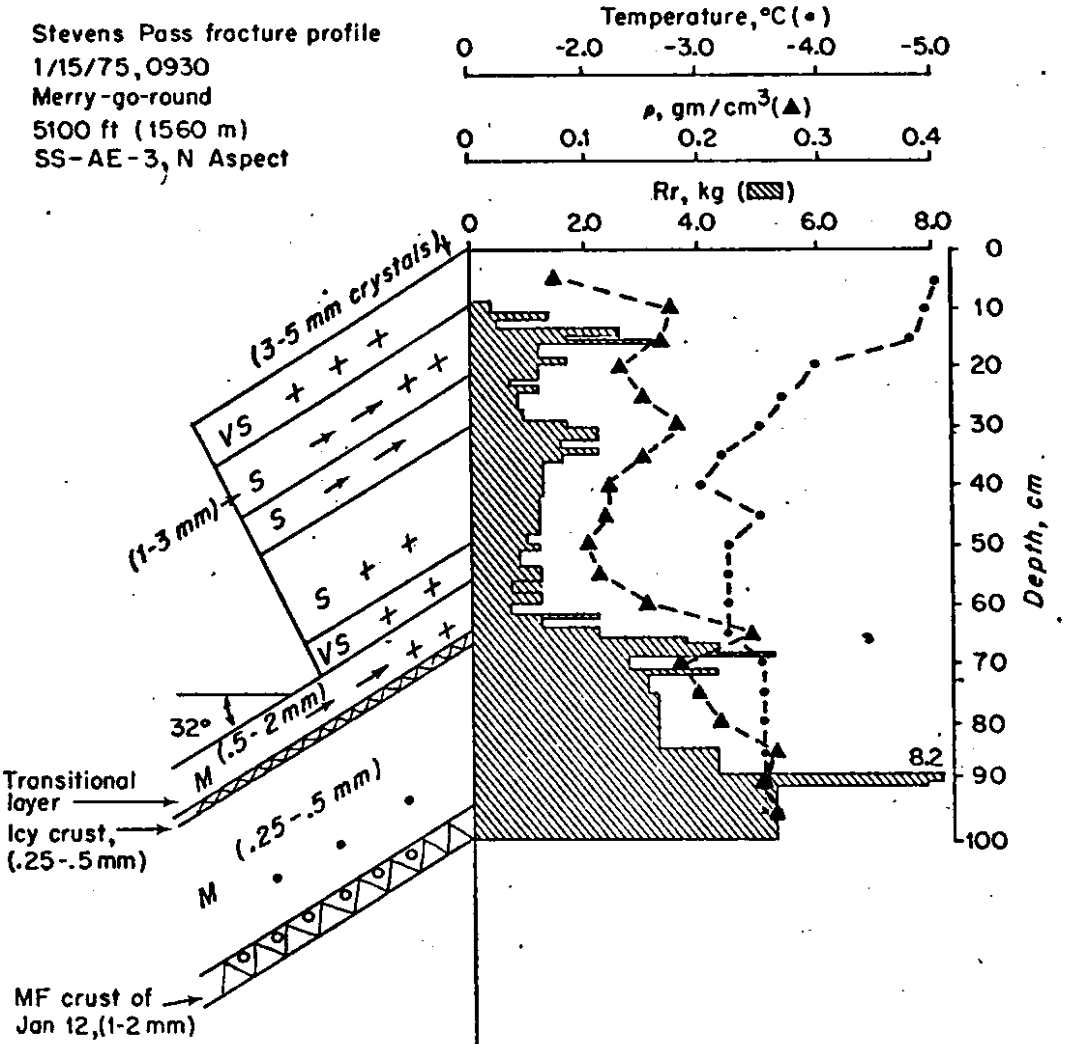

Figure 8. Surface Weather Map for 1600 PST, 1/16/75. Surface isobars and plotted station weather data are shown, and are described in Figure 1.

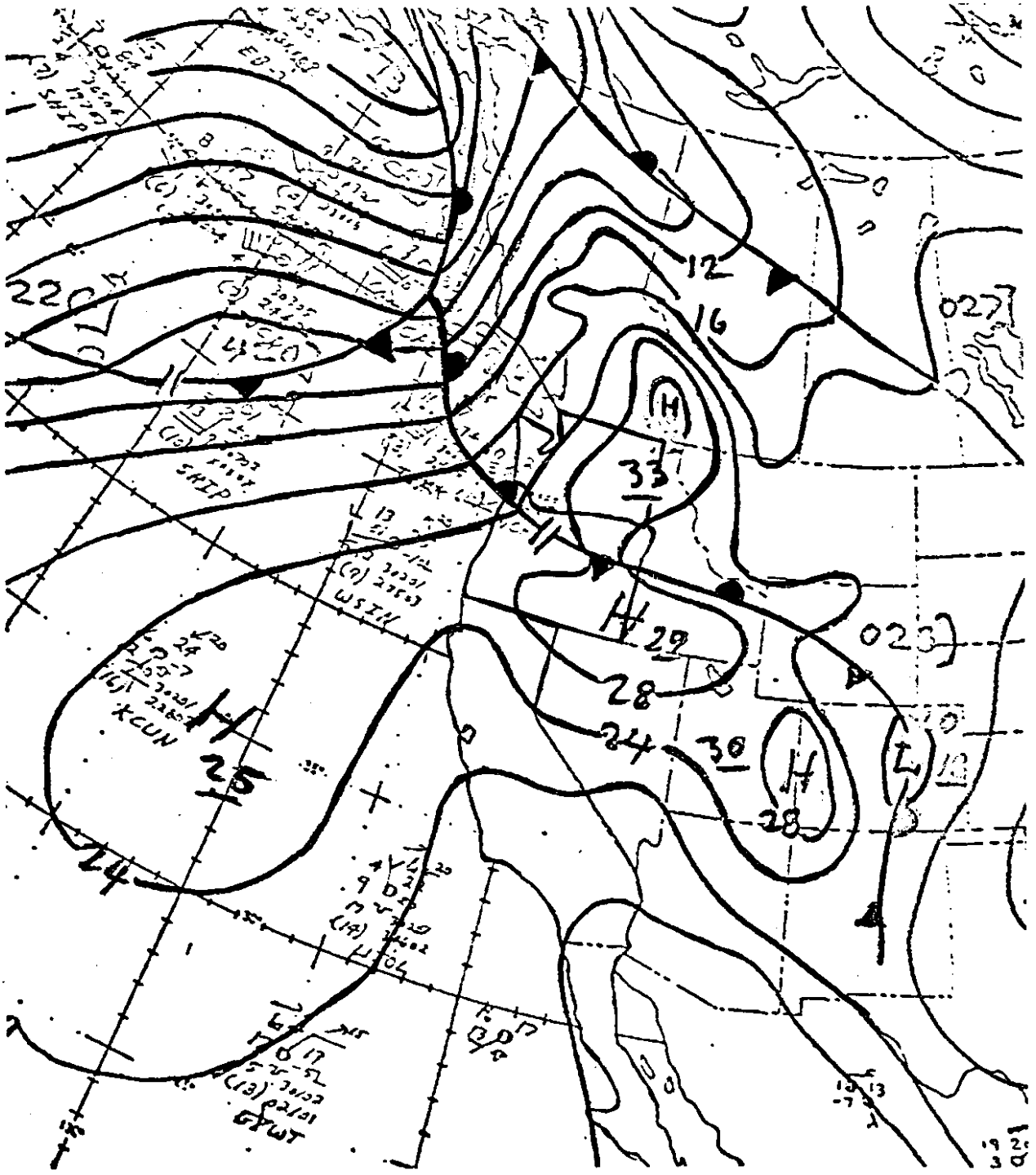

Figure 9 . Snowpit Study at Stevens Pass, 1/18/75. See Figure 3 for explanation of snow profile data.

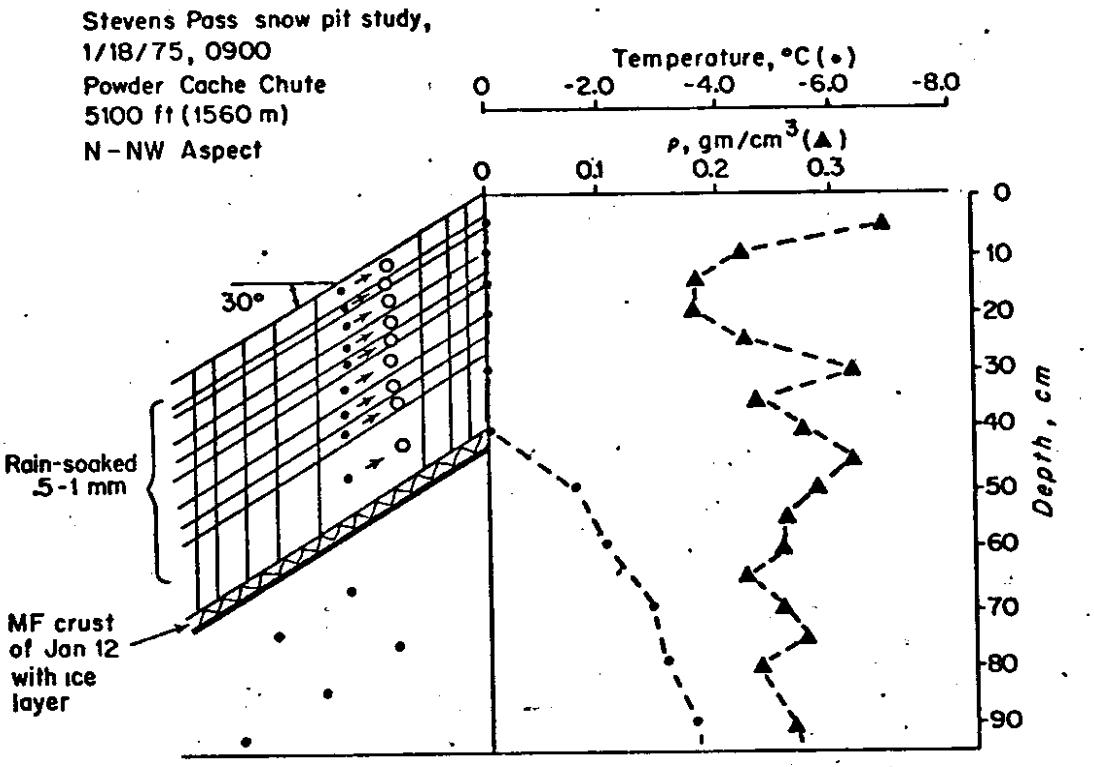

Figure 10. Fracture-line Profile of Slab Avalanche at Stevens Pass, 1/25/75. See Figure 3 for explanation of snow profile data.

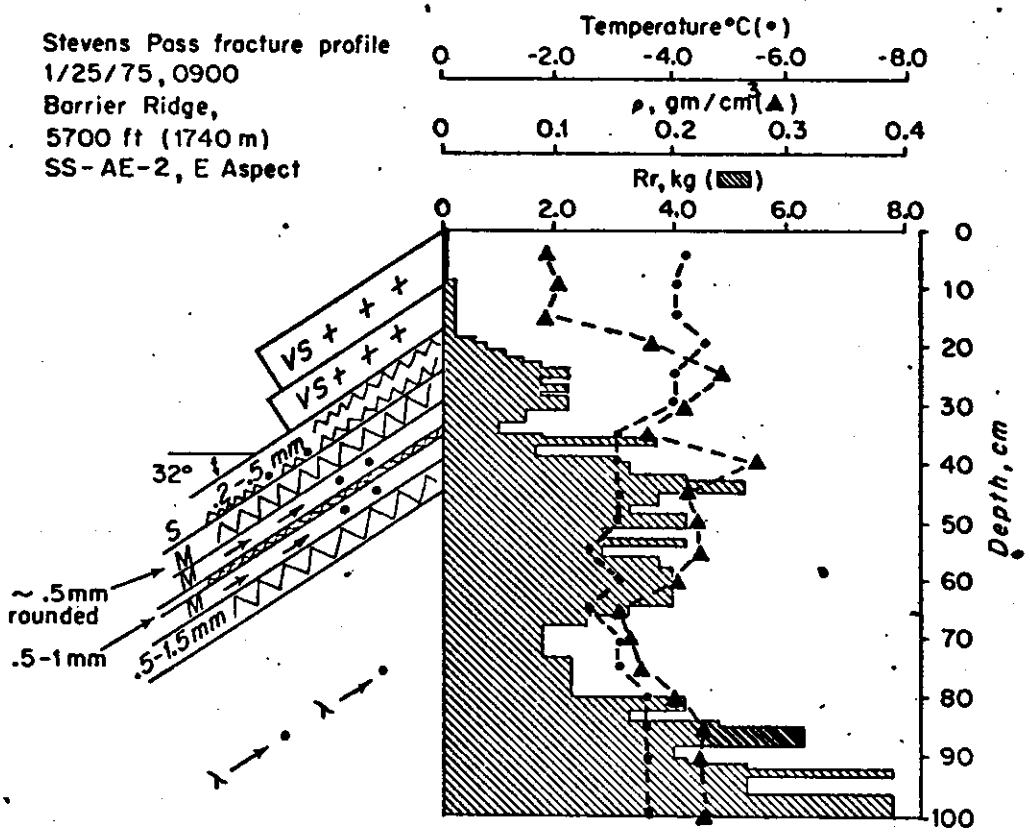

Figure 11. 500 mb Weather Maps for 0400 PST, 1/27/75-1/30/75. 500 mb height contours, isotherms and winds are shown, and are described in Figure 6 (b).

(a) 500 mb Map, 0400 PST, 1/27/75.

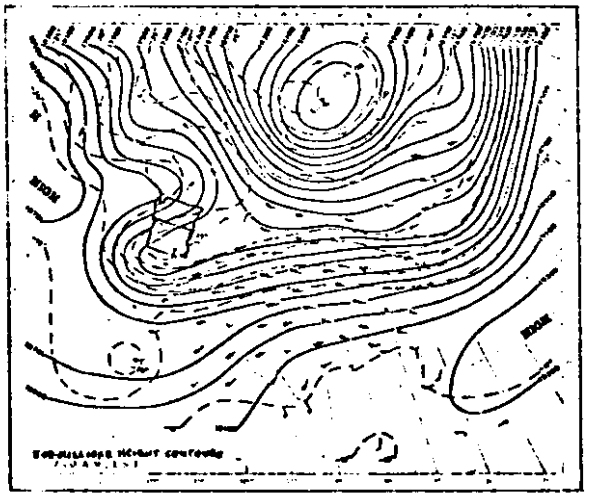

(b) 500 mb Map, 0400 PST, 1/28/75.

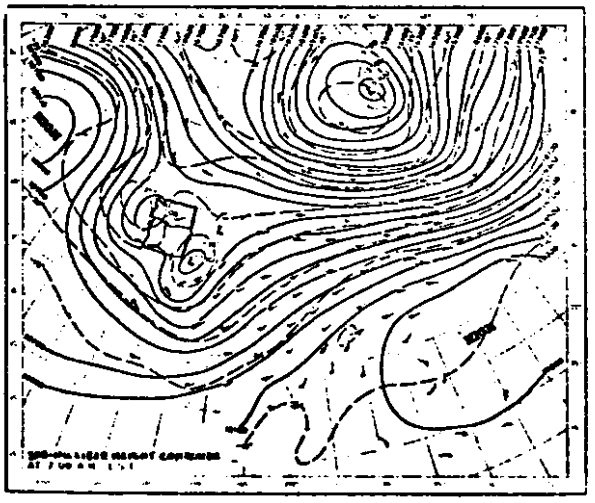

(c) 500 mb Map, 0400 PST, 1/29/75.

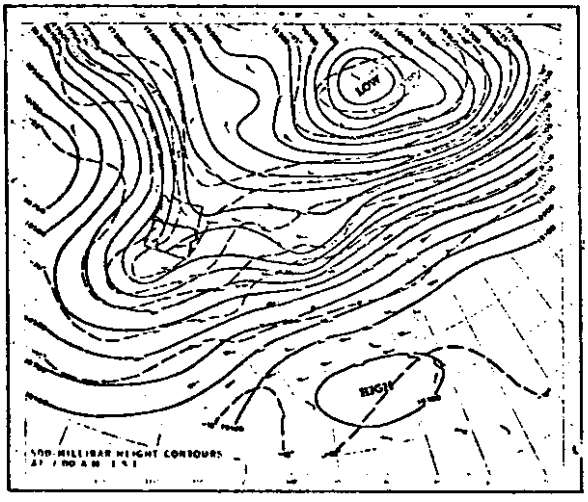

(d) 500 mb Map, 0400 PST, 1/30/75.

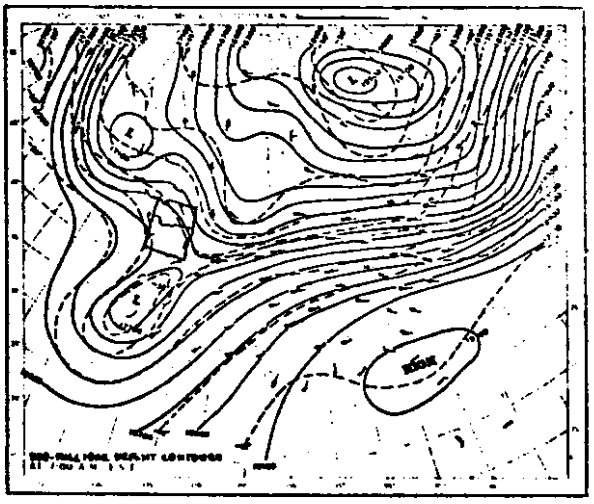

Figure 12. 500 mb Weather Maps for 0400 PST, 2/1/75-2/4/75. 500 mb height contours, isotherms and winds are shown, and are described in Figure 6 (b).

(a) 500 mb Map, 0400 PST, 2/1/75.

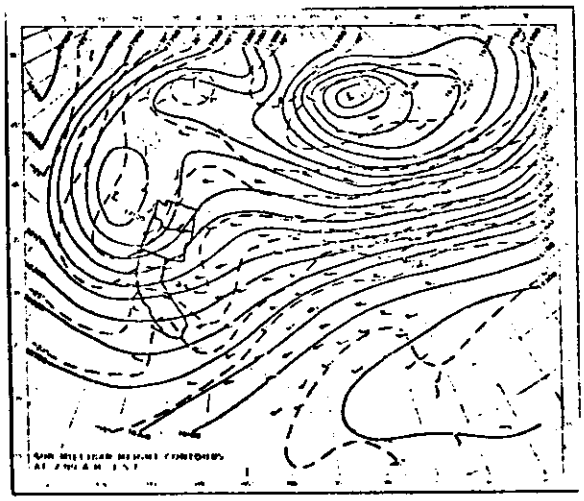

(b) 500 mb Map, 0400 PST, 2/2/75.

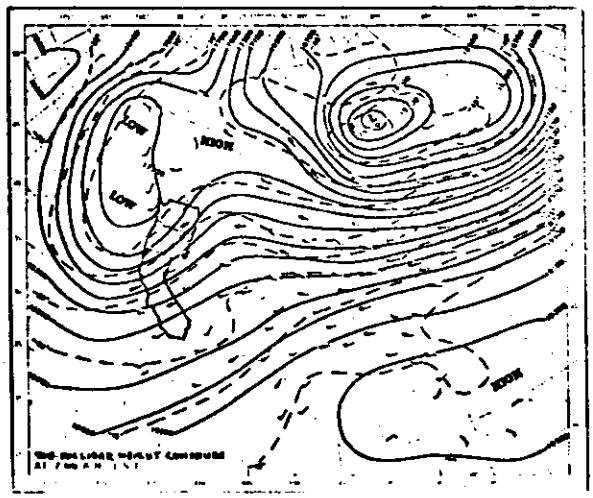

(c) 500 mb Map, 0400 PST, 2/3/75.

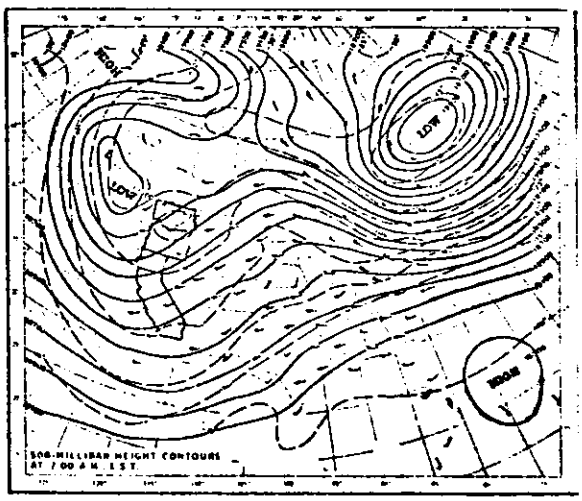

(d) 500 mb Map, 0400 PST, 2/4/75.

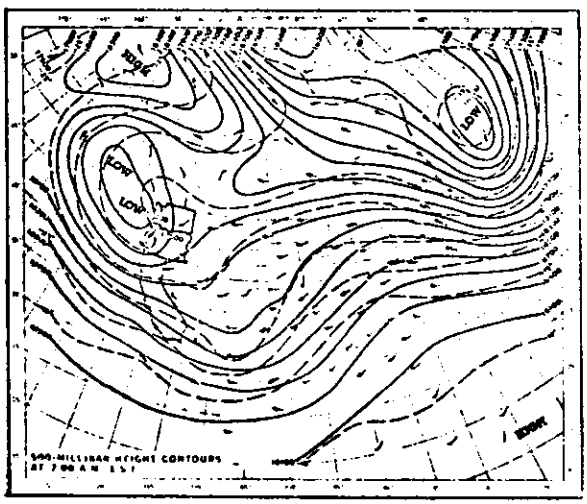

Figure 13. Surface Weather Maps for 1600 PST, 1/31/75, and 0400 PST, 2/3/75. Surface isobars and plotted station weather data are shown, and are described in Figure 1.

(a) Surface Map, 1600 PST, 1/31/75.

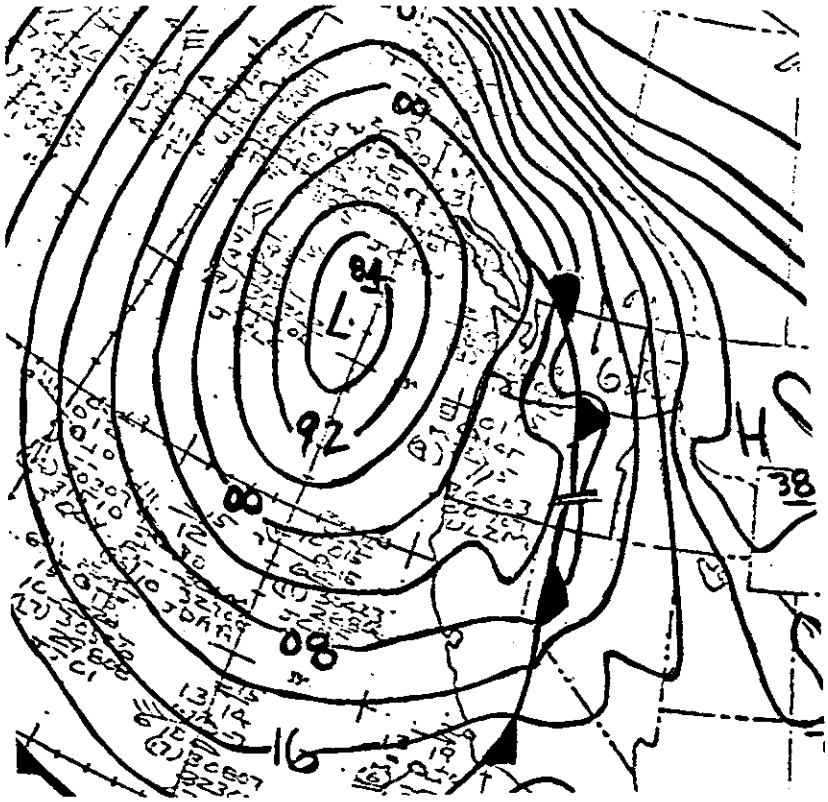

(b) Surface Map, 0400 PST, 2/3/75.

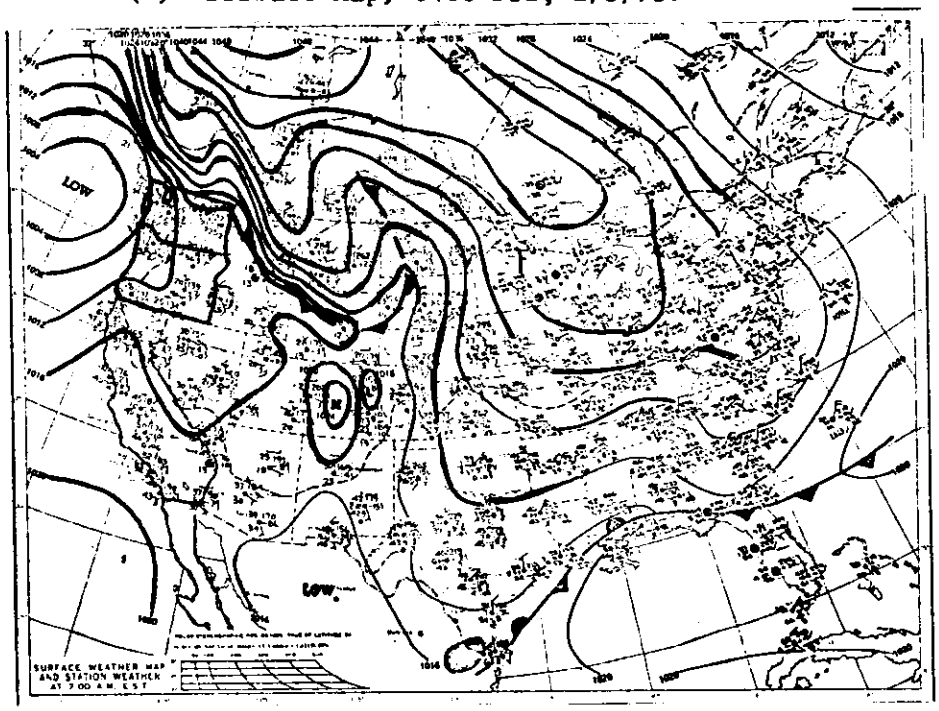

Figure 14. Snowpit Study at Stevens Pass, 1/31/75. See Figure 3 for explanation of snow profile data.

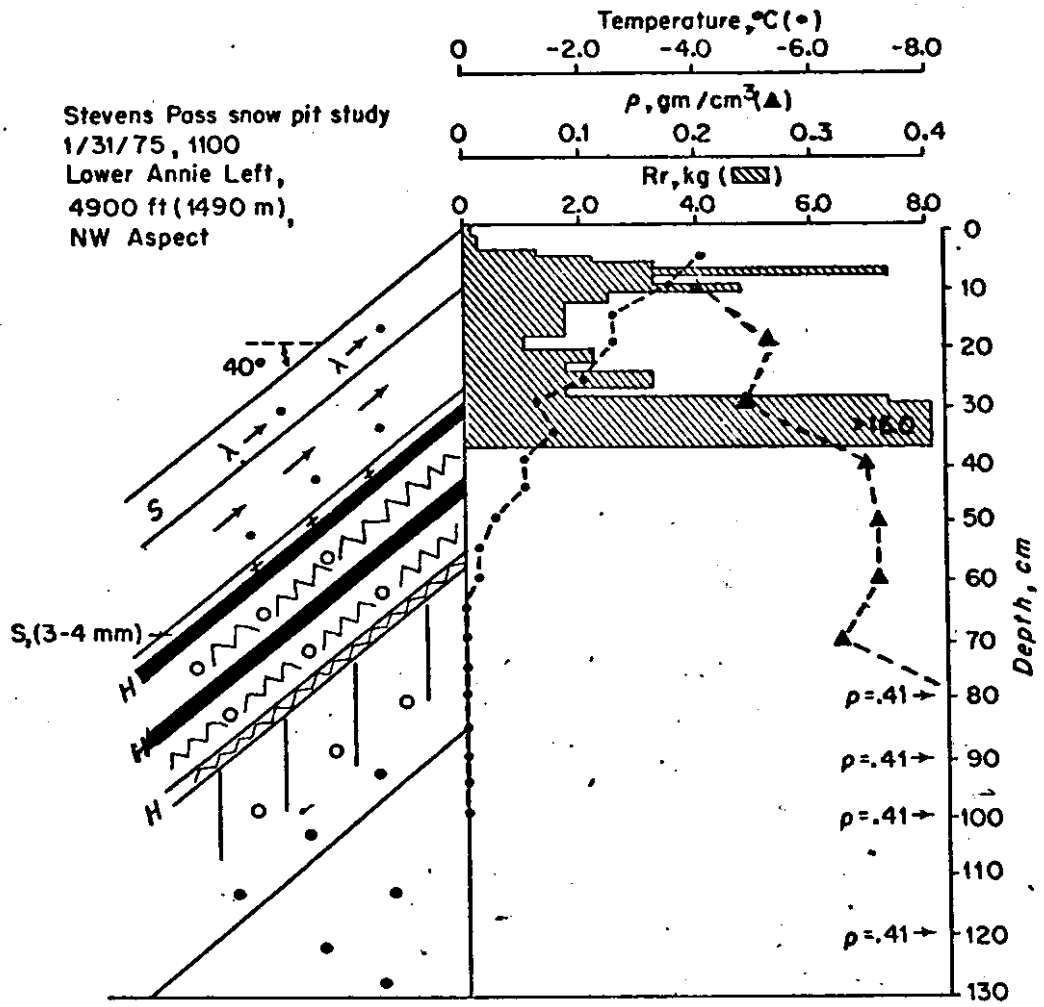

Figure 15. Fracture-line Profile of Slab Avalanche at Stevens Pass, 2/1/75. See Figure 3 for explanation of snow profile data.

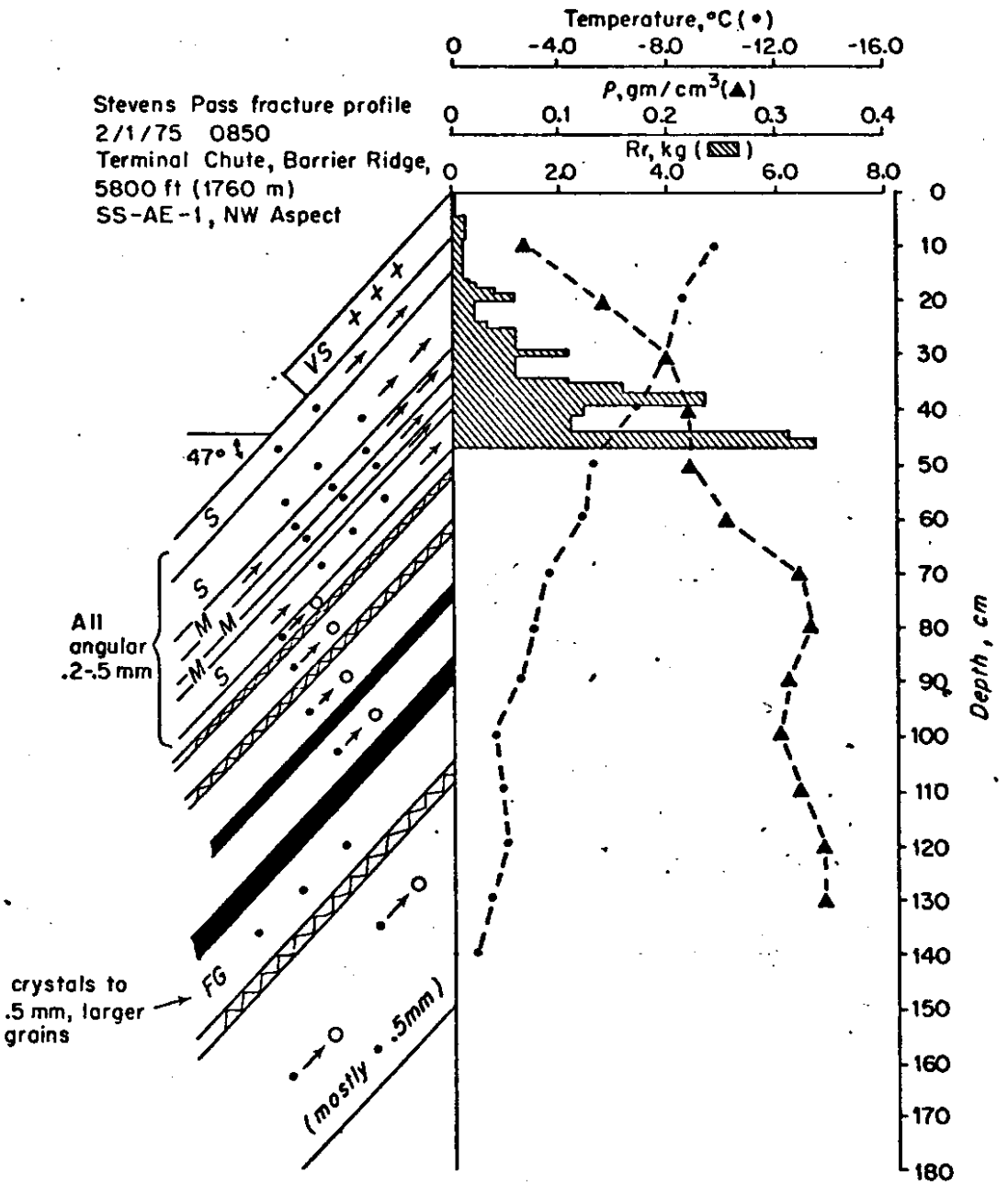

Figure 16. Snowpit Study at Stevens Pass, 2/5/75. See Figure 3 for explanation of snow profile data.

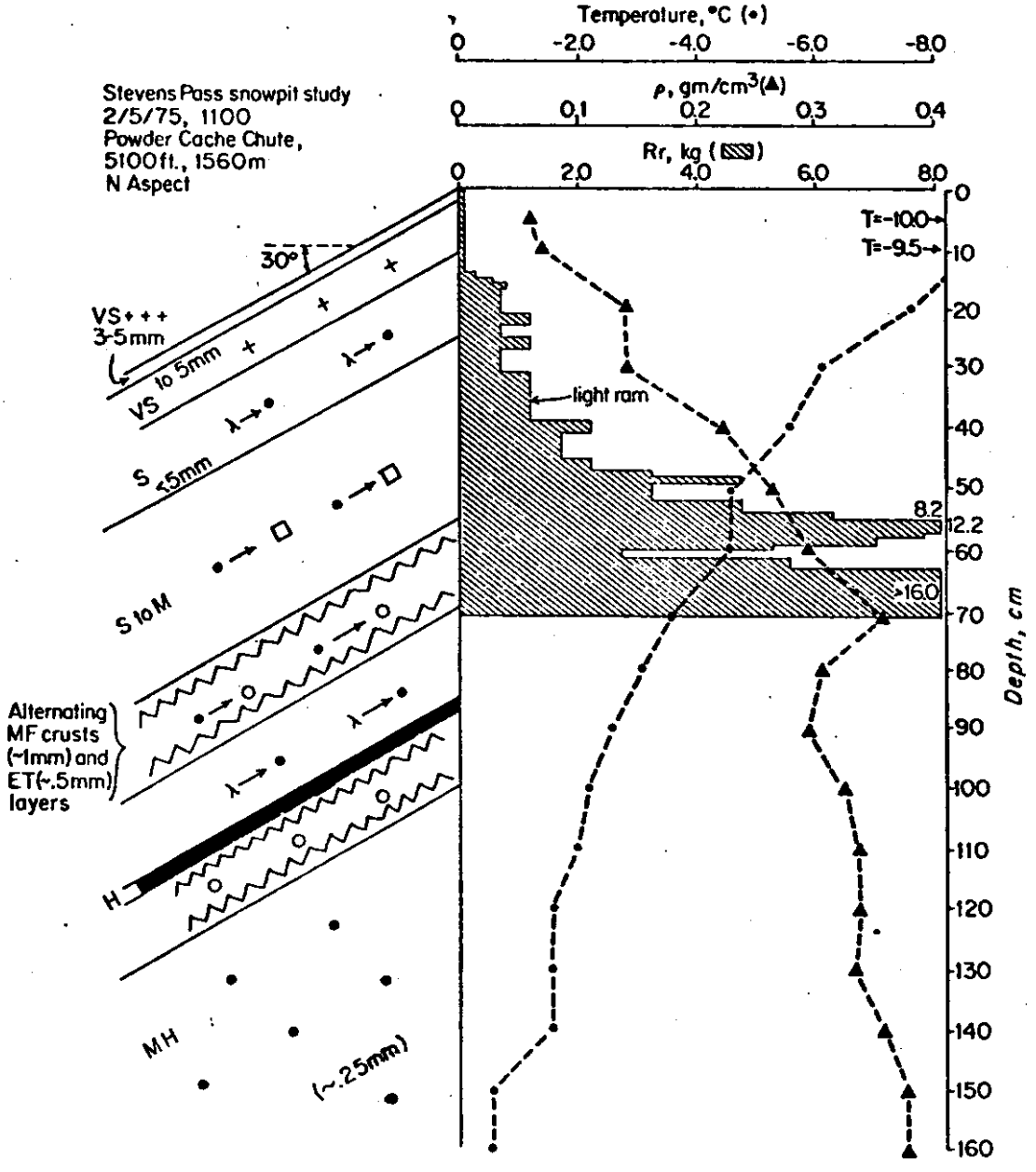

Figure 17. Fracture-line Profile of Slab Avalanche at Stevens Pass, 2/7/75. See Figure 3 for explanation of snow profile data.

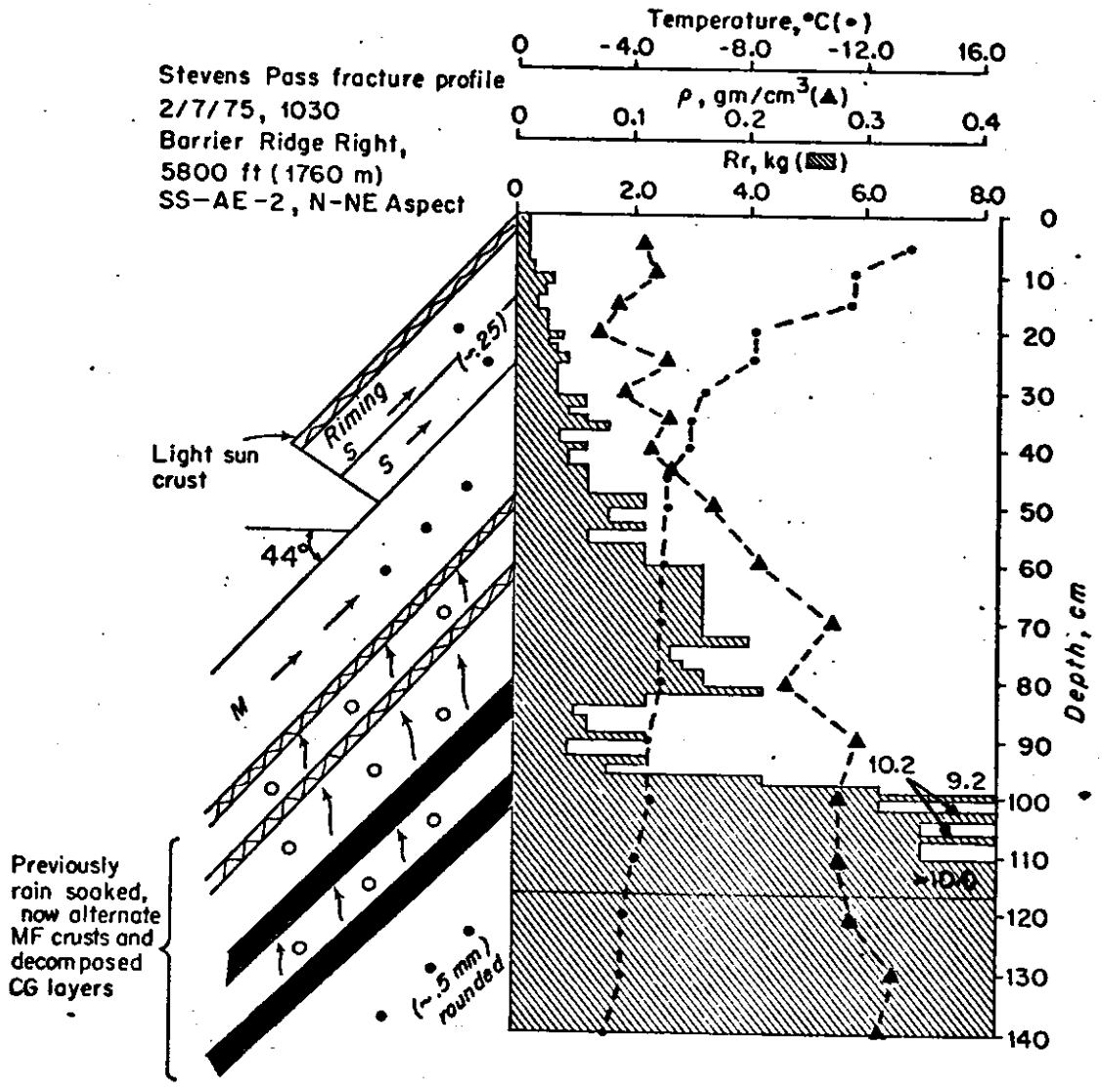

Figure 18. 500 mb Weather Maps for 0400 PST, 2/9/75 and 2/10/75. 500 mb height contours, isotherms and winds are shown, and are described in Figure 6 (b).

(a) 500 mb Map, 0400 PST, 2/9/75.

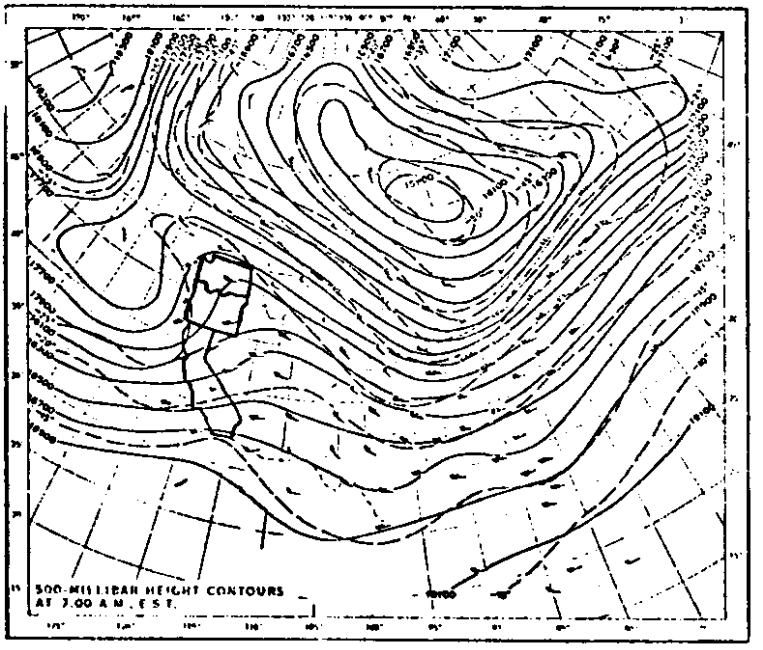

(b) 500 mb Map, 0400 PST, 2/10/75.

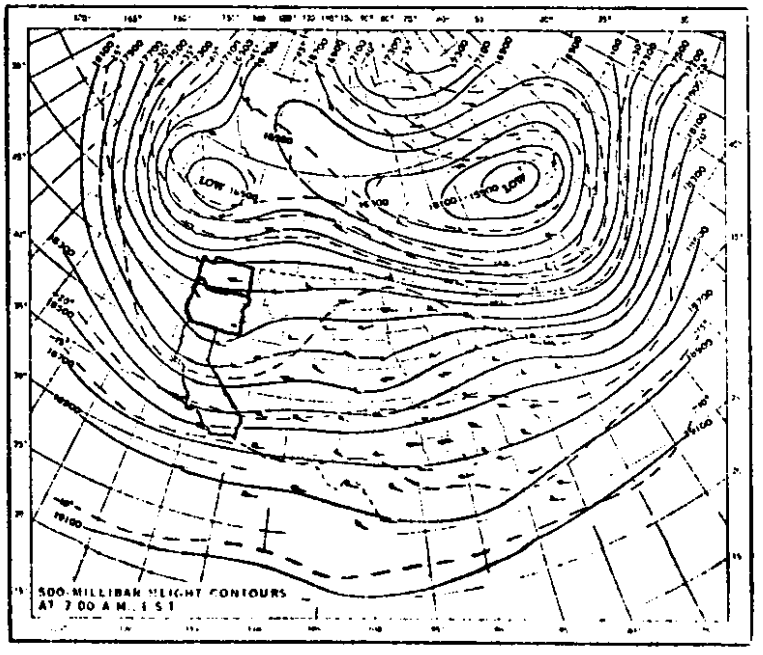

Figure 19. Fracture-line Profile of Slab Avalanche at Stevens Pass, 2/14/75. See Figure 3 for explanation of snow profile data.

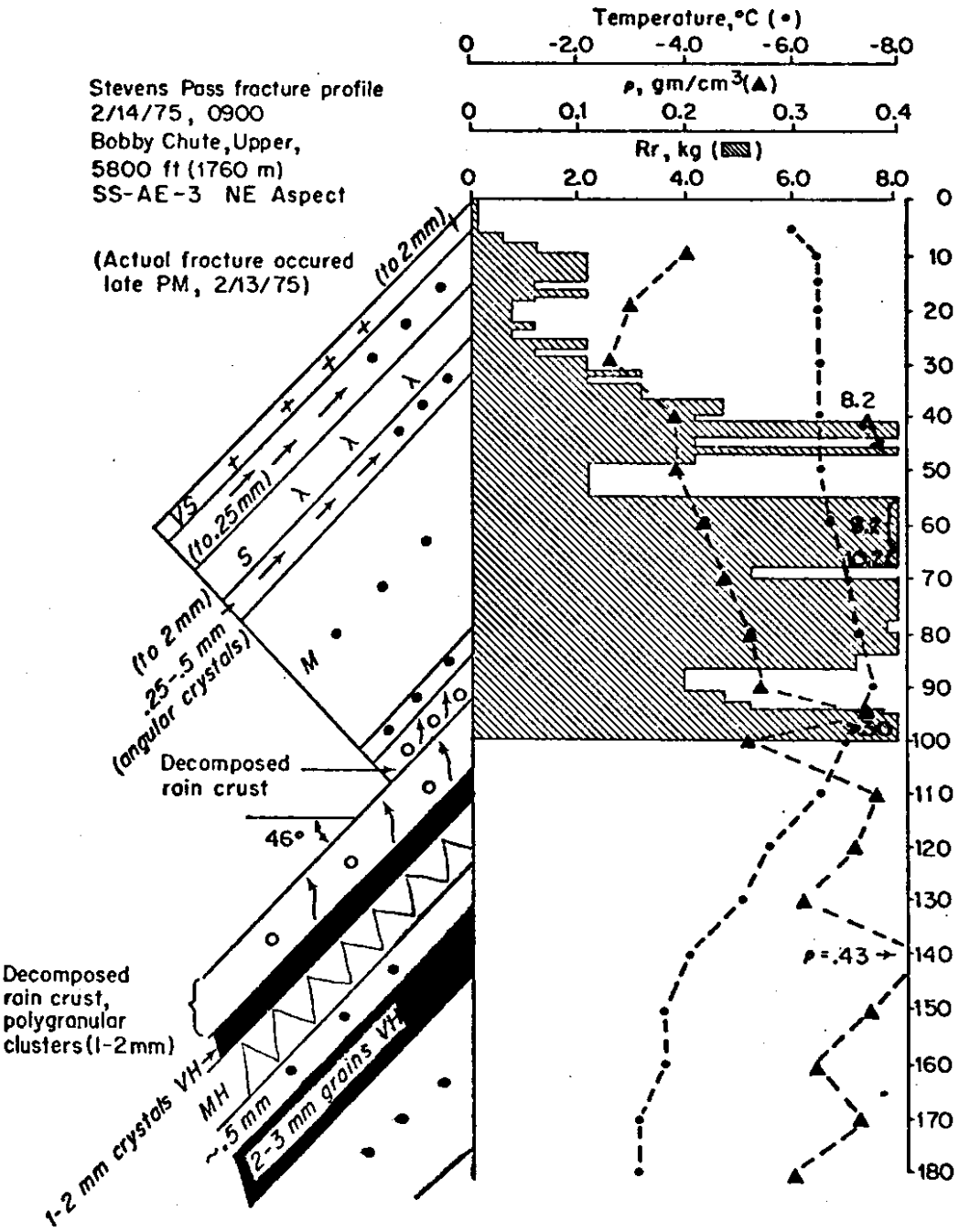

Figure 20. Fracture-line Profile of Slab Avalanche at Stevens Pass, 2/15/75. See Figure 3 for explanation of snow profile data.

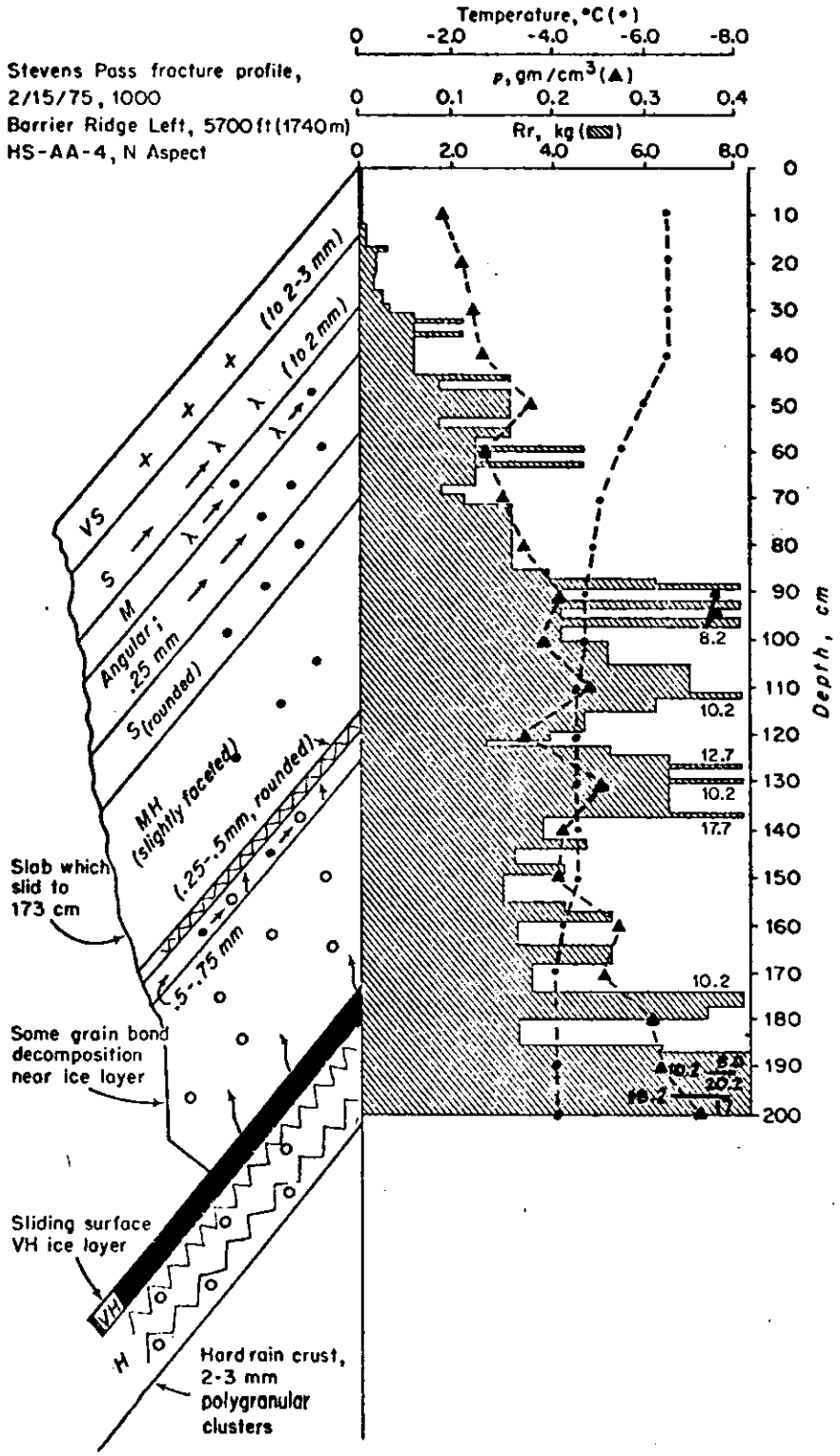

Figure 21. Surface Weather Maps for 0400 PST, 2/12/75, and 1000 PST, 2/19/75. Surface isobars and plotted station weather data are shown, and are described in Figure 1.

(a) Surface Map, 0400 PST, 2/12/75.

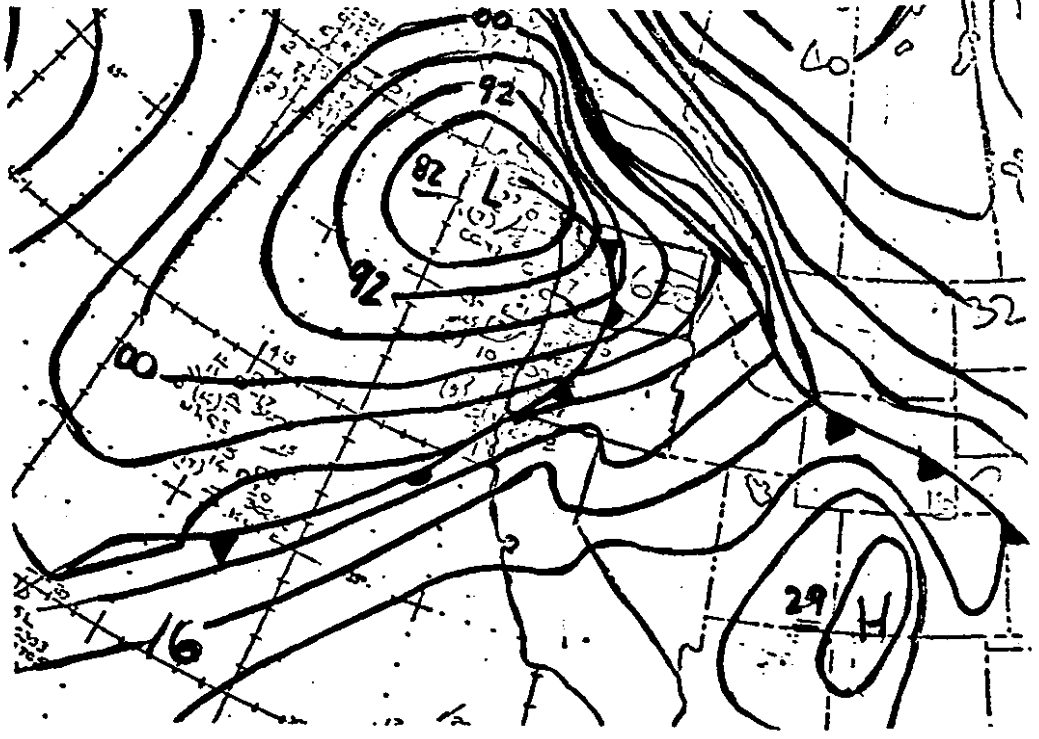

(b) Surface Map, 1000 PST, 2/19/75.

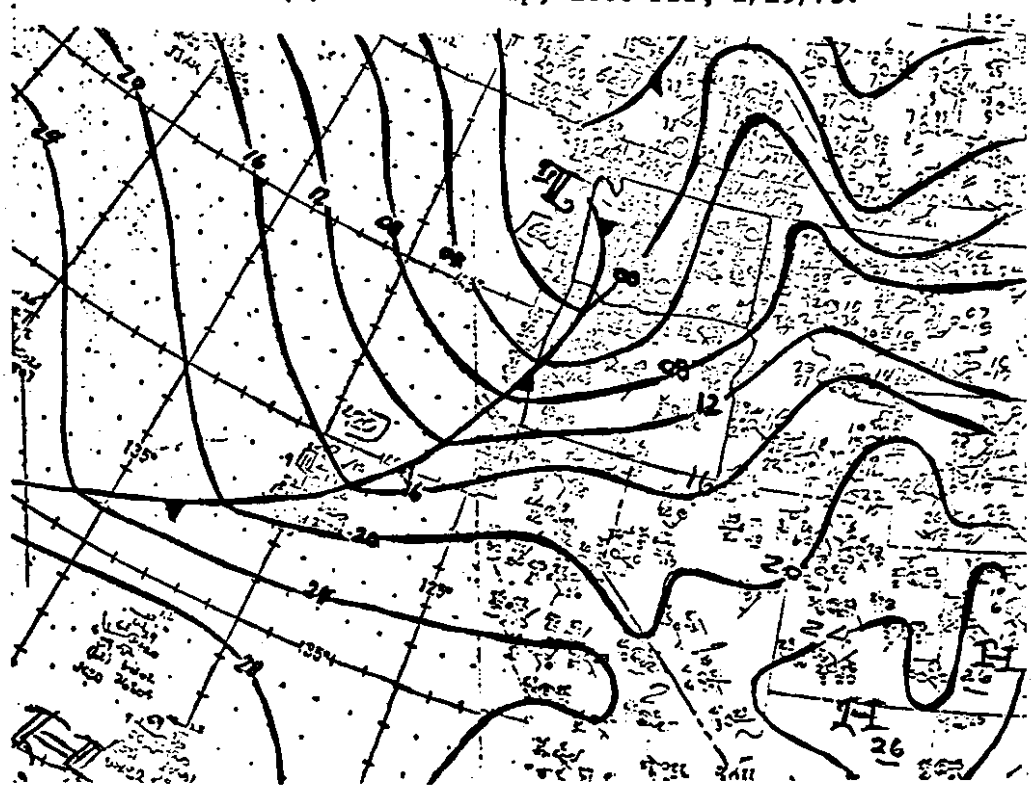

Figure 22. Twenty-four Hour New Snow Depth, Water from Rain and Avalanche Occurrences for Stevens Pass, January-March, 1975.

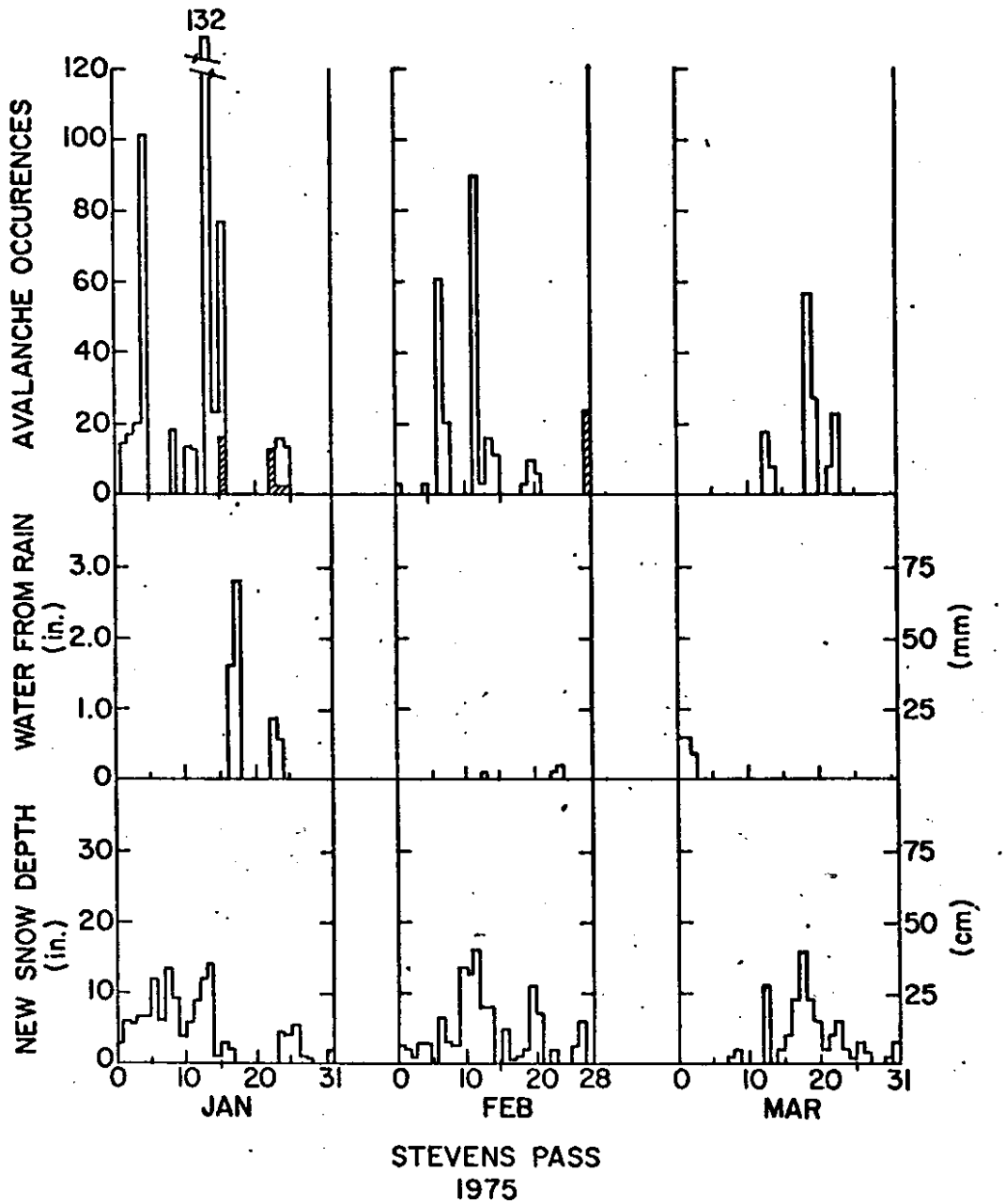

Figure 23. Twenty-four Hour New Snow Depth, Water from Rain and Avalanche Occurrences for Snoqualamie Pass, January-March, 1975. The abbreviation NA above any time periods indicates that the particular observations for the day(s) shown were not available.

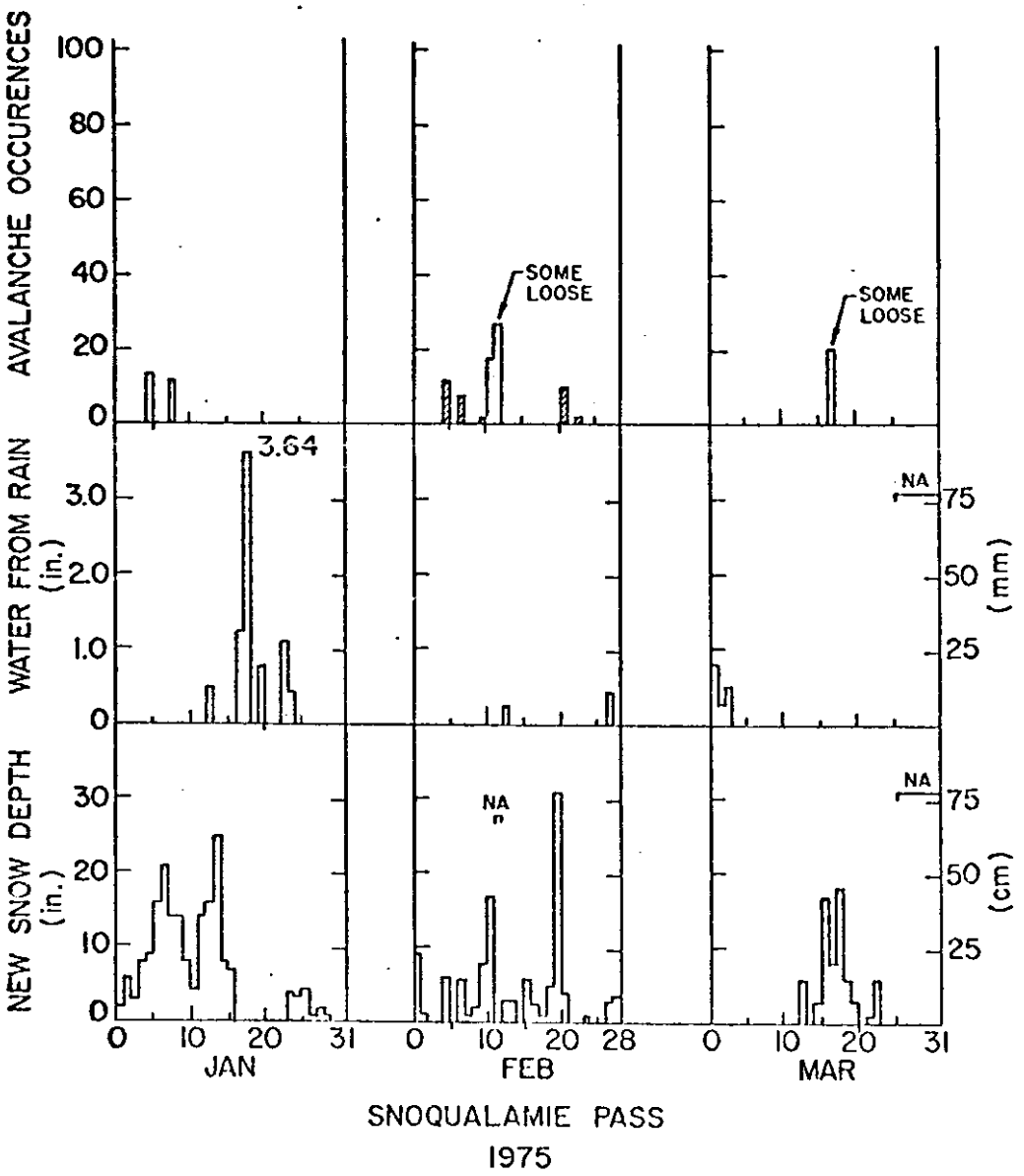

Figure 24. Twenty-four Hour New Snow Depth, Water from Rain and Avalanche Occurrences for Crystal Mountain, January-March, 1975.

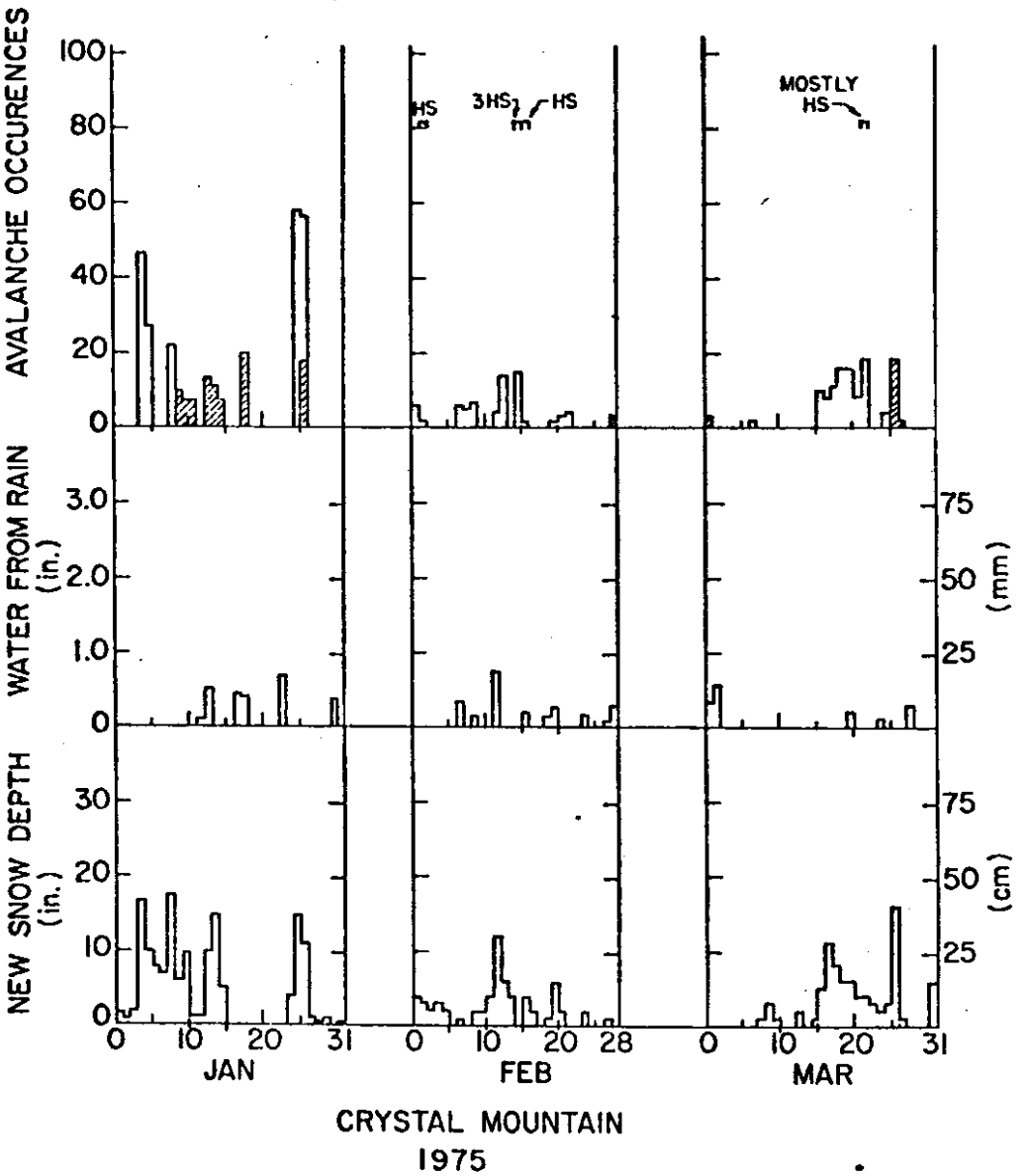

Figure 25. Twenty-four Hour New Snow Depth, Water from Rain and Avalanche Occurrences for Washington Pass, January-March, 1975.

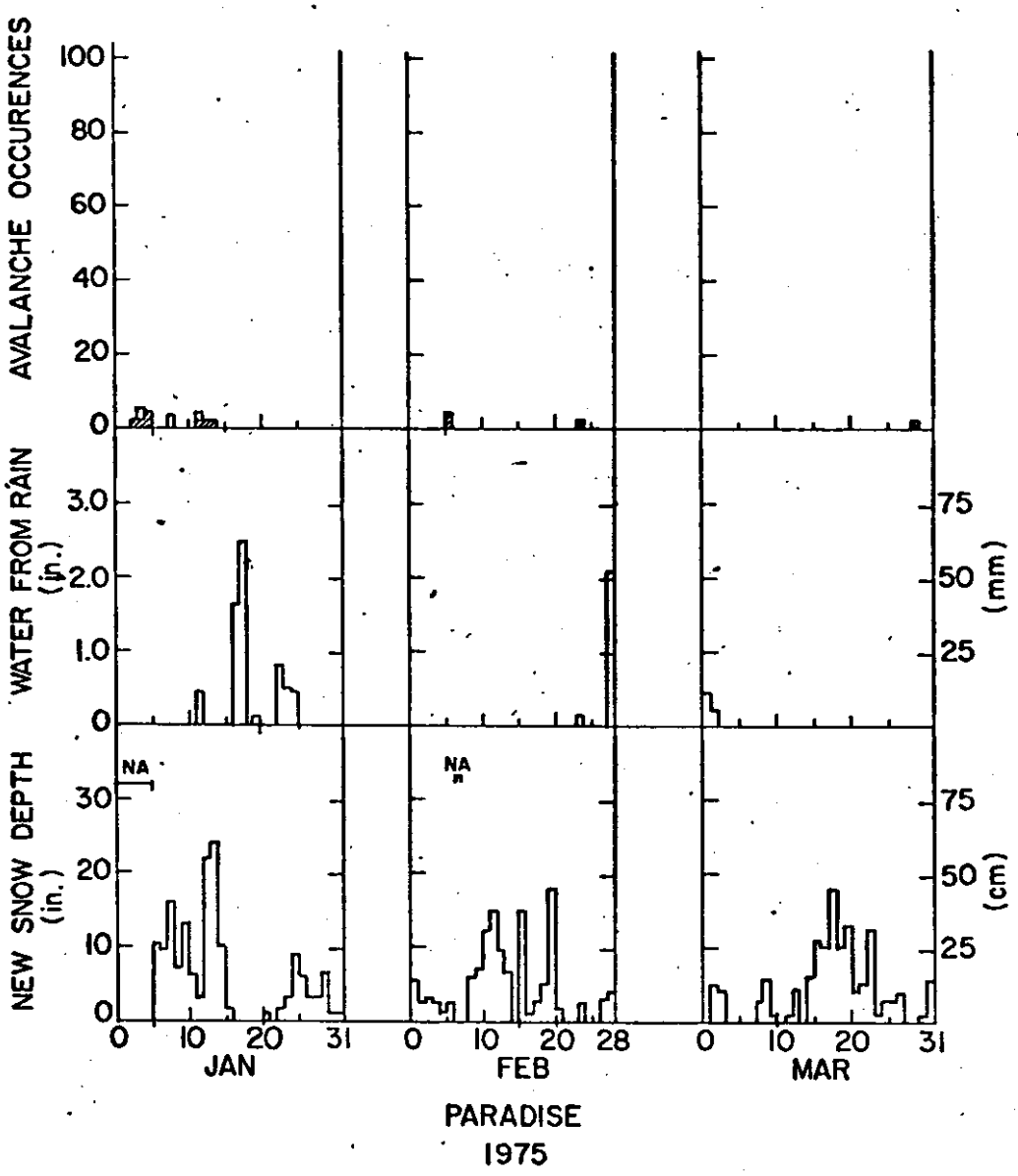

Figure 26. Fracture-line Profile of Slab Avalanche at Stevens Pass, 2/20/75. See Figure 3 for explanation of snow profile data.

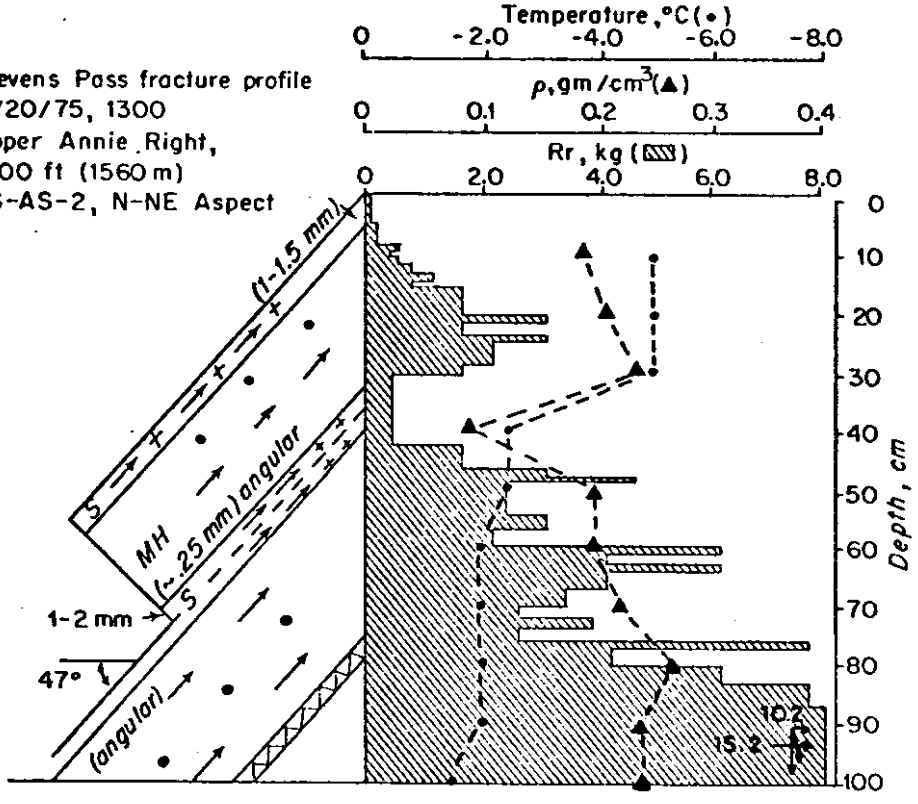

Figure 27. Fracture-line Profile of Slab Avalanche at Stevens Pass, 2/22/75. See Figure 3 for explanation of snow profile data.

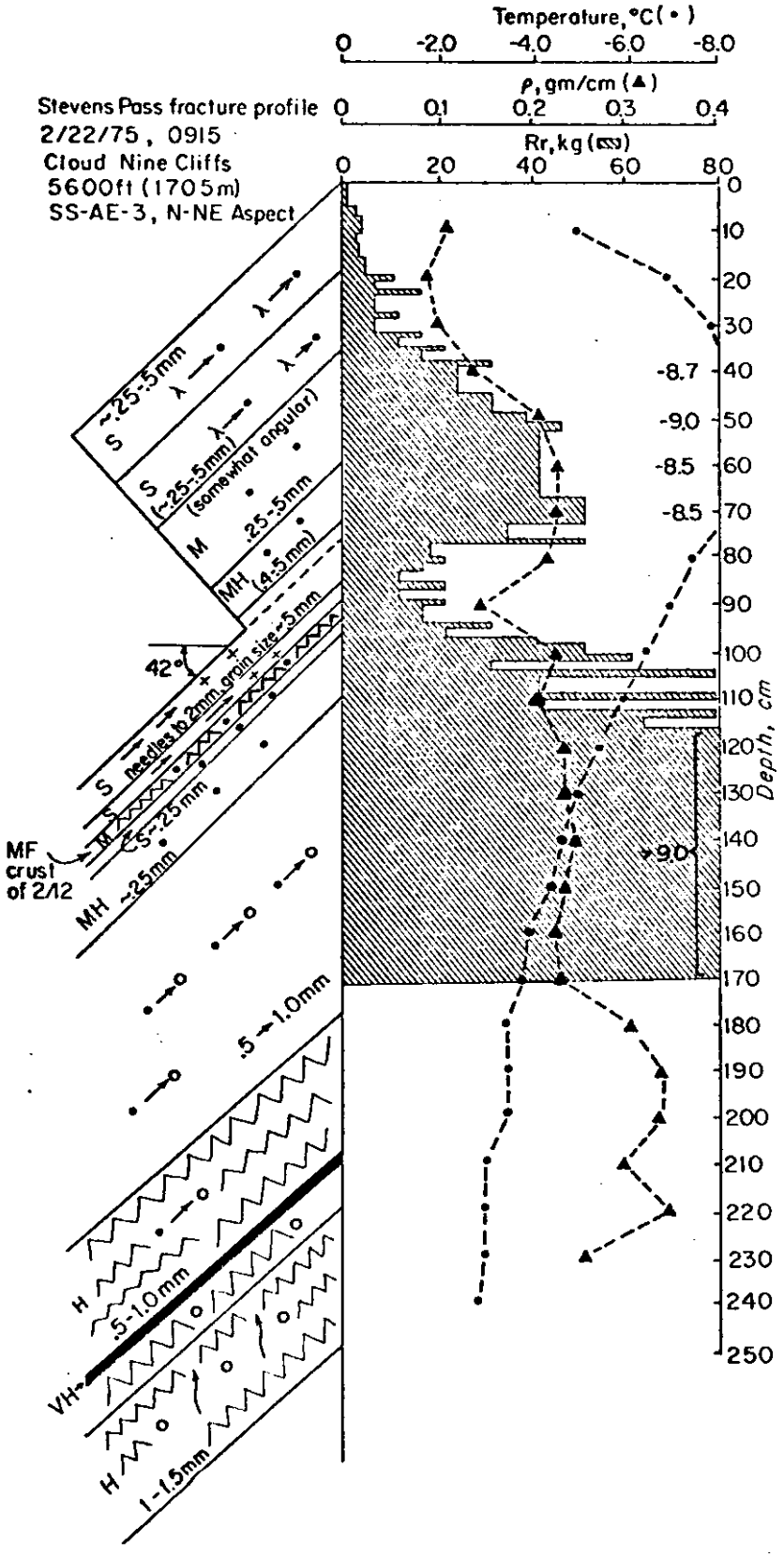

Figure 28. Surface and 500 mb Weather Maps for 0400 PST, 2/28/75. Appropriate map data for surface and 500 mb maps are explained in Figures 1 and 6(b), respectively.

(a) Surface Map, 0400 PST, 2/28/75.

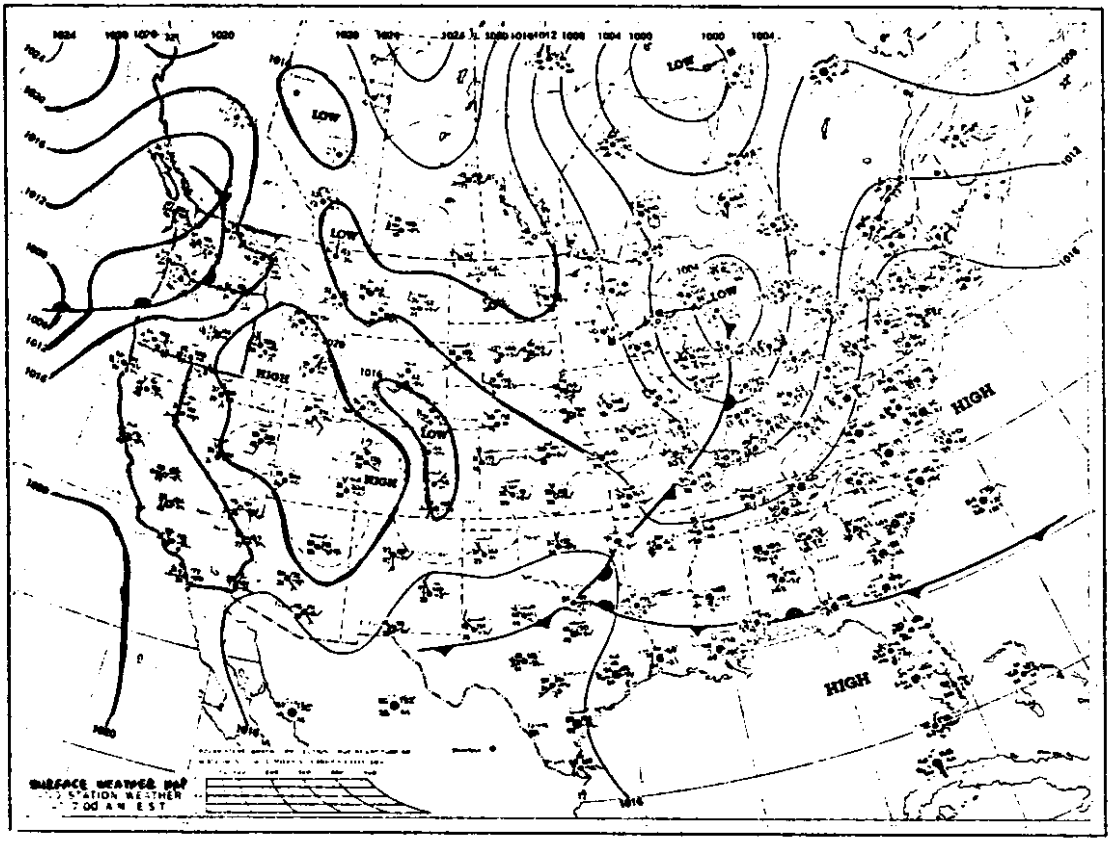

(b) 500 mb Map, 0400 PST, 2/28/75.

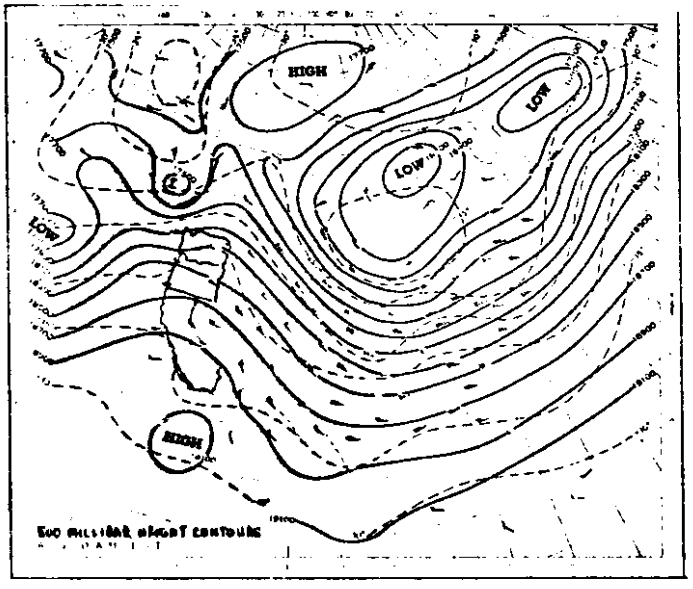

Figure 29. 500 mb Weather Maps for 0400 PST, 3/4/75. 3/6/75 and 3/10/75. 500 mb height contours, isotherms and winds are shown, and are described in Figure 6 (b).

(a) 500 mb Map, 0400 PST, 3/4/75.

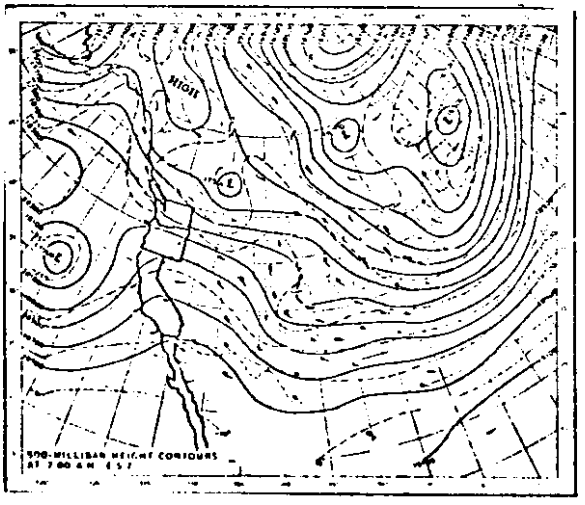

(b) 500 mb Map 0400 PST, 3/6/75.

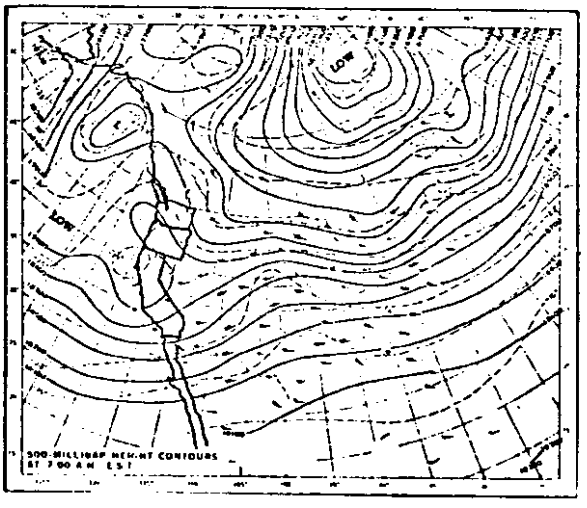

(c) 500 mb Map, 0400 PST, 3/10/75.

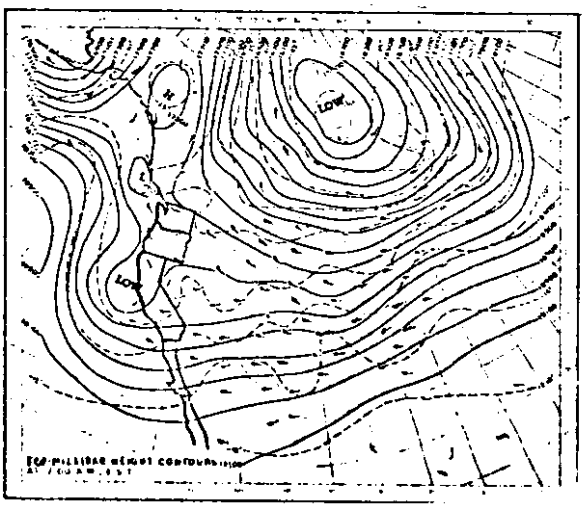

Figure 30. Fracture-line Profile of Slab Avalanche at Stevens Pass, 3/13/75. See Figure 3 for explanation of snow profile data.

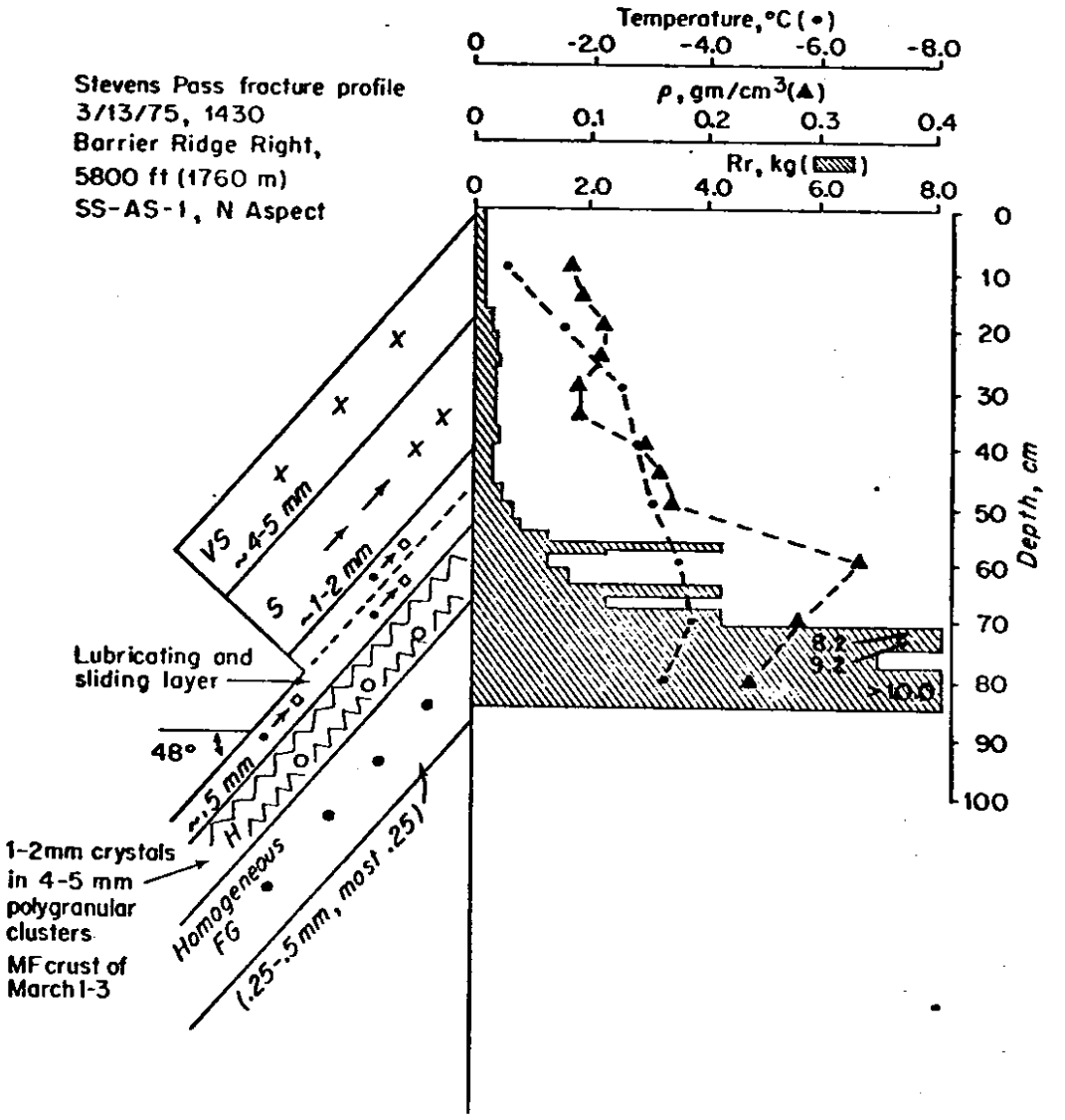

Figure 31. Snowpit Study at Stevens Pass, 3/16/75. See Figure 3 for explanation of snow profile data.

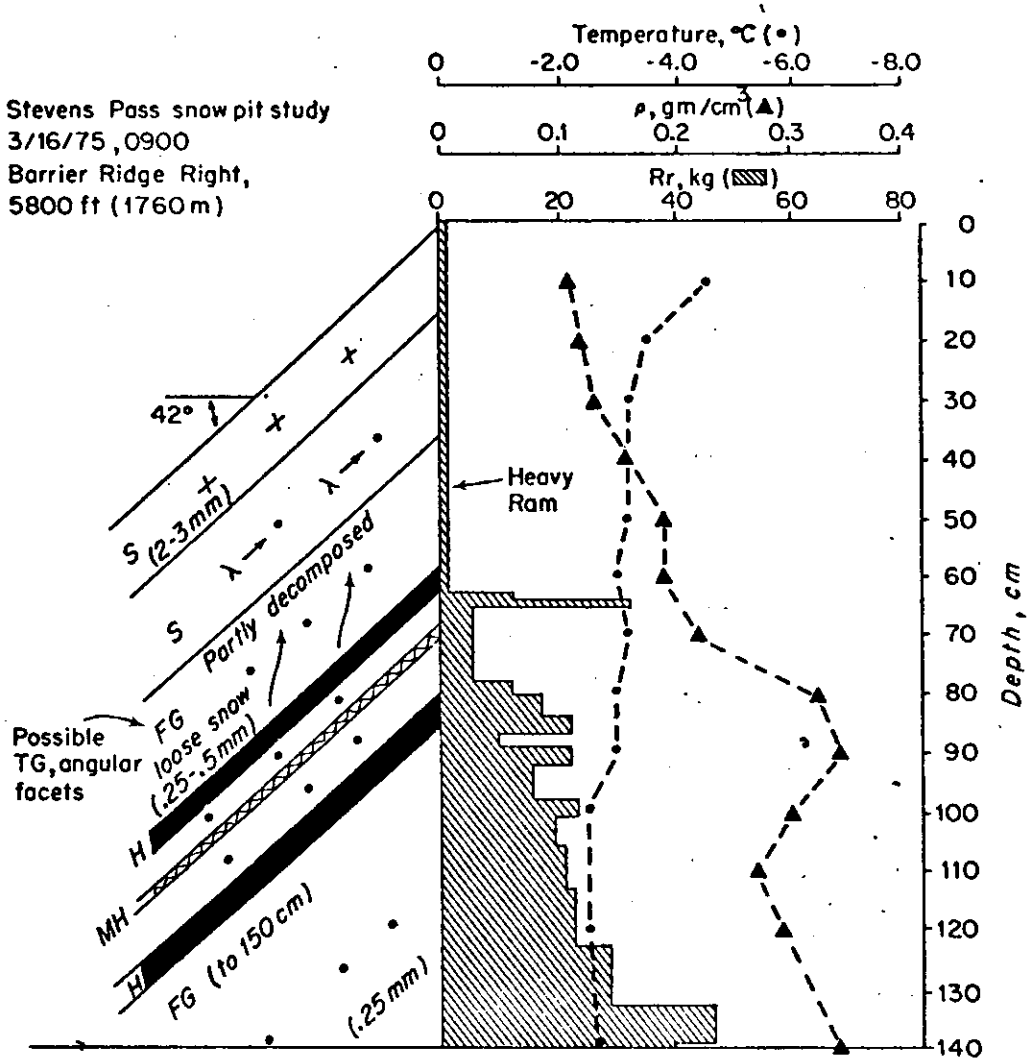

Figure 32. Surface and 500 mb Weather Maps for 0400 PST, 3/17/75. Appropriate map data for surface and 500 mb maps are explained in Figures 1 and 6(b), respectively.

(a) Surface Map, 0400 PST, 3/17/75.

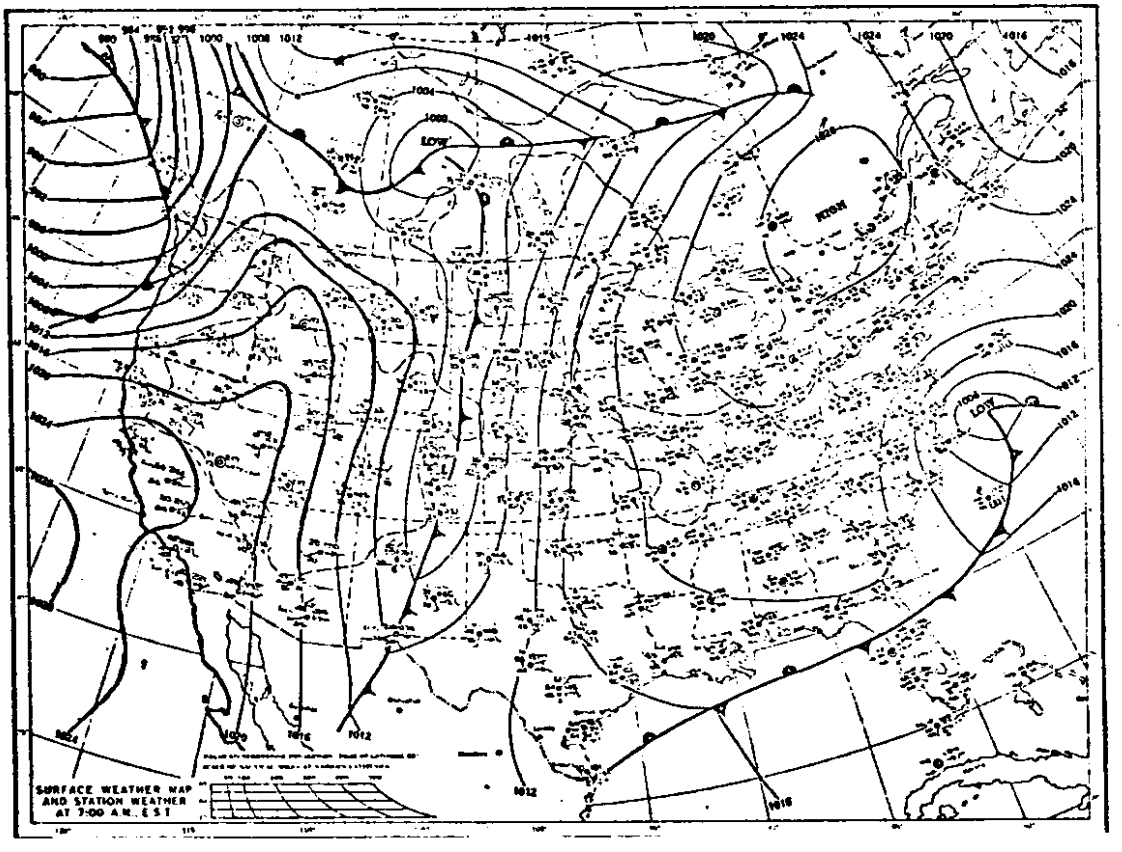

(b) 500 mb Map, 0400 PST, 3/17/75.

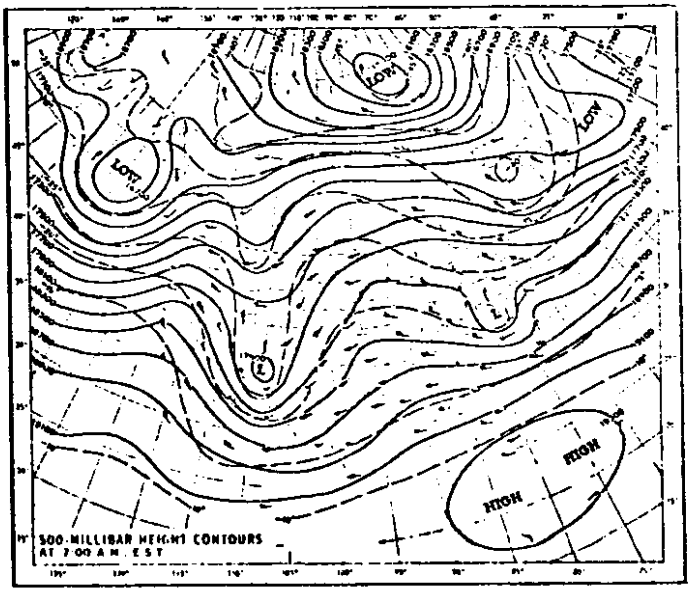

Figure 33. Surface Weather Map for 0500 PST, 3/22/75. Surface isobars and plotted station weather data are shown, and are described in Figure 1.

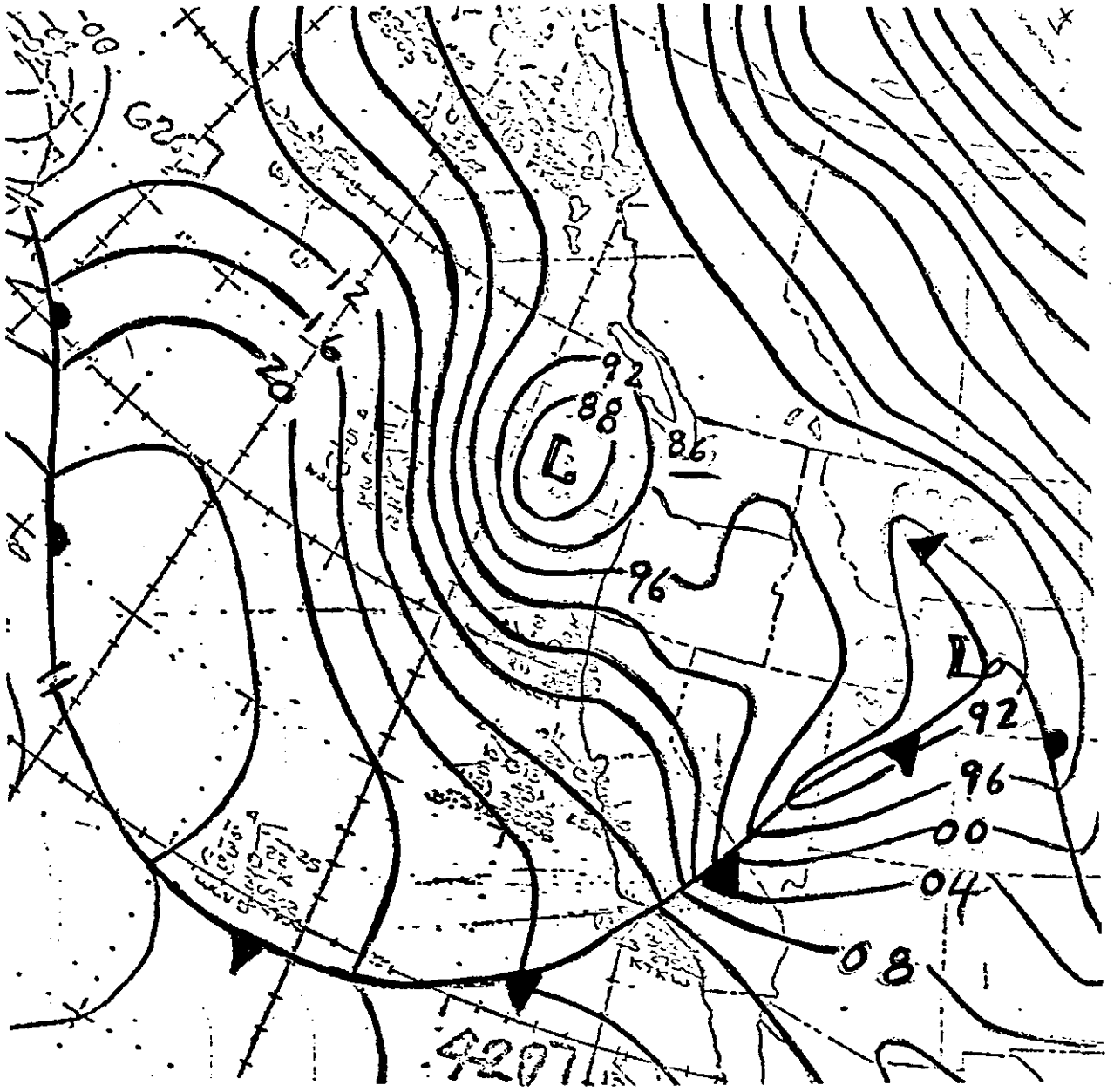

Figure 34. Surface Weather Map for 2300 PST, 3/24/75. Surface isobars and plotted station weather data are shown, and are described in Figure 1.